STRATOSPHERIC SULFATE AEROSOL:

A MICROPHYSICAL MODEL

by

Michael J. Mills

S.B., Massachusetts Institute of Technology, 1989

M.S., University of Colorado, 1993

A thesis submitted to the

Faculty of the Graduate School of the

University of Colorado in partial fulfillment

of the requirement for the degree of

Doctor of Philosophy

Department of Astrophysical, Planetary and Atmospheric Sciences

1996

This thesis for the Doctor of Philosophy degree by

Michael J. Mills

has been approved for the

Department of

Astrophysical, Planetary, and Atmospheric Sciences

by

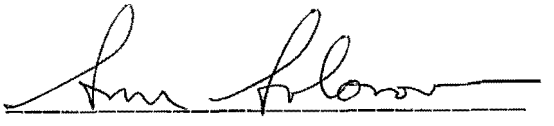

Susan Solomon

Linnea Avallone

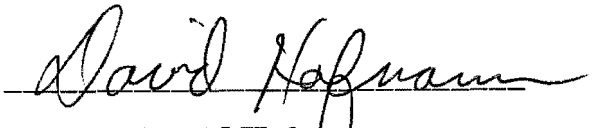

David Hofmann

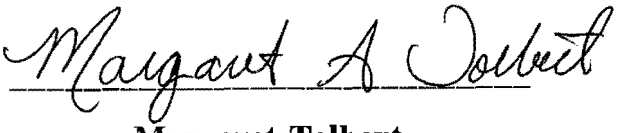

Margaret Tolbert

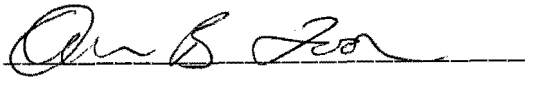

Owen Brian Toon

Date 25 November 1996

Mills, Michael J. (Ph.D., Astrophysical, Planetary and Atmospheric Sciences)

Stratospheric Sulfate Aerosol: A Microphysical Model

Thesis directed by Susan Solomon

Sulfate aerosol plays many important roles in the chemical and radiative budgets of the stratosphere. The predominant source of sulfate is large volcanic eruptions. However, an ambient layer of aerosol is observed even in volcanically quiescent periods, the sources of which are not quantitatively known. The regions and causes of new particle production are also not understood. In particular, an anomalous layer of small particles of uncertain origin is observed near 30 km in polar regions each spring. The vertical extent of stratospheric aerosol is also uncertain, limiting our knowledge of the impact of heterogeneous chemistry.

In order to address these questions of stratospheric aerosol theory, I have developed a numerical model of sulfate aerosol microphysics. I have incorporated this model into the Garcia-Solomon two-dimensional model of atmospheric dynamics and chemistry. Model calculations show carbonyl sulfide to be a very minor source of stratospheric aerosol, while tropospheric SO_2 is potentially very important. Additional sources of stratospheric sulfate are also indicated. Because anthropogenic emissions are a major source of SO_2 to the free troposphere, these results suggest that human impact on stratospheric sulfate in volcanically quiescent periods is substantial.

The model shows that the observed layer of new particles near 30 km in polar spring results from rapid oxidation of SO_2 shortly after the return of sunlight. This SO_2 is produced in the mesosphere by sulfuric acid photolysis, and descends to the stratosphere in polar winter. Spring oxidation rapidly produces sulfuric acid vapor, which nucleates in lingering cold temperatures. Particles grow rapidly to observable size by condensation of additional sulfuric acid vapor.

Heterogeneous reaction of N_2O_5 on sulfate aerosol in descending mesospheric air produces a layer of nitric acid in our model near 40 km in polar winter similar to that observed. The model shows that the aerosol layer extends upward to altitudes above 40 km in polar winter, despite strong descent in the mean circulation. This extension results from very cold temperatures in polar winter, which reduce equilibrium vapor pressures. Because observations of aerosol at such high altitudes are not available, these calculations represent an important theoretical advance.

Acknowledgments

I could not have performed this research without the guidance and support of my advisor, Susan Solomon. If I ever wondered about the relevance of atmospheric research to human problems, I needed only to look at Dr. Solomon's outstanding record of contributions to our understanding of the vital issue of ozone depletion. I am grateful for the opportunities she gave me to collaborate with her on a wide variety of atmospheric modeling problems, supplemented with a rare chance to make atmospheric measurements in Antarctica. Dr. Solomon's insight and experience have been invaluable to my research, and her candor and judgment motivated me to complete this thesis. My time with her will continue to benefit me throughout my career.

I thank my other committee members for the time they have taken on my behalf. Brian Toon and David Hofmann shared with me much of their extensive knowledge of aerosol modeling and measurements, respectively. Each have provided me with insightful suggestions and comments which will aid the future publication of this research. I am also grateful to Linnea Avallone for her very thorough reading of this text. Her comments demonstrated impeccable editorial skill as well as experience in the field, and have made this thesis more readable and cogent. Maggie Tolbert has been a source of great encouragement and cheer throughout my graduate studies. Her very thorough Atmospheric Chemistry course made her my favorite classroom professor.

A number of other researchers contributed to this work. Rolando Garcia developed the dynamical code for the model, and helped me to understand how it works. I would like to thank Bob deZafra for providing me with his nitric acid observations, to which I have compared my model calculations. Ken Carslaw was so kind as to permit use of his parameterization for ternary solution aerosol composition in the model. Jing-Xia Zhao was very patient in helping me to understand her new method for calculating binary homogenous nucleation rates from classical theory.

The NASA Global Change Research Fellowship provided funding support for much of this research. Funding from this fellowship allowed me to travel to numerous conferences over the course of three years, at which I interacted profitably with many of the scientists whose work is cited throughout this thesis.

Many colleagues at the NOAA Aeronomy Lab have guided me with their knowledge, encouragement, and friendship. Many thanks to Lori Perliski, Ryan Sanders, Roy Miller, Alex Weaver, Bob Portmann, John Daniel, and Sherry Stephens of the Middle Atmosphere Group. I must also acknowledge my fellow inhabitants of Trailer A: Jonathan Williams, Jane Olson, and Alison Grimsdell. Without their sense of fun and games I would doubtless have graduated earlier, albeit without my present knowledge of African capitals and countless sundry trivia. They have kept my laughing chops wriggling all through. Thanks also to Leslie Hartten, without whose M&M supply I would have often gone hungry.

As throughout my life, my mother, father, and sister have been there for me with love and encouragement in my years of graduate research. It is with great affection that I acknowledge their contribution to this thesis work. My family set me on the path of learning at an early age, and has supported my goals and choices ever since.

In the years of my graduate work it was not easy to be gay, lesbian, bisexual, or transgendered in the State of Colorado. I could not have endured the very real trauma that was the 1992 anti-gay referendum Amendment 2 without the love, support, and tenacity of a close group of friends and fellow activists. Among these are Karl Kruszynski, Vincent Cawley, Jim Davis-Rosenthal, Joe Hopper, Paul Chasnoff, Christopher DeWinter, Sue Larson, and Elliott Trice. In the years since, many more have joined my circle, and have stood with me through a variety of challenges, triumphs, and losses. It is to these dear friends among many courageous Coloradans that I dedicate this thesis.

Les Ballons

by Oscar Wilde

Against these turbid turquoise skies
 The light and luminous balloons
 Dip and drift like satin moons,
Drift like silken butterflies;

Reel with every windy gust,
 Rise and reel like dancing girls,
 Float like strange transparent pearls,
Fall and float like silver dust.

Table of Contents

Figures

Tables

Chapter 1

Stratospheric Aerosol

1.1 Background

Although the Earth's atmosphere is often thought to be composed solely of gases, suspended throughout are liquid and solid particles whose importance to atmospheric chemistry has only recently been appreciated. We observe the scattering of light from atmospheric particles as the beautiful sunsets, long noticed to follow major volcanic eruptions. The duration of such effects, often several years, is indicative of both the magnitude of volcanic perturbations on ambient atmospheric particles, and of the penetration of this perturbation into the stratosphere.

In 1961 Junge, *et al.* published the first *in situ* measurements confirming the presence of a suspension of particles, or aerosol, in the stratosphere. Vaporization measurements determined the particles to be liquid solutions of sulfuric acid and water (Rosen, 1971). The pioneering measurements of Junge followed a period of unusually low volcanic activity, leading to the concept of an "ambient" aerosol, which may be independent of large volcanic eruptions. Carbonyl sulfide (OCS), a gas originating from natural and anthropogenic sources on the earth's surface, has been thought to be a major source of this ambient layer, due to its substantial lifetime and mixing ratio in the troposphere, and photochemical destruction in the stratosphere (Crutzen, 1976).

Aerosol has long been recognized as an important factor in the radiative budget of the stratosphere. Several recent studies have examined the impact on stratospheric dynamics of radiative heating caused by aerosol following major volcanic eruptions (Brasseur and Granier, 1992; Kinne *et al.*, 1992; Schoeberl *et al.*, 1993; Tie *et al.*, 1994). This heating is calculated to force upward vertical motions in the tropics, leading to a reduction in column ozone there. It has also been suggested that scattering of solar radiation in volcanic aerosol affects photodissociation rates and hence abundances of stratospheric species (Fiocco *et al.*, 1978; Michelangeli *et al.*, 1989; Pitari and Rizi, 1993).

Much interest in stratospheric aerosol has been generated in the last decade with the recognition of the importance of heterogeneous reactions to the chemistry of the polar stratosphere in winter and spring. These reactions take place between atmospheric gases and compounds on the surface or in the bulk of solid or liquid particles. Heterogeneous reaction rates are therefore proportional to either the surface area or the volume of particles available. In addition, the solubility of key gases (e.g. HCl) in liquid often increases dramatically at low stratospheric temperatures. The effects of heterogeneous chemistry in the stratosphere were most dramatically observed in one of its coldest regions, where such reactions are responsible for liberating anthropogenic chlorine to destroy nearly all of the ozone at some altitudes over Antarctica each spring (Farman *et al.*, 1985; Solomon *et al.*, 1986; Solomon, 1988).

Since the discovery of the Antarctic ozone hole, the importance of heterogeneous chemistry has been recognized as extending to mid-latitudes due to the global presence of sulfate aerosol (Hofmann and Solomon, 1989). Enhancements in stratospheric sulfur due to volcanic eruptions are therefore of concern as perturbations to stratospheric chemistry. Several calculations relying on measurements of aerosol surface area indicate that heterogeneous chemistry on volcanic aerosol has significant effects on stratospheric nitrogen and ozone (Fahey *et al.*, 1993; Mills *et al.*, 1993;

Solomon *et al.*, 1996). Two-dimensional microphysical calculations of volcanic aerosol have implicated heterogeneous chemistry in observed ozone depletion at middle and high latitudes (Tie *et al.*, 1994).

Interaction between the effects of aerosol on stratospheric chemistry and the distribution of particles amongst various sizes can be explicitly calculated with a model of aerosol microphysics. Microphysical processes of aerosol include nucleation, condensation, coagulation, and sedimentation. Although much can be learned by including observed profiles of aerosol surface area in models without microphysical codes, a microphysical model is required to predict aerosol behavior under hypothetical conditions or in regions of the atmosphere where observations are unavailable. A microphysical model, for example, could calculate the aerosol produced by a single source, absent other influences. Microphysical models can also aid in the interpretation of observations by determining relationships between observed quantities and aerosol parameters, such as surface area, mass, or particle number. The work of Toon, Turco, and coworkers (Toon, *et al.*, 1979; Turco, *et al.*, 1979a,b) has been seminal for many who have followed in developing microphysical models of stratospheric aerosol.

1.2 Thesis Goals

While much has been learned from previous studies, a number of outstanding questions remain concerning volcanic and ambient stratospheric aerosol. Which are the dominant nonvolcanic sources of sulfate aerosol? What does this tell us about man's impact on global aerosol? What is the lifetime of aerosol in the stratosphere? Are volcanic influences ever removed from stratospheric aerosol? What impact does man have on stratospheric aerosol from current tropospheric SO_2 pollution? What impact might future anthropogenic sources, such as from a proposed fleet of stratospheric aircraft, have? Where are new aerosol particles formed? What is the extent of heterogeneous reactions on aerosol? I address these and other questions with a microphysical model I have developed for this purpose.

My analysis begins with a thorough examination of nonvolcanic aerosol. My first goal is to assess the importance of carbonyl sulfide to stratospheric sulfate. I use the microphysical model to calculate the layer that would be produced by this source alone. I then add observed mixing ratios of sulfur dioxide to the model troposphere to determine its relative importance to the stratosphere. I compare these calculations to stratospheric observations to check the accuracy of the microphysical simulation and to judge whether additional sources are indicated.

I have used the model to examine several observed phenomena in polar regions. The first is a distinct layer of small particles that forms near 25 km in polar spring. The microphysical model should be able to reproduce such observations, lending a better understand of the cause. The second is a distinct layer of nitric acid that forms near 40 km in polar winter. The model indicates that this layer is generated by heterogeneous reactions on aerosol.

1.3 Thesis Outline

This thesis describes a detailed model of sulfate aerosol microphysics that I have incorporated into the Garcia-Solomon 2-dimensional model of atmospheric dynamics and chemistry. It also discusses several important findings that have resulted.

Chapter 2 describes chemistry, transport, and sources of sulfur-bearing gases added to the Garcia-Solomon model. I begin by describing the model's numerical integration techniques, which make use of chemical families. I then describe the model's derivation of atmospheric dynamics. The mean circulation is calculated from governing equations, and is driven by parameterizations of gravity and planetary wave breaking. The effects of sub-grid-scale motions are parameterized as eddy diffusion.

In section 2.2 I consider various sources of nonvolcanic stratospheric sulfur. Carbonyl sulfide has long been thought to contribute significantly to sulfate aerosol, due to its long lifetime and large mixing ratio in the troposphere, and its dissociation in

the stratosphere. Sulfur dioxide is also observed in large abundance throughout the free troposphere, and also contributes to sulfate aerosol upon reaching the stratosphere. Reduced sulfur compounds such as dimethyl sulfide and CS_2 are considered as well. I then describe the oxidation pathways from source gases to sulfuric acid, and present some calculated altitude profiles of gas-phase sulfur compounds.

In chapter 3 I explain how microphysical aerosol processes are simulated numerically. New particles are formed by binary homogenous nucleation according to classical theory. Existing particles grow and shrink by exchanging water, sulfuric acid, and nitric acid with the vapor phase. Coagulation occurs when two particles collide, reducing particle number and increasing particle size. Small particles move with the air that suspends them, according to mean circulation and diffusive processes described in chapter 2. Larger particles can sediment through air at significant rates, a process which I calculate explicitly.

In chapter 4 I compare model calculations of aerosol from various sources to aerosol observed in volcanically quiescent periods. In doing so I address a number of questions. Can carbonyl sulfide alone produce the bulk of this nonvolcanic aerosol? How significant is sulfur dioxide from the troposphere? Are other sources required to explain observations? Have aerosol levels unperturbed by volcanic influences ever been observed? What is the lifetime of stratospheric aerosol?

In chapter 5 I show how the microphysical model explains two anomalous phenomena in polar winter. The first is the anomalous "CN layer," a sharply defined layer of new particles observed shortly after the end of polar night near 30 km. The second is the formation of a distinct layer of nitric acid near 40 km in polar air in mid-winter. The model also explains much of the observed denitrification of the lower stratosphere.

Chapter 6 is a final summary and discussion of the thesis conclusions. Further research suggested by this work is discussed.

Chapter 2

The Two-Dimensional Chemical-Dynamical Model

The presence of the stratospheric sulfate aerosol depends on the transport of sulfur-bearing compounds to the stratosphere, and their chemical oxidation to sulfuric acid. I calculate these processes interactively with other chemistry and dynamics in the Garcia-Solomon model. Model calculations rely on knowledge of natural and anthropogenic sources and sinks of sulfur, and laboratory measurements of reaction rates for chemical pathways through intermediate compounds. In this chapter I discuss these chemical pathways, sources and sinks, and describe the Garcia-Solomon model to which they were added.

The model used for this project was developed by R. Garcia and S. Solomon and was modified for this study. The model's vertical dimension spans 56 pressure levels, selected to correspond approximately to two kilometer altitude intervals from 2 to 112 km above sea level. The horizontal dimension is divided into 36 latitudes from 89.5°S to 89.5°N, giving a resolution of approximately five degrees. Details of the photochemistry and dynamics of the model are described in Garcia *et al.* (1992) and Garcia and Solomon (1994). The first section of this chapter discusses the numerical integration methods employed in the model's photochemical scheme, incorporating the effects of dynamics on chemical constituents. The second section details the photochemical reactions involving sulfur-bearing species that were added to this

model. I then present calculated profiles and distributions for various gas-phase sulfur species, comparing to observations where available.

2.1 Photochemistry and Transport

The chemical reactions considered in the Garcia-Solomon model are discussed in Garcia and Solomon (1994). A numerical photochemical model must calculate changes in abundances of individual chemical species due to each of these reactions in which it either participates as a reactant or results as a product. In addition, the effects of transport processes must be included in calculations of chemical abundances.

Numerical Integration Methods

Chemistry and dynamics define a continuity equation for each chemical species in the following differential form:

$$\frac{dn_k}{dt} = \sum_i P_i - \sum_j L_j n_k - T_k \qquad 2.1$$

Here n_k is the number density of a chemical species [molecules/cm^3], P_i represents each photochemical production rate [molecules/cm^3/s], L_j represents each photochemical loss rate [/s], and T_k is density change due to transport [molecules/cm^3/s]. The loss term may be expressed as $L_j \cdot n_k$ because the rate of each loss reaction is proportional to the concentration of the species that is lost. The model solves this continuity equation for each chemical species at each altitude and latitude by numerically integrating over discrete timesteps.

Numerical integration of equation 2.1 requires that the equation be expressed in terms of a finite difference over such a timestep, Δt. Either the initial or the resultant concentration (n_k) may be substituted as a factor in the loss term, thus:

$$\frac{n_k(t+\Delta t)-n_k(t)}{\Delta t} = \sum_i P_i - n_k(t+\Delta t)\cdot\sum_j L_j - T_k \qquad 2.2$$

or

$$\frac{n_k(t+\Delta t)-n_k(t)}{\Delta t} = \sum_i P_i - n_k(t)\cdot\sum_j L_j - T_k \qquad 2.3$$

Equation 2.2, which uses the resultant density in the loss term, is the semi-implicit form of the continuity equation. The solution of this semi-implicit form is always stable, but fails to conserve mass. Equation 2.3 expresses the finite difference in the explicit form, leading to the forward Euler finite difference solution:

$$n_k(t+\Delta t) = n_k(t) + \left(\sum_i P_i - n_k(t)\sum_j L_j - T_k\right)\Delta t \qquad 2.4$$

This solution is stable and mass-conserving provided that the chosen timestep is less than one-fifth of the total lifetime of the given species (Brasseur and Solomon, 1986, p. 200).

The total lifetime of a species is the time it would take for the species concentration to decay to 1/e of its initial value if production were shut off. Lifetime is separated into photochemical and dynamical components, thus:

$$\frac{1}{\tau_{tot}} = \frac{1}{\tau_{chem}} + \frac{1}{\tau_{dyn}} \qquad 2.5$$

$$\text{where } \tau_{chem} \equiv \frac{n_k}{n_k\sum_j L_j} = \frac{1}{\sum_j L_j} \quad \text{and} \quad \tau_{dyn} \equiv \frac{n_k}{|T_k|}$$

These mathematical formulations illustrate that chemical and dynamical lifetimes are equivalent to the current species concentration divided by its current rate of loss. Hence in an equilibrium situation, where a species concentration remains constant in the atmosphere, a lifetime may be considered as the time for a number of molecules

equivalent to its current concentration to cycle through chemical and dynamical loss processes.

The dynamical lifetime may be further divided into lifetimes for the various dynamical processes (i.e. diffusion, advection) included in the model. More will be said about these processes later in this section. In general, these processes transport molecules in the stratosphere over distances representative of the model's grid resolution on timescales of weeks to months. Thus it is easy to chose integration timesteps that are always shorter than the dynamical lifetimes of species.

Timescales for chemistry in the stratosphere pose a more difficult problem. Photochemical lifetimes vary among all of the model's individual species from microseconds to years. Individual lifetimes may vary on a comparable scale with altitude and latitude. Numerical integration by forward Euler differencing with timesteps that are always less than the smallest chemical lifetime in the system would consume tremendous computing resources. The Garcia-Solomon model utilizes "families" of chemical species to solve these systems, as discussed, for example, in Brasseur and Solomon (1986) and Turco and Whitten (1974).

Chemical families are defined such that species within the family interchange rapidly via chemical reaction, but only slowly convert to species outside the family. A family lifetime may be defined in terms of the ratio of the total family concentration to the rate of loss of all family members to species outside the family. This family lifetime must be at least five times longer than the model's photochemical timestep, so that forward Euler differencing of the total family concentration remains stable and mass-conserving. The family sum thus derived is then partitioned among constituent species using suitably stable methods.

The lifetime of each constituent is tested to determine whether a forward Euler (explicit) or photochemical equilibrium solution is possible. Long-lived constituents violate the condition for family chemistry, and are integrated explicitly via forward

Euler differencing (equation 2.4). Separate transport terms are calculated for long-lived constituents, and their concentrations are subtracted from the family sum. The remaining family concentration may be partitioned among the short-lived members.

Partitioning of family concentration among short-lived species makes use of photochemical equilibrium solutions. When photochemistry occurs sufficiently rapidly, concentrations are assumed to have reached equilibrium values at the next timestep. The photochemical equilibrium solution is derived by setting the rate of change in constituent number density to zero in equation 2.1, leading to the result

$$n_k = \frac{\sum_i P_i}{\sum_j L_j} \qquad 2.7$$

When two constituents interchange rapidly, the equilibrium assumption allows their densities to be expressed in terms of the ratio of one to the other. These concepts are best conveyed by a simple example.

In sunlit regions of the stratosphere above 30 km, ozone is relatively short-lived, having a photochemical lifetime of less than 30 minutes. The only loss process that destroys ozone on such a short timescale, however, is photolysis to produce atomic and molecular oxygen. Atomic oxygen is much shorter-lived than ozone in the stratosphere, having a lifetime ranging between 0.01 and 10 seconds. Its only rapid loss mechanism is reaction with molecular oxygen and a third body to produce ozone. These conditions suggest the grouping of ozone and atomic oxygen into the odd oxygen family.

The lifetime of the odd oxygen family is significantly longer than that of either ozone or atomic oxygen. Loss processes for odd oxygen are numerous, and include catalytic cycles with oxides of nitrogen, chlorine, bromine, and hydrogen, as well as pure oxygen chemistry. Neglecting heterogeneous processes, the lifetime of odd oxygen ranges from hours in the upper stratosphere to years in the lower stratosphere.

Thus the model integrates the continuity equation for total odd oxygen using the forward Euler method, accounting for transport processes as well as chemical production and loss of odd oxygen.

Partitioning of the resultant family concentration between atomic oxygen and ozone makes use of the dominant chemistry affecting atomic oxygen production and loss. This chemistry is described approximately by the following differential equation:

$$\frac{\partial[O]}{\partial t} \approx J_{O_3}[O_3] - k_a[O][O_2][M] \qquad 2.8$$

Because of the short lifetime of atomic oxygen, its concentrations reach equilibrium within a model timestep. The time differential on the left side of the equation is therefore set to zero. This photochemical equilibrium assumption leads to the following approximate expression of the dominant partitioning:

$$\frac{[O]}{[O_3]} \approx \frac{J_{O_3}}{k_a[O_2][M]} \qquad 2.9$$

This expression provides a simple partitioning for odd oxygen, provided the chemical lifetimes involved are sufficiently short. Where ozone is long-lived, such as at night or in the lower stratosphere, its density is integrated explicitly, using its own transport term. In such regimes, the remaining odd oxygen is partitioned into atomic oxygen.

The model used in this study defines six chemical families, listed in table 2.1. The model tests the conditions for family chemistry as described above. Hence the definition of each family varies to include only those constituent species whose photochemical lifetimes are sufficiently short. Table 2.2 lists source gases and the lower boundary conditions the model applies to them (representative of the atmosphere for the year 1990). In addition to the compounds listed in Tables 2.1 and 2.2, the model includes H_2O, CH_2O, CH_3O_2, and additional sulfur species discussed in section 2.2.

Table 2.1 Chemical families in the model. Families consisting of one species are not shown.

Chemical Family	Abbreviation	Constituent list
Odd oxygen	O_x	O, O_3
Odd nitrogen	NO_x	N, NO, NO_2, NO_3, N_2O_5, HNO_4
Odd hydrogen	HO_x	H, OH, HO_2
Odd chlorine	ClO_x	Cl, ClO, HOCl, Cl_2O_2 OClO, Cl_2, $ClONO_2$, BrCl
Odd bromine	BrO_x	Br, BrO, HOBr, HBr, $BrONO_2$, BrCl,
Odd sulfur	SO_x	S, SO, SO_2

Table 2.2 Chemical mixing ratios at the model's lower boundary (accurate for 1990).

Species	Lower BC	Species	Lower BC
Halocarbons:		**Others:**	
CFC11 ($CFCl_3$)	270.1 pptv	N_2O	310 ppbv
CFC12 (CF_2Cl_2)	465.3 pptv	CH_4	1715 ppbv
CFC113 ($C_2F_3Cl_3$)	70.5 pptv	CO_2	354 ppmv
CCl_4	108.2 pptv	H_2	500 ppbv
Methyl Chloroform (CH_3CCl_3)	153.2 pptv	HCl	100 pptv
Methyl Bromide (CH_3Br)	13.6 pptv	Methyl Chloride (CH_3Cl)	600 pptv
H1301 (CF_3Br)	1.7 pptv	HNO_3	200 pptv, lat>30 50 pptv, lat<30
H1211 (CF_2ClBr)	2.9 pptv	CO	latitude dependent, from Fishman and Crutzen (1978)
HCFC22 ($CHClF_2$)	105.8 pptv	H_2O_2	300 pptv
HCFC141b ($C_2H_2Cl_2F$)	0.3 pptv	O_x	25 ppbv
		NO_x	40 pptv, lat>30 15 pptv, lat<30

Model Transport

Chemical constituents in the model experience transport due to advection, dynamical wave forcing, and motions smaller than grid scale. Vertical and meridional winds, which advect species, are calculated from solutions to the governing equations, and are consistent with model-calculated temperatures. The Garcia-Solomon model includes the parameterization of Lindzen (1981) for the effect of dissipating gravity waves, and the parameterization of Garcia (1991) of planetary wave breaking in the stratosphere. Additional motions of air on scales smaller than the model's grid are parameterized as a diffusive process.

The mean circulation of the middle atmosphere is driven to a large extent by eddy motions, particularly gravity and planetary wave breaking. Steady and conservative waves, however, do not affect the mean circulation. Two-dimensional models must deal with complex three-dimensional atmospheric dynamics in terms of zonal averages and parameterized eddies, or waves, which depart from this mean. Straightforward Eulerian averages around latitude circles, however, will not readily remove steady and conservative waves from the mean, due to the fact that these waves do not travel strictly along latitude circles. The resultant zonal averages are not characteristic of the mean meridional motion from a Lagrangian perspective. The development of the Transformed Eulerian Mean (TEM), with the work of Boyd (1976), Andrews and McIntyre (1976, 1978), and Dunkerton (1978), decoupled steady and conservative waves from the mean circulation. Breaking waves, on the other hand, can force the TEM circulation through eddy forcing terms.

The Garcia-Solomon model calculates the residual circulation by solving the Transformed Eulerian Mean (TEM) form of the governing equations.

Momentum equation

$$\frac{\partial \overline{u}}{\partial t} + \overline{v}^* \left(\frac{\partial \overline{u}}{\partial y} - f \right) + \overline{w}^* \frac{\partial \overline{u}}{\partial z} = F_p + F_g + D_u \qquad 2.10$$

Gradient wind equation $$\frac{\partial \bar{u}}{\partial z}\left(f+\frac{2\bar{u}}{a}\tan\phi\right)=-\frac{R}{H}\frac{\partial \bar{T}}{\partial y} \qquad 2.11$$

Continuity equation $$\frac{1}{\cos\phi}\frac{\partial}{\partial y}\left(\bar{v}^{*}\cos\phi\right)+\frac{1}{\rho_o}\frac{\partial}{\partial z}\left(\rho_o \bar{w}^{*}\right)=0 \qquad 2.12$$

Thermodynamic equation $$\frac{\partial \bar{T}}{\partial t}+\bar{v}^{*}\frac{\partial \bar{T}}{\partial y}+\bar{w}^{*}\frac{\partial \bar{T}}{\partial z}+\frac{HN_o^2}{R}\bar{w}^{*}=Q+D_H \qquad 2.13$$

In these equations $\bar{u}$ is the zonal velocity, $\bar{v}^{*}$ and $\bar{w}^{*}$ are residual meridional and vertical velocities, and $\bar{T}$ is temperature deviation from the global average profile. Overbars indicate zonal averages of these variables. The model coordinates are log-pressure altitude, z (assuming a 7 km scale height, H); latitude, ϕ (or horizontal distance $y = R_0\phi$, where R_0 is the radius of the Earth); and time, t. f is the Coriolis parameter and N_0 is the Brunt-Vaisala frequency for the reference profile. The remaining terms, Q, F_g, F_p, D_u, and D_H represent forcing terms due to diabatic heating, gravity waves, planetary waves, and diffusion of momentum and heat due by sub-grid scale motions.

Given the mean meridional circulation $\bar{v}^{*}, \bar{w}^{*}$, the model derives $\bar{u}$ from equation 2.10, and subsequently $\bar{T}$ from equation 2.11. This temperature field is then used to calculate the infrared heating term to the diabatic forcing, Q, and as is explained below, is distinct from the temperature field used in model chemistry. In order to solve the continuity equation, 2.12, the model defines a streamfunction, $\bar{\chi}^{*}$, such that $\bar{v}^{*}$ and $\bar{w}^{*}$ are proportional to its z- and y-derivatives, respectively. Manipulation of all four equations leads to an elliptic equation in terms of $\bar{\chi}^{*}$ and the forcing terms. This streamfunction equation is diagnostic, having no time derivatives, and thus can be used to generate $\bar{v}^{*}$ and $\bar{w}^{*}$ at the next timestep given the current $\bar{u}$ and $\bar{T}$. Finally, $\bar{v}^{*}$ and $\bar{w}^{*}$ are used in the thermodynamic equation, 2.13, to get the temperature field used in model chemistry.

Advection of chemical species by the meridional circulation is calculated using a semi-Lagrangian code. Each model gridpoint is traced half a timestep along its back-trajectory, calculated from wind fields $\bar{v}^*$ and $\bar{w}^*$, which are then bilinearly interpolated at this new coordinate. The parcel is then followed back another half timestep, and mixing ratios are bilinearly interpolated at this point of origin. The advection contribution to the chemical transport term per timestep is then calculated simply as the mixing ratio difference between each gridpoint and its point of origin. This semi-Lagrangian scheme is more accurate than finite difference methods for advection of steep gradients, and conserves mass. Inclusion of higher-order interpolation would be an improvement necessary only for highly localized species with gradients that the model could not resolve, and could lead to mass-conservation problems (Garcia and Solomon, 1994).

Although true molecular diffusion is not an important process in the atmospheres, it is traditional and appropriate to parameterize sub-grid scale parcel motions as a diffusive process. Coefficients for vertical and horizontal eddy diffusion, K_{zz} and K_{yy}, are specified in the troposphere, consistent with the rapid mixing inherent to this region (Garcia *et al.*, 1992). Throughout the stratosphere the background diffusivity is small ($K_{yy} = 10^4\ m^2s^{-1}$ and $K_{zz} = 0.1\ m^2s^{-1}$) and the diffusion coefficients are dominated by the effects of gravity- and planetary-wave breaking, via parameterizations discussed in Garcia and Solomon (1985) and Garcia *et al.* (1992).

2.2 Sources and Photochemistry of Stratospheric Sulfur

Figure 2-1 shows the chemical pathways transforming sulfur from source gases to sulfuric acid, as included in the model. The corresponding sulfur reactions added to the Garcia-Solomon model are listed in table 2.3. The source gases shown in figure 2-1 represent the four most important reduced sulfur compounds in the atmosphere:

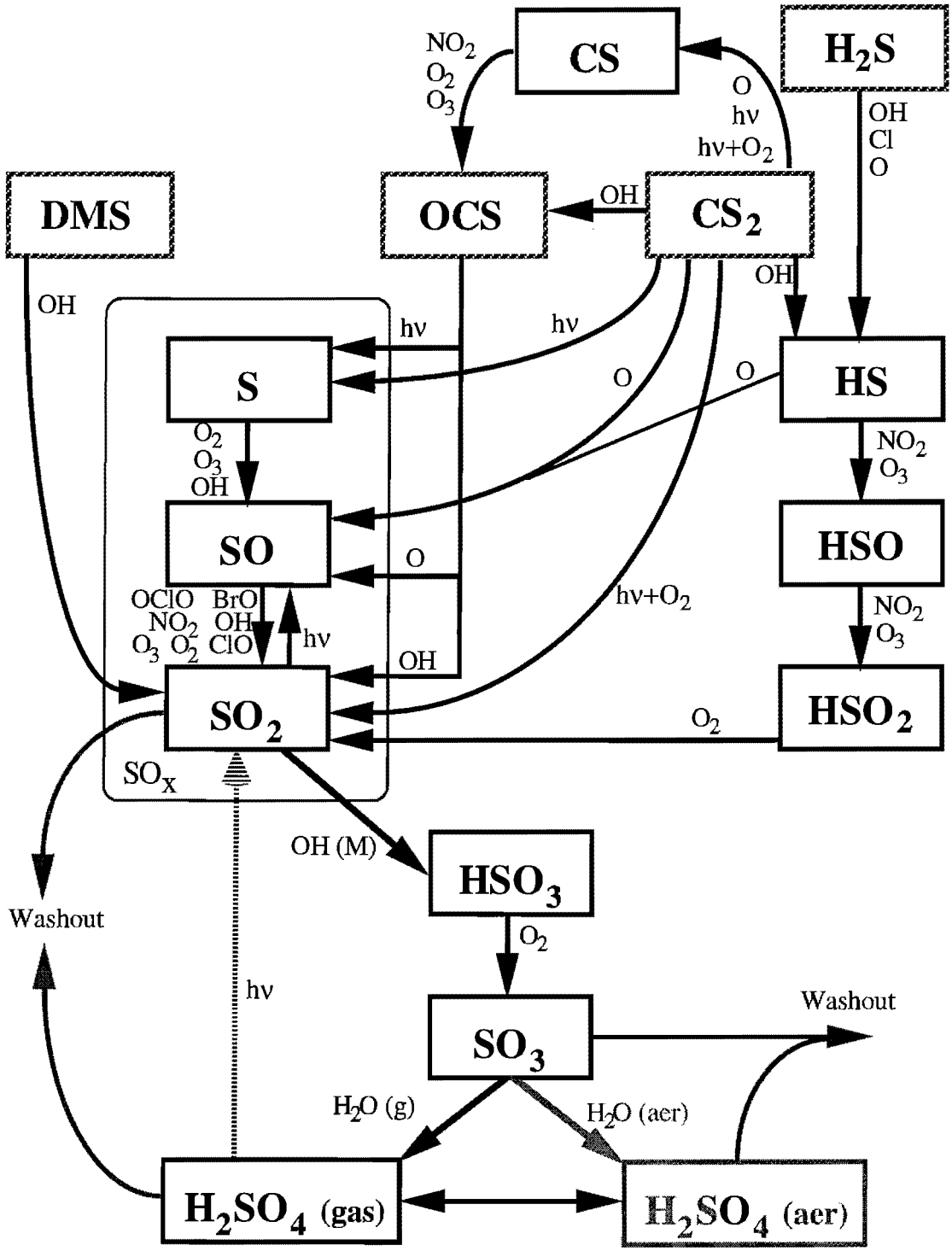

Figure 2-1 Sulfur photochemistry

Table 2.3 Sulfur reactions

a) 2-body reactions

	Reaction	Rate (cm^3/s)	Notes	Source
R1	$OH + OCS \rightarrow products \rightarrow SO_2$	$1.1x10^{-13} \exp(-1200/T)$		1
R2	$O + OCS \rightarrow CO + SO$	$2.1x10^{-11} \exp(-2200/T)$		1
R3	$O + H_2S \rightarrow OH + SH$	$9.2x10^{-12} \exp(-1800/T)$		1
R4	$O + CS_2 \rightarrow CS + SO$	$3.2x10^{-11} \exp(-650/T)$		1
R5	$OH + H_2S \rightarrow SH + H_2O$	$6.0x10^{-12} \exp(-75/T)$		1
R6	$OH + CS_2 \rightarrow OCS + SH$	$\frac{1.25x10^{-16} \exp(4550/T)}{T + 1.81x10^{-3} \exp(3400/T)}$	Valid at 1 atm pressure of air, approximate for troposphere	1,2
R7	$OH + CH_3SCH_3 \rightarrow H_2O + CH_2SCH_3 \rightarrow SO_2$	$1.2x10^{-11} \exp(-260/T)$		1
R8	$OH + S \rightarrow H + SO$	$6.6x10^{-11}$		1
R9	$OH + SO \rightarrow H + SO_2$	$8.6x10^{-11}$		1
R10	$Cl + H_2S \rightarrow HCl + SH$	$5.7x10^{-11}$		1
R11	$ClO + SO \rightarrow Cl + SO_2$	$2.8x10^{-11}$		1
R12	$BrO + SO \rightarrow Br + SO_2$	$5.7x10^{-11}$		1
R13	$S + O_2 \rightarrow SO + O$	$2.3x10^{-12}$		1
R14	$S + O_3 \rightarrow SO + O_2$	$1.2x10^{-11}$		1
R15	$SO + O_2 \rightarrow SO_2 + O$	$2.6x10^{-13} \exp(-2400/T)$		1
R16	$SO + O_3 \rightarrow SO_2 + O_2$	$3.6x10^{-12} \exp(-1100/T)$		1
R17	$SO + NO_2 \rightarrow SO_2 + NO$	$1.4x10^{-11}$		1
R18	$SO + OClO \rightarrow SO_2 + ClO$	$1.9x10^{-12}$		1
R19	$SO_3 + H_2O \rightarrow products \rightarrow H_2SO_4$	$6.0x10^{-15}$		3
R20	$SH + O_3 \rightarrow HSO + O_2$	$9.0x10^{-12} \exp(-280/T)$		1
R21	$SH + NO_2 \rightarrow HSO + NO$	$2.9x10^{-11} \exp(240/T)$		1
R22	$SH + O \rightarrow H + SO$	$1.6x10^{-10}$		3
R23	$HSO + O_3 \rightarrow HSO_2 + O_2$	$1.0x10^{-13}$		1
R24	$HSO + NO_2 \rightarrow HSO_2 + NO$	$9.6x10^{-12}$		1

R25	$HSO_2 + O_2 \rightarrow HO_2 + SO_2$	3.0×10^{-13}	1
R26	$HOSO_2 + O_2 \rightarrow HO_2 + SO_3$	$1.3 \times 10^{-12} \exp(-330/T)$	1
R27	$CS + O_2 \rightarrow OCS + O$	2.9×10^{-19}	1
R28	$CS + O_3 \rightarrow OCS + O_2$	3.0×10^{-16}	1
R29	$CS + NO_2 \rightarrow OCS + NO$	7.6×10^{-17}	1

1. DeMore *et al.* (1994) 2. Hynes *et al.* (1988) 3. DeMore *et al.* (1992)

b) Three-body Reactions

		Low Pressure Limit[a] $k_0(T) = k_0^{300} (T/300)^{-n}$		High Pressure Limit[b] $k_\infty(T) = k_\infty^{300} (T/300)^{-m}$	
	Reaction	k_0^{300}	n	k_∞^{300}	m
T1	$OH + SO_2 \xrightarrow{M} HOSO_2$	(3.0±1.0) (-31)	3.3±1.5	(1.5±0.5) (-12)	$0 \pm {}^{0}_{2}$

Note: $k(Z) = k(M,T) = \left(\frac{k_0(T)[M]}{1 + (k_0(T)[M]/k_\infty(T))} \right) 0.6^{\{1 + [\log_{10}(k_0(T)[M]/k_\infty(T))]^2\}^{-1}}$

The values quoted are suitable for air as the third body, M.

a Units are $cm^6/molecule^2$-sec.

b Units are $cm^3/molecule$-sec.

c) Photolytic Sulfur Reactions

	Reaction	Source
J1	$CS_2 + h\nu \rightarrow S + CS$	Okabe (1978)
J2	$CS_2 + h\nu + O_2 \rightarrow SO_2 + CS$	Wine *et al.* (1981)
J3	$OCS + h\nu \rightarrow CO + S$	Molina *et al.* (1981)
J4	$SO_2 + h\nu \rightarrow SO + O$	Okabe (1978), Yung and DeMore (1982)
J5	$H_2SO_4 + h\nu \rightarrow SO_2$	$J5 = 0.3 \bullet J_{HCl}$, based on Rinsland *et al.* (1995) and recommendations of DeMore *et al.* (1994) for HCl cross-sections

carbonyl sulfide (OCS), carbon disulfide (CS_2), dimethyl sulfide (DMS), and hydrogen sulfide (H_2S). Reduced sulfur compounds are produced naturally by bacteria living near the ocean surface. OCS and CS_2 are also produced anthropogenically. Sulfur dioxide pollution is possibly an additional source of stratospheric sulfur, though SO_2 in the atmosphere may also result from the oxidation of reduced sulfur compounds. Anthropogenic emissions of SO_2, OCS, and CS_2 are the greatest source of sulfur to the atmosphere. Understanding to what extent sulfur from each source reaches the stratosphere is key in assessing the human impacts on the stratosphere. In this section I discuss the importance of surface and volcanic emissions of each of these gases and their oxidation pathways.

Carbonyl Sulfide

It has been suggested that carbonyl sulfide represents the dominant source of sulfur to the stratosphere in the absence of direct volcanic injections (Crutzen, 1976). The most abundant of sulfur-bearing compounds in the troposphere, OCS is produced by biological and volcanic sources, as well as by anthropogenic processes, such as coal burning. Unlike other reduced sulfur compounds, OCS does not react rapidly with OH in the troposphere. Its photochemical lifetime in the troposphere is greater than 60 years, allowing it to enter the stratosphere without significant reactive loss.

This long lifetime also means that OCS is nearly uniformly distributed throughout the troposphere, where it is observed to have a mixing ratio near 500 pptv (Sandalls and Penkett, 1977; Maroulis *et al.*, 1978; Torres *et al.*, 1980). Bandy *et al.* (1992b) concluded from a time series of OCS measurements in the Northern Hemisphere that there is no trend in OCS mixing ratio, and calculated a mean measured value of 512 pptv. The model sets a boundary condition of 510 pptv of OCS at the lowest altitude. Once it reaches the stratosphere, OCS is decomposed chiefly by

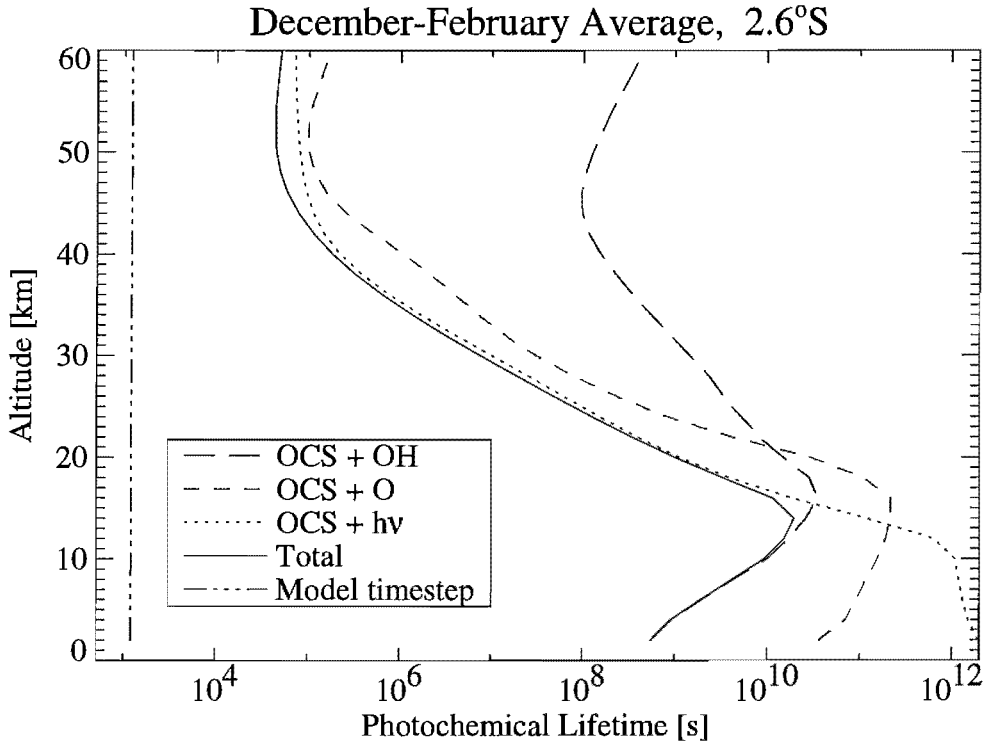

Figure 2-2 Timescale for OCS loss due to reaction with OH, reaction with O, and photolysis, and total OCS lifetime calculated in the model. The model's 1 hour timestep for OCS chemistry is also indicated.

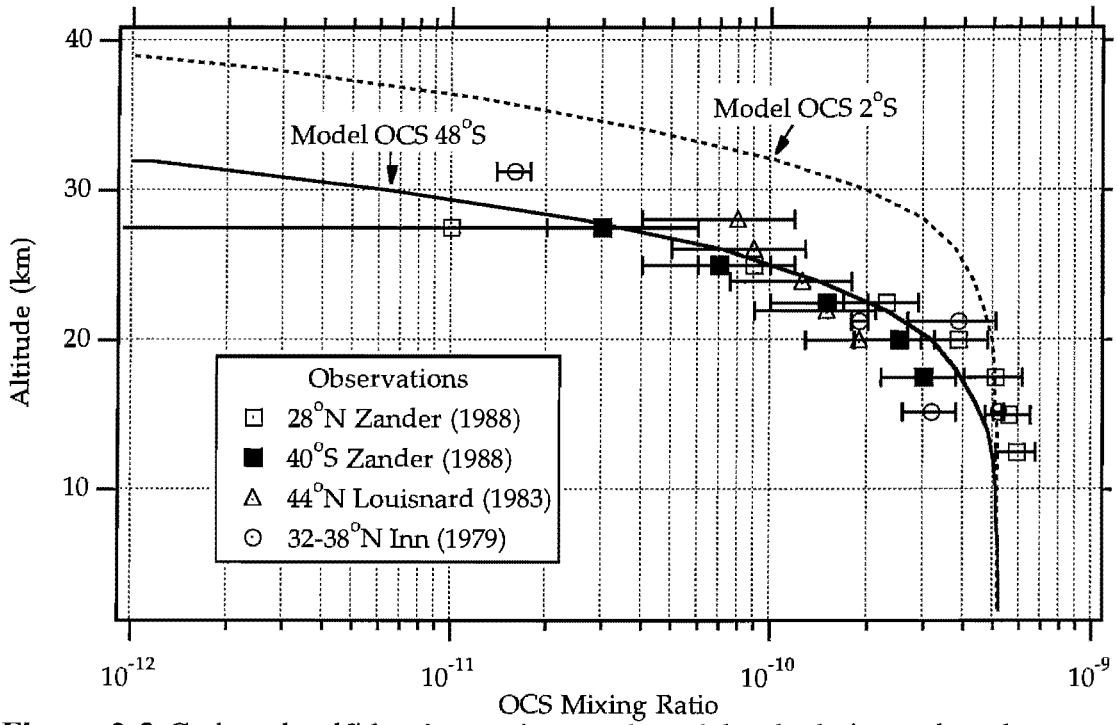

Figure 2-3 Carbonyl sulfide observations and model calculations plotted versus altitude. Model calculations are for day 240 (September 1).

ultraviolet light, with additional loss to OH and O (Molina *et al.*, 1981; DeMore *et al.*, 1994). Figure 2-2 shows the lifetimes for each of these processes as calculated in the model. The calculated vertical profiles of OCS in the stratosphere and troposphere compare well to mid-latitude observations, shown in figure 2-3 (Inn *et al.*, 1979; Louisnard *et al.*, 1983; Zander *et al.*, 1988). In the tropics, the model calculates that higher altitudes are required for dissociation of OCS. The two-dimensional nature of this model shows clearly that OCS can provide little active sulfur to the tropics below 25 km.

Sulfur Dioxide Pollution

Other than carbonyl sulfide, a number of significant nonvolcanic sources of atmospheric sulfur are known, all of which oxidize in the troposphere. Sulfur dioxide is an anthropogenic pollutant produced directly by coal burning, petroleum burning, processing of non-ferrous ores, and possibly biomass burning (Möhler and Arnold, 1992) These emissions have been estimated to account for between 10 and 45 percent of the total sulfur involved in the atmospheric balance, indicating the large uncertainty associated with the global sulfur cycle (Seinfeld, 1986, p. 9-11). The extent to which this pollution reaches the upper troposphere is uncertain and appears to be highly variable and dependent on meteorological factors. Many vertical profiles obtained by aircraft measurements over continental land masses show SO_2 decreasing in the boundary layer, due to reaction with radicals such as OH and oxidation in clouds, and reaching altitude-independent mixing ratios of 40 to 90 pptv in the middle and upper troposphere (Warneck, 1988, p.523-524). Other observations show steady or sharp increases in SO_2 mixing ratios from the boundary layer to continentally derived air in the free troposphere (Maroulis *et al.*, 1980; Andreae *et al.*, 1988) Maroulis *et al.* (1980) also report that average mixing ratios in the free troposphere are 35% higher in the Northern Hemisphere than the Southern Hemisphere, and nearly twice as high over

continents as oceans. Both of these increases indicate entrainment of anthropogenic SO_2 emissions in the free troposphere. Sulfur from aircraft exhaust has also been suggested as an SO_2 source to the free troposphere (Hofmann, 1995).

Reduced Sulfur Compounds and Sulfur Dioxide in the Free Troposphere

Maroulis *et al.* also reported that in remote ocean areas, SO_2 increases in the free troposphere relative to the boundary layer, suggesting additional sources of SO_2 there. Oceanic measurements showed a 60% increase from the boundary layer to the free troposphere, while continental measurements showed a 40% increase. The observations suggested that mixing ratios of 30 to 150 pptv were typical even in remote ocean regions. More recent measurements in air thought to be unperturbed by continental influences confirm SO_2 increases in the free troposphere relative to the boundary layer, with mixing ratios between 40 and 50 pptv (Berresheim *et al.*, 1990). While Maroulis *et al.* tried to explain the SO_2 increase as resulting from OCS oxidation by OH, later revision of this rate coefficient made clear that carbonyl sulfide does not dissociate in the troposphere to any significant extent. This left the need for an additional source of SO_2 in the mid-troposphere (Rodhe and Isaksen, 1980).

Determination of sources of the observed SO_2 in the free troposphere is of direct interest to stratospheric aerosol studies. Golombek and Prinn (1993) used the Maroulis data and those of Jaeschke *et al.* (1976) as input to a stratospheric aerosol model and found that sulfur originating in the troposphere as SO_2 may be the primary source of stratospheric aerosol below 20 km. SO_2 is somewhat stable in the free troposphere, where its loss to OH is slow (20 to 100 days) and removal from deposition is reduced compared to the boundary layer. Free tropospheric SO_2 is therefore somewhat well-mixed, providing a source of sulfuric acid (H_2SO_4) throughout the troposphere. Particle measurements indicate that gas-to-particle nucleation of sulfuric acid and water in the tropical upper troposphere may be the

source of much of the stratospheric aerosol (Brock *et al.*, 1995). Further, SO_2 observations near the tropopause indicate that sulfur present as SO_2 in the troposphere may dominate the stratospheric sulfur budget (Möhler and Arnold, 1992).

Chatfield and Crutzen (1984) explained the SO_2 observations of Maroulis and others as resulting from oxidation of reduced sulfur compounds that are transported to the mid-troposphere in strong updraft regions of the tropics. Using a model of deep convection in clouds, Chatfield and Crutzen studied reduced sulfur compounds with such varied lifetimes as those listed in table 2.4. They pointed out that eddy diffusion is not an adequate parameterization for tropospheric transport of compounds with vertically varying lifetimes, such as SO_2. Hence earlier models, such as that of Rodhe and Isaksen (1980), had been unable to transport reduced sulfur compounds to the free troposphere rapidly enough to account for apparent SO_2 production there. In Chatfield and Crutzen's model, convective clouds in the tropics could transport compounds so rapidly, albeit intermittently, that even short-lived reduced sulfur compounds could contribute to SO_2 in the upper troposphere. The same mechanism could pump SO_2 originating at the ground or in the boundary layer. The model of Costen *et al.* (1988) extended the possible importance of cloud pumping to extratropical marine regions.

Table 2.4 Reduced sulfur compounds and tropospheric lifetimes considered by Chatfield and Crutzen (1984)

Compound Name	Chemical Formula	Tropospheric Lifetime
carbonyl sulfide	OCS	months, years
carbon disulfide	CS_2	2-6 days
hydrogen sulfide	H_2S	2 days
dimethyl sulfide	$(CH_3)_2S$	8 hours to 2 days
methyl mercaptan or methane thiol	CH_3SH	2 hours
dimethyl disulfide	CH_3SSCH_3	15 minutes

This prediction was supported by the DMS and SO_2 observations of Berresheim *et al.* (1990).

The extent to which SO_2 mixing ratios in the free troposphere are influenced by reduced sulfur compounds is a continuing matter of uncertainty and some dispute. Chatfield and Crutzen concluded that dimethyl sulfide plays the major role in SO_2 production in the remote marine troposphere. Thornton *et al.* (1996), however, calculate that DMS could account for at most 18 pptv of SO_2, assuming all DMS is converted to SO_2. Further, the measurements of Bandy *et al.* (1992a) suggest that the yield of SO_2 from DMS must be low. Thornton *et al.* (1996) propose instead that high levels of SO_2 in the remote marine troposphere result from long-range transport of continental pollution.

With little certainty as to the sources, I rely on the observed variation between 10 and 150 pptv to bracket the model's SO_2 boundary conditions in the troposphere (Chatfield and Crutzen, 1984; Pham *et al.*, 1995). The absence of a simulation of tropospheric phenomena such as cloud pumping in the present model precludes a realistic treatment of reduced sulfur compounds. I therefore assume that, to the extent to which they may influence SO_2 in the free troposphere, reduced sulfur compounds have been fully oxidized by the time they reach the model's lower boundary.

While CS_2 is expected to be a small source of SO_2, it is significant as the only atmospheric precursor of OCS. Photooxidation, as described in Wine *et al.* (1981), is expected to dominate CS_2 destruction in the troposphere, although reaction with OH is competitive. Anthropogenic emissions are responsible for about 60%, and oceans for about 40%, of the CS_2 in the atmosphere. Measurements are scarce and highly variable, indicating 20 to 150 pptv typical of industrial regions, and 5 to 25 pptv over oceans (Chatfield and Crutzen, 1984; Tucker *et al.*, 1985; Pham *et al.*, 1995, and sources therein). These measurements indicate that CS_2 likely has a minor effect on tropospheric mixing ratios of OCS and SO_2.

Oxidation

Mechanisms by which SO_2 oxidizes to gas-phase sulfuric acid are relatively well-known. As shown in figure 2-1, some reduced sulfur compounds oxidize to produce atomic sulfur (S) and sulfur monoxide (SO) in addition to SO_2. These species may be considered equivalent to SO_2, as they react with O_2 to form SO_2 on the order of a second or less. In the stratosphere SO_2 photodissociates to SO on a timescale of a day to a month, providing a small interchange between these two species. Oxidation of SO_2 proceeds by reaction with OH, producing HSO_3. As is suggested by measurements of SO_2 in the free troposphere, this reaction is slow. The model calculates lifetimes on the order of months for SO_2 oxidation throughout the stratosphere and free troposphere.

Once oxidation of SO_2 occurs, the resultant HSO_3 reacts quickly with O_2 to form SO_3. SO_3 is known to react with H_2O in the gas phase to form H_2SO_4, though the mechanism is uncertain, and only an upper limit for this reaction is given in current recommendations (DeMore *et al.*, 1994). I use this upper limit as the reaction rate in the model in order to produce gas-phase H_2SO_4. In the moist troposphere this reaction is known to be rapid, and formation of SO_3 is considered equivalent to formation of H_2SO_4 (Seinfeld, 1986, p. 164). The model calculates this reaction to occur rapidly (τ<1 second) in the drier stratosphere as well. Recent measurements suggest that SO_3 oxidation may proceed by reaction with the water dimer (Kolb *et al.*, 1994). Rinsland *et al.* (1995) calculate that this mechanism would proceed on a timescale of 1 hour at 20 km and 60 days at 40 km. In the bulk of the aerosol layer, however, SO_3 is more likely to condense on existing liquid particles and react with water in them to produce sulfate. Condensation will be discussed in greater detail in the next chapter.

Atmospheric sulfur oxidation is complete with the formation of gas-phase sulfuric acid, which plays a key role in the formation and evolution of stratospheric aerosol. The dominant loss mechanisms for gas-phase H_2SO_4 in the stratosphere are

nucleation of new particles and condensation on existing particles. In the troposphere, H_2SO_4 is scavenged and removed by rainout as is discussed in the next section. In the upper stratosphere, where liquid aerosol evaporates, photolysis of gas-phase H_2SO_4 is thought to occur. Photolysis cross sections have not been measured successfully, however. Rinsland *et al.* (1995) inferred H_2SO_4 photolysis rates by comparing model calculations to upper stratosphere profile observations of SO_2 retrieved from the space shuttle. The model in that study assumed H_2SO_4 photolysis cross sections proportional to those of HCl. The model was found to best fit the observations with H_2SO_4 photolysis rates set at 0.3 times those calculated for HCl. Model calculations without H_2SO_4 photolysis compared poorly to the SO_2 observations. The Garcia-Solomon model calculates HCl photolysis rates based on cross sections recommended in DeMore *et al.* (1994). Calculations in this study include H_2SO_4 photolysis at 0.3 times the HCl rate, except for cases described otherwise.

Rainout

Tropospheric rainout is an important process for the ultimate removal of chemical species from the atmosphere. The timescale on which rain removes species is not well known. Clearly, rainout is fast enough to remove highly soluble species from the troposphere before they enter the stratosphere. For such highly soluble species as HCl, H_2SO_4, and SO_3 , the model sets an arbitrary 4-day lifetime for rainout in the troposphere. Such an estimate is fast enough to remove soluble species in the troposphere, and is therefore adequate for study of stratospheric chemistry.

SO_2, however, has an intermediate solubility and may be only partially removed by rainout. Large volcanic eruptions produce large quantities of both SO_2 and HCl. While SO_2 clearly enters the stratosphere, where it causes great enhancements in sulfate aerosol, essentially all of the volcanic HCl is removed by rain in the volcanic cloud as it rapidly rises through the troposphere. SO_2 does oxidize to some extent in clouds,

however, and is removed from the troposphere as acid rain. Pham *et al.* (1995) report that in-cloud oxidation accounts for 90% of total chemical sinks for SO_2 in the troposphere. Many of these chemical aqueous processes are poorly understood, and the development of an interactive cloud and precipitation code necessary to account for the variable nature of SO_2 rainout removal is outside the scope of this study. Our purposes are best served by a simple rainout parameterization. Warneck (1988, p. 398) calculates a residence time of 40 days for in-cloud scavenging of SO_2. Results shown in future chapters rely on fixed concentrations of SO_2 in the troposphere, corresponding to observations. The model thus avoid uncertainties in rainout rates and the more detailed sulfur chemistry of the troposphere.

Calculated Sulfur Profiles

Figure 2-4 shows altitude profiles of major sulfur-bearing species at mid-latitudes on day 240 (September 1) for a typical scenario. Model cases A and B include 200 and 400 pptv, respectively, of SO_2 throughout the troposphere. The SO_2 measurements of Möhler and Arnold (1992), which penetrated the stratosphere by several kilometers, indicate a much sharper drop in mixing ratio above the tropopause than the model calculates at mid-latitudes. These measurements, however, were made in northern Scandinavia. A calculated polar profile, shown in figure 2-4, indicates a somewhat better comparison to these observations.

Between 20 and 30 km SO_2 mixing ratios increase in the tropics and mid-latitudes due to production by OCS oxidation. Above 25 km, SO_2 mixing ratios are largely insensitive to variation in tropospheric mixing ratio, as OCS becomes the dominant source. Above the top of the liquid sulfate layer (35 to 40 km) SO_2 profiles are sensitive to sulfuric acid photolysis rates. The two case profiles presented in figure 2-4 represent no H_2SO_4 photolysis, and photolysis rates equal to 0.3 times photolysis

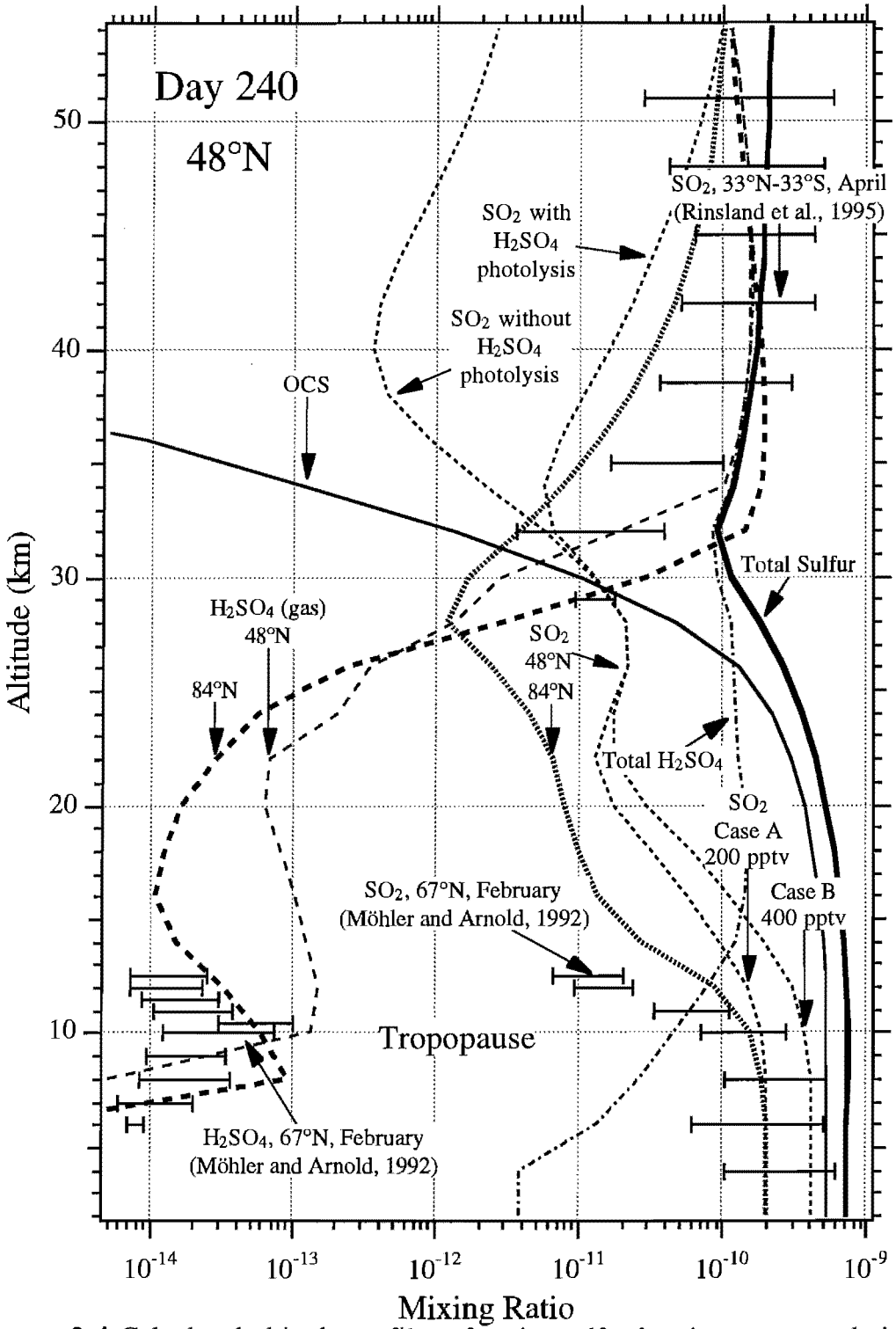

Figure 2-4 Calculated altitude profiles of major sulfur-bearing compounds in the stratosphere at 48°N on day 240 (September 1).

rates for HCl. Observations presented in Rinsland *et al.* (1995) show tropical and mid-latitude SO_2 increasing from ~10 pptv at 30 km to ~100 pptv at 50 km. Consistent with calculations presented in that paper, our model best fits this data with H_2SO_4 photolysis included.

Total H_2SO_4 is partitioned between gas-phase sulfuric acid and liquid sulfate. Vertical profiles of calculated gas-phase sulfuric acid in polar regions compare well to the observations of Möhler and Arnold (1992) near the tropopause at 67°N. As with SO_2, our model indicates variation in gas-phase sulfuric acid with latitude and season, presenting a significant advantage over one-dimensional models.

Total sulfur in figure 2-4 is seen to vary with altitude suggesting that sulfur is not conserved in the stratosphere. As is discussed in Chapter 3, sulfate is lost by sedimentation of liquid aerosol. In Chapter 4 I show that rates of removal from the stratosphere by sedimentation are sensitive to the details of particle size distributions and the mass of sulfate present.

Chapter 3

Aerosol Microphysics

Sulfuric acid formed by gas-phase sulfur oxidation provides the source of new particles in the stratosphere. Throughout most of the stratosphere, the composition of these particles is dominated by sulfate ($SO_4^=$), formed by the solution of sulfuric acid in water. Particles grow, shrink, and move due to interactions with atmospheric gases and with each other. Microphysical processes affecting particle size distributions are calculated in the model interactively with chemistry and dynamics. These processes are nucleation; condensation and evaporation of H_2SO_4, H_2O, and HNO_3; uptake of SO_3; coagulation; transport; sedimentation; and tropospheric deposition (rainout).

Particles in the model are distributed amongst 45 size bins, which are treated similarly to individual chemical species. The size bins are spaced geometrically, each bin containing twice the number of sulfate molecules (hence volume) as the previous bin. This scheme allows coverage of 13 orders of magnitude in particle volume, or 4 orders of magnitude in particle radius.

The model calculates total sulfuric acid (vapor plus sulfate) from the balance among chemical production, loss due to rainout, and change due to transport. Nucleation, condensation, and evaporation affect the partitioning of this total between gas and aerosol phases. The model solves the following two finite difference equations for total and gas-phase sulfuric acid mixing ratios:

$$\frac{[H_2SO_4]_{t+\Delta t}^{gas+liq} - [H_2SO_4]_t^{gas+liq}}{\Delta t} = \underset{production}{k_{19}[SO_3][H_2O]} + \qquad 3.1$$

$$T_{gas+liq} - \sum_{i=1}^{45} C_i^{SO_3} n_i - \lambda^g [H_2SO_4]_t^{gas} - \lambda^{liq} [H_2SO_4]_t^{liq}$$

transport SO_3 *condensation* *deposition*

$$\frac{[H_2SO_4]_{t+\Delta t}^{gas} - [H_2SO_4]_t^{gas}}{\Delta t} = \underset{production}{k_{19}[SO_3][H_2O]} + \qquad 3.2$$

$$T_{gas} - J \cdot Na_{crit} - \sum_{i=1}^{45} C_i^{H_2SO_4} n_i - \sum_{i=1}^{45} C_i^{SO_3} n_i - \lambda^g [H_2SO_4]_t^{gas}$$

transport *nucleation* *acid condensation, evaporation* SO_3 *condensation* *deposition*

where J (particles/cm^3/s) is the nucleation rate, Na_{crit} is the average number of acid molecules in newly nucleated particles, $C_i^{H_2SO_4}$ and $C_i^{SO_3}$ (molecules/s) are the fluxes of acid and SO_3 molecules to a particle in size bin i, n_i (particles/cm^3) is the population of size bin i, and λ^g and λ^{liq} (/s) are parameterized rainout rates for sulfuric acid gas and aerosol, respectively, in the troposphere. Each of these parameters is discussed in further detail in subsequent sections.

Equations 3.1 and 3.2 allow the model to time-integrate concentrations of total and gas-phase sulfuric acid. The difference between these two quantities is the total concentration of sulfate in aerosol, which the model partitions amongst the 45 particle size bins. Particle size distributions evolve over time due to nucleation, condensation, evaporation, coagulation, and particle transport, as is discussed in the subsequent sections. The model calculates this evolution by time-integrating the effects of each of these processes on existing particle size distributions.

3.1 Nucleation

Pure gases of sulfuric acid or water will not nucleate to form liquid particles at stratospheric temperatures and pressures. When both gases are present, however, nucleation theory does favor the formation of binary solutions of sulfuric acid and water at cold stratospheric temperatures. New particles may form by heterogeneous nucleation on involatile nuclei (transported from the ground or produced by meteoric ablation), or in their absence by direct gas-to-particle conversion. Such homogeneous nucleation has been suggested as an important mechanism in the production of sulfate particles in the upper tropopause and in the polar winter stratosphere (Hamill *et al.*, 1990).

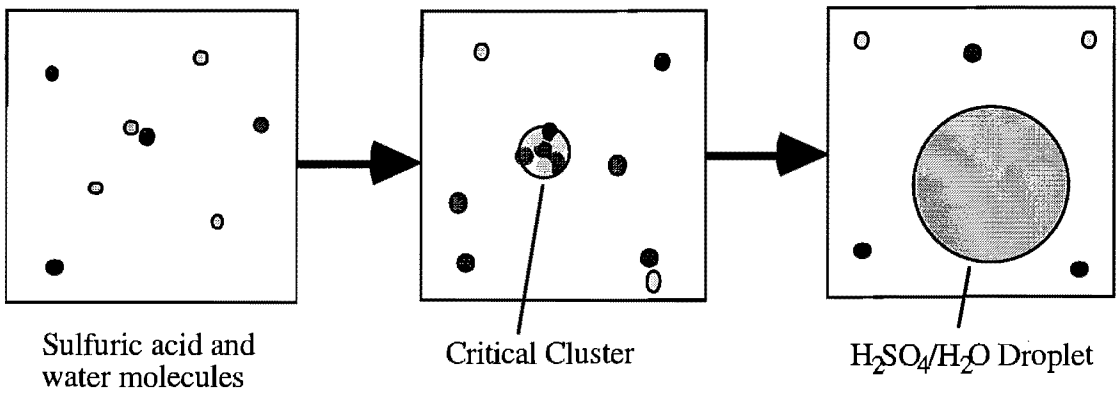

Figure 3-1 Formation of new particles by binary homogeneous nucleation of sulfuric acid and water.

An estimation of the formation rates of new particles by either homogeneous or heterogeneous nucleation is possible via classical binary nucleation theory. This theory rests on a number of speculative assumptions and extrapolations, but is useful in predicting where nucleation is favored in the atmosphere. The calculation for heterogeneous nucleation is proportional to that for homogeneous nucleation, leading to a result that both processes are favored under the same conditions. It is therefore reasonable to disregard heterogeneous nucleation in the present model, thus avoiding speculation as to sources, evolution, and size distributions of involatile nuclei.

Under most stratospheric conditions, very small clusters of sulfuric acid and water molecules are energetically favored to fall apart. The energy required to form these small clusters, ΔG, generally increases with their size. Under some conditions, however, there exists some critical size greater than which this Gibbs free energy of formation actually decreases with further additions. When clusters larger than this critical size are able to form, further growth is favored, and nucleation has occurred.

Calculation of nucleation rates requires determination of the critical Gibbs free energy, ΔG^*, for formation of the critical stable liquid nucleus. Previous efforts determined ΔG^* by calculating formation energies for many clusters, varying the number of sulfuric acid and water molecules to determine the critical value (Heist and Reiss, 1974). A significant computational reduction is achieved, however, by employing a change of variables, to composition (weight percent H_2SO_4) and particle radius. This method, developed by Zhao (1993), gives a straightforward, non-iterative solution for nucleation rates.

The model calculates nucleation rates at each gridpoint for which ambient sulfuric acid vapor pressure exceeds the equilibrium vapor pressure. Calculation of nucleation rates by this method begins with determination of the acid composition, ω^*, of the critical nucleus. The work of Zhao showed that this value may be obtained numerically as the root to the following equation:

$$\ln\left(\frac{p_{H_2O}}{p^o_{H_2O}}\right)\cdot\left[1+\frac{d\ln\rho}{d\omega}\omega^*\right]-\frac{M_{H_2O}}{M_{H_2SO_4}}\ln\left(\frac{p_{H_2SO_4}}{p^o_{H_2SO_4}}\right)\cdot\left[1+\frac{d\ln\rho}{d\omega}\omega^*\right]=0 \qquad 3.3$$

where ω is the weight fraction sulfuric acid of the embryo, ρ [g/cm^3] is its density, p_{H_2O} and $p_{H_2SO_4}$ are the ambient partial pressure of water and sulfuric acid, $p^o_{H_2O}$ and $p^o_{H_2SO_4}$ are the equilibrium vapor pressures over the cluster, and M_{H_2O} and $M_{H_2SO_4}$ are molecular weights. The critical radius, r^*, and Gibbs free energy, ΔG^*,

are then calculable given the surface tension, σ, at the critical composition and ambient temperature:

$$r^* = \frac{2\sigma\left(\omega^*, T\right)}{Y\left(\omega^*, T, p_{H_2O}, p_{H_2SO_4}\right)} \tag{3.4}$$

$$\Delta G^* = \frac{4}{3}\pi r^{*2}\sigma\left(\omega^*, T\right) \tag{3.5}$$

$$J = J_o e^{-\Delta G^*/k_B T} \tag{3.6}$$

where Y is a mathematical function, T is temperature, and J is the calculated nucleation rate. The pre-exponential factor, J_0, defined thus (Jaecker-Voirol and Mirabel, 1988):

$$J_o = \beta_{H_2SO_4} A^* N_{H_2O} \frac{Z}{\sin^2 \phi} \tag{3.7}$$

where $\beta_{H_2SO_4}$ (/cm^{2}s) is the impingement rate of sulfuric acid molecules, A^* (cm^2) is the surface area of the critical nucleus, N_{H_2O} (/cm^3) is water vapor density, Z is a non-equilibrium factor set to 0.25, and ϕ is the angle of particle growth in the coordinate system of acid molecules vs. water molecules. Previous nucleation calculations (Hamill *et al.*, 1977a; 1982; 1990; Zhao and Turco, 1995), appear to have neglected these latter two factors, altering calculated nucleation rates by an order of magnitude or more.

Confidence in the calculated nucleation rates rests on the soundness of the underlying theory and the certainty of a number of measured physical properties that enter the resulting calculation. One such property critical to the calculation is the surface tension of sulfuric acid/water solutions. Nucleation rates vary exponentially with the calculated critical Gibbs free energy, which varies as the cube of the critical surface tension. However, no measurements exist in the literature for surface tensions of sulfuric acid/water solutions at stratospheric temperatures. My calculations rely on extrapolations of the measurements of Sabinina and Turpugow (1935) at 10 to 50°C. It

is not clear, however, that macrophysical properties such as surface tension are applicable to small clusters of molecules such as those involved in nucleation in the atmosphere. Equilibrium vapor pressures of water and sulfuric acid, and measured densities of sulfuric acid/water solutions are other measured properties that enter the nucleation calculation. I have developed parameterizations for the measured and calculated values of each of these properties, and tested the sensitivity of calculated nucleation rates to uncertainties therein.

Surface Tension

Figure 3-2 shows the surface tension data points from Sabinina and Turpugow at 10 to 50°C. Some previous nucleation models (Zhao, 1993) have relied on a 4th-order polynomial fit to this data developed by Hamill *et al.* (1982) Unfortunately, such high-order fits do not perform well on extrapolations. Figure 3-2 shows the

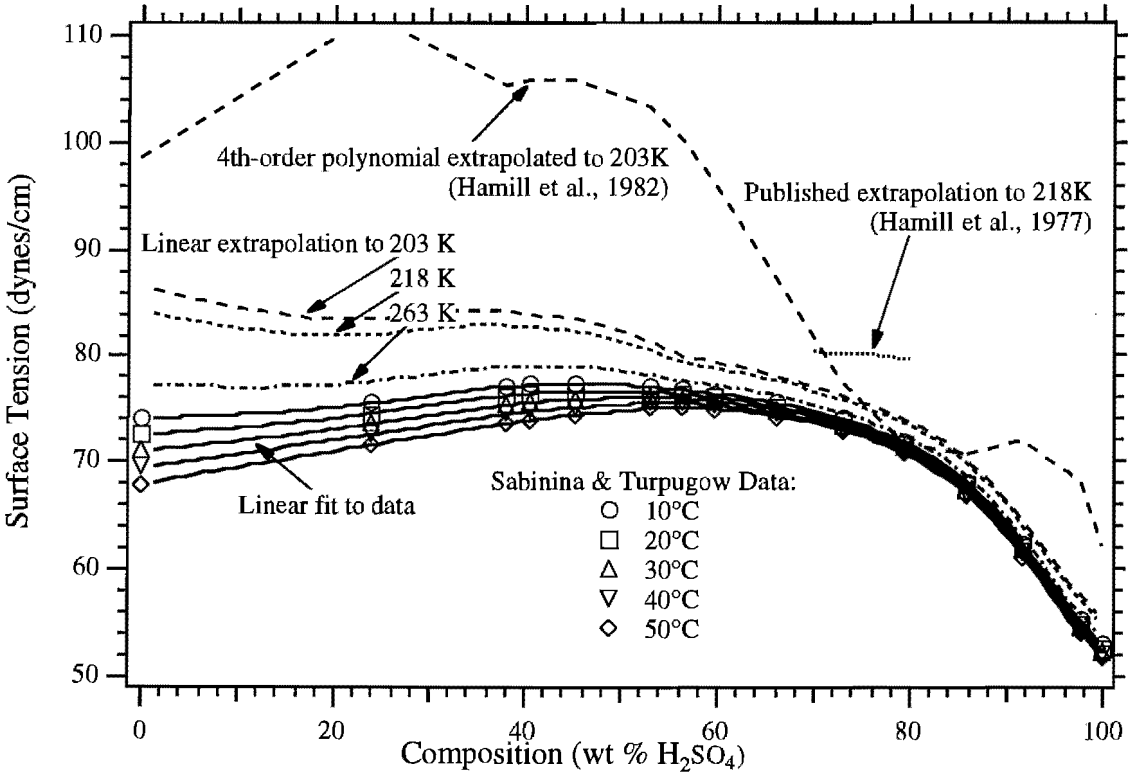

Figure 3-2 The surface tension measurements of Sabinina and Turpugow (1935), and various extrapolations to stratospheric temperatures.

extrapolation of this parameterization to 203K. A simple linear fit seems more reasonable for extrapolation purposes. The nucleation calculation of Hamill *et al.* (1977) relies on an extrapolation for surface tension at 218K that is also in strong disagreement with the linear extrapolation in the published range (see Figure 3-2). Given these discrepancies I have tested the sensitivity of calculated nucleation rates to surface tension parameterizations.

Figure 3-3 shows calculated nucleation rates varying only surface tension among three parameterizations. Rates are shown over the range of stratospheric conditions in the model: temperatures vary from 180 to 260K and ambient water vapor concentrations between 10^{11} and 10^{16} molecules/cm^3. Sulfuric acid vapor

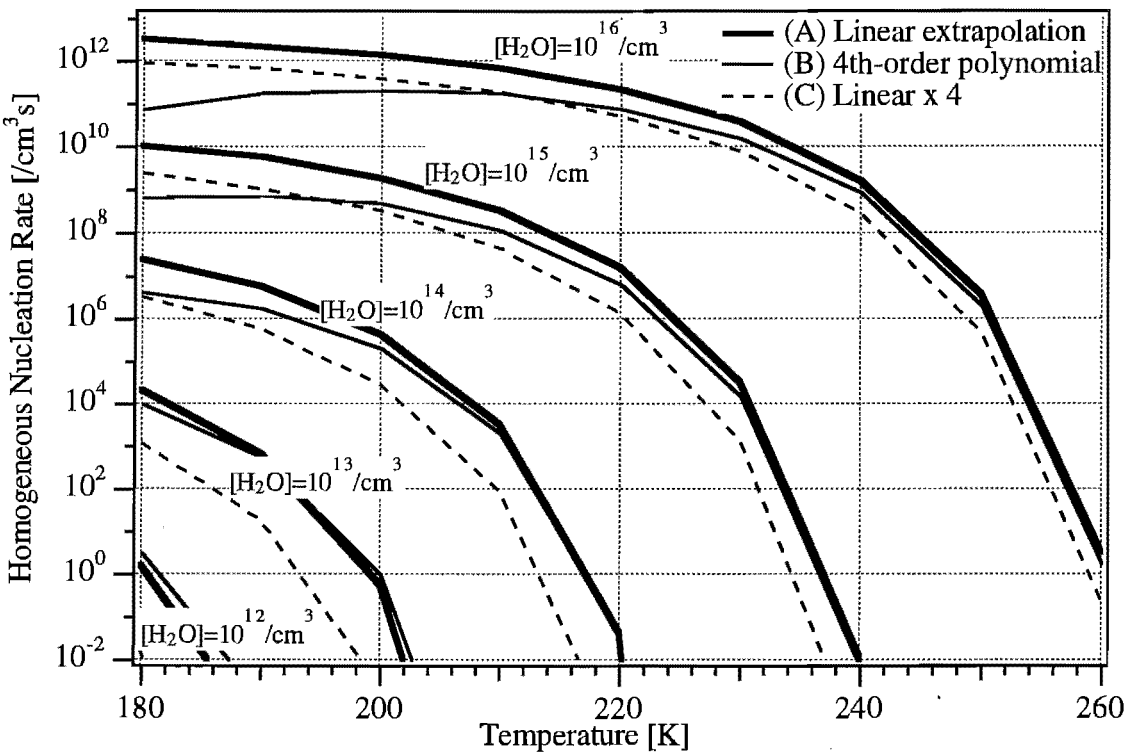

Figure 3-3 Sensitivity of calculated nucleation rates to parameterized surface tension. Nucleation rates are calculated using (case A, thick solid lines) a linear extrapolation of surface area to temperature, (case B, thin solid lines) the 4th-order polynomial fit of Hamill *et al.* (1982), and (case C, dashed lines) a linear extrapolation with four times the sensitivity to temperature as case A. Case C approximates to the parameterization of Hamill *et al.* (1977). Sulfuric acid concentrations were set equal to 10^{-8} times water vapor concentrations for these calculations.

concentrations are set at eight orders of magnitude less than water vapor, in rough accord with most of the modeled stratosphere. The three surface tension parameterizations are: (A) the model's linear extrapolation (thick solid lines), (B) the 4th-order polynomial extrapolation (thin solid lines), and (C) a parameterization extrapolated linearly with four times the sensitivity of case A, to approximate the extrapolation of (Hamill *et al.*, 1977b).

At temperatures above 190K the nucleation discrepancies between case A and case B are of an order of magnitude or less. These variations are small compared to the variations of nucleation rates with temperature. The temperature at which nucleation becomes significant ($J > 1.0$ /cm^{3}s) is the same in both cases. This resiliency reflects the fact that the composition of critical nuclei resulting from homogeneous nucleation is generally between 65 and 90 weight percent acid. In this range of composition, the 4th-order polynomial extrapolation approximates well the linear extrapolation. Discrepancies increase, however, at very low temperatures, where nucleation rates in case B begin to decrease with decreasing temperature.

Case C (dashed lines in Figure 3-3) approximates the published extrapolation of Hamill *et al.* (1977). At most temperatures and vapor pressures, the case C nucleation rates are reduced from the case A rates by an order of magnitude or more. The temperature at which nucleation becomes significant is reduced by 1 to 3 degrees in case C. Nucleation rates diverge from case A to a greater extent in case C than case B, at most stratospheric temperatures. This demonstrates the importance of surface tension data in the 65 to 90 weight percent range, which is the only range where case B approximates case A.

While the sensitivity of calculated nucleation rates to these extrapolations of the Sabinina and Turpugow data is small relative to the sensitivity to temperature, these results argue for further measurements of surface tension of H_2SO_4/H_2O solutions at stratospheric temperatures. Other measurements presented in Timmermans (1960)

predate and show some disagreement with Sabinina and Turpugow. No data is found in the literature for temperatures below 0°C. More recent data at lower temperatures would lend confidence to calculated nucleation rates. The model incorporates the case A parameterization: a linear extrapolation of the Sabinina and Turpugow data in temperature, with linear interpolation in composition.

Density

The model's nucleation calculations rely on temperature extrapolations of measurements of H_2SO_4/H_2O solution densities made at 0 to 100°C, tabulated in the International Critical Tables (NRC, 1928). Recent measurements have confirmed that these data may be linearly extrapolated to stratospheric temperatures with excellent accuracy (Beyer *et al.*, 1995). Previous workers have relied on a 5th-order polynomial extrapolation in temperature (Hamill *et al.*, 1982; Zhao, 1993). I have calculated nucleation rates using both linear and 5th-order polynomial extrapolation. The extreme linearity of the original data is such that the polynomial only departs significantly from linearity at extremely dilute or extremely concentrated solutions. Since calculated nucleation rates depend on the properties of 60 to 90 weight percent acid solutions, the discrepancy in resulting nucleation rates is insignificant. Our model incorporates a linear extrapolation of the ICT density measurements in temperature, with linear interpolation in composition.

Equilibrium Vapor Pressures

Several authors have investigated the equilibrium vapor pressures of water and sulfuric acid over solutions. The values used most often for water are those calculated by Gmitro and Vermeulen (1964) from thermodynamic properties reported by Giauque *et al.* (1960). Recently Zhang *et al.* (1993) measured equilibrium water vapor pressures between 190 and 240K and reported poor agreement with the Gmitro and Vermeulen calculations. Nucleation rates calculated using parameterizations based on

these two works are contrasted in Figure 3-4. Zhang's refinement is seen to have little relative effect where nucleation is most important (at high nucleation rates). However, nucleation will remain significant at temperatures 2 to 4 degrees higher under the Gmitro and Vermeulen parameterization. Our model makes use of Zhang's parameterization based on his measurements for water equilibrium vapor pressure.

Gmitro and Vermeulen also report calculations of sulfuric acid equilibrium vapor pressures over solutions. Roedel (1979), however, was the first to measure sulfuric acid vapor pressure at room temperature. His measurement suggested a correction factor of 0.086 to the Gmitro and Vermeulen values. Roedel also discussed the dependence of the nucleation rate on sulfuric acid vapor pressure. Ayers *et al.*

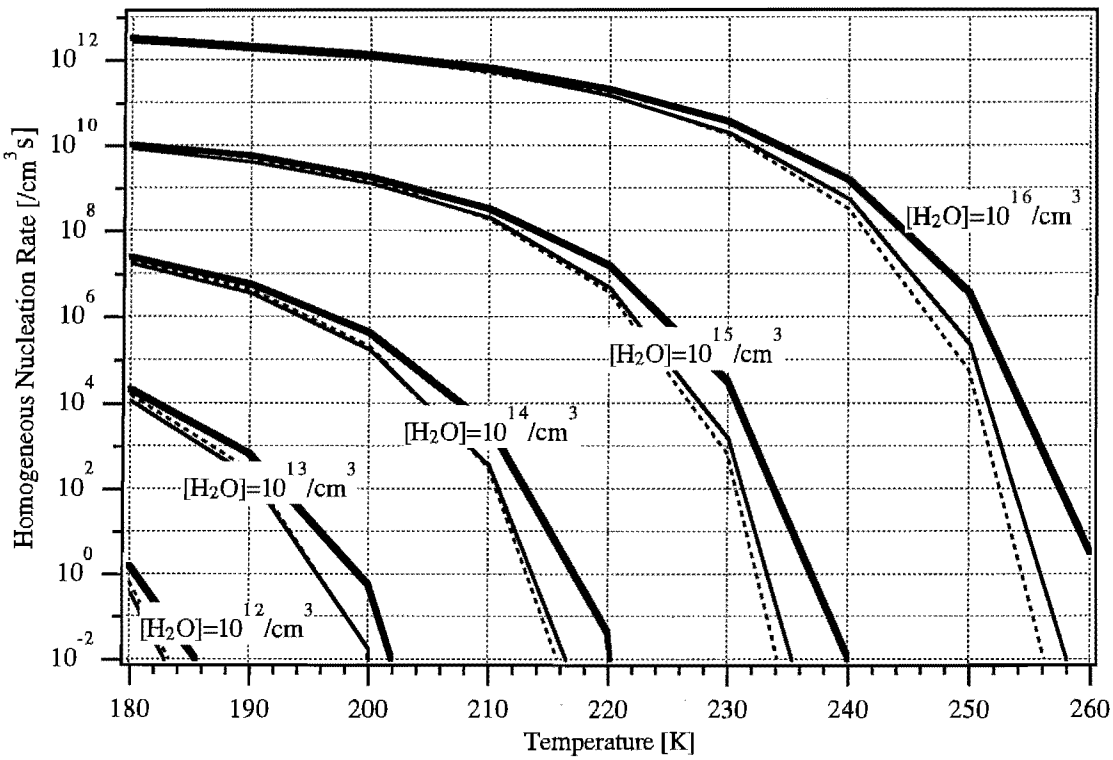

Figure 3-4 Sensitivity of calculated nucleation rates to water and sulfuric acid vapor pressures. The thick solid lines use the Gmitro and Vermeulen (1964) parameterization for water vapor pressure, and the Ayers *et al.* (1980) parameterization for sulfuric acid vapor pressure. The thin solid lines use the Zhang *et al.* (1993) parameterization for water vapor pressure, and the Ayers *et al.* (1980) parameterization for sulfuric acid vapor pressure. The dashed lines use the Gmitro and Vermeulen (1964) parameterizations for both water and sulfuric acid vapor pressure. Sulfuric acid concentrations were set equal to 10^{-8} times water vapor concentrations for these calculations.

(1980) measured the sulfuric acid vapor pressure over a 98 wt % H_2SO_4 solution at 338 to 445K, and extrapolated to confirm Roedel's measurement. Ayers *et al.* suggest a parameterization, which is incorporated in our model. Comparison between the thick solid line (Ayers) and the dashed line (Gmitro and Vermeulen) in Figure 3-4 reveals the sensitivity of calculated nucleation rates to this choice of sulfuric acid equilibrium vapor pressure parameterization. The discrepancy is similar to that for choice of water equilibrium vapor pressure parameterization.

Accuracy of calculated nucleation rates

Wyslouzil *et al.* (1991) have measured binary nucleation for sulfuric acid-water systems. They find extremely poor agreement with the nucleation theory presented above, measuring rates 10 orders of magnitude higher or lower (depending on temperature) than those predicted. Unfortunately, the data they present are not sufficient to parameterize nucleation as a mathematical function of temperature and vapor pressures of sulfuric acid and water. Nucleation rates vary exponentially with such conditions, and any such parameterization would involve rather speculative extrapolation over many orders of magnitude. Wyslouzil *et al.*, however, do suggest a correction factor to classical binary nucleation theory, which is a nearly linear exponential function of the number of acid molecules in the critical nucleus, Na_{crit}. I have parameterized Wyslouzil's correction thus:

$$\frac{J_{empirical}}{J_{theory}} = \exp\left(-26.8 + 2.03 \cdot Na_{crit} - 0.01 \cdot Na_{crit}^2\right) \qquad 3.8$$

As shown in figure 3-5, the effect of this correction factor on calculated nucleation rates far exceeds sensitivities to uncertainties in measured parameters. Wyslouzil's data suggest gaps in the classical theory of binary homogeneous nucleation.

I have tested the sensitivity of the completed microphysical model to this very significant nucleation rate correction. The correction factor reduces new particle

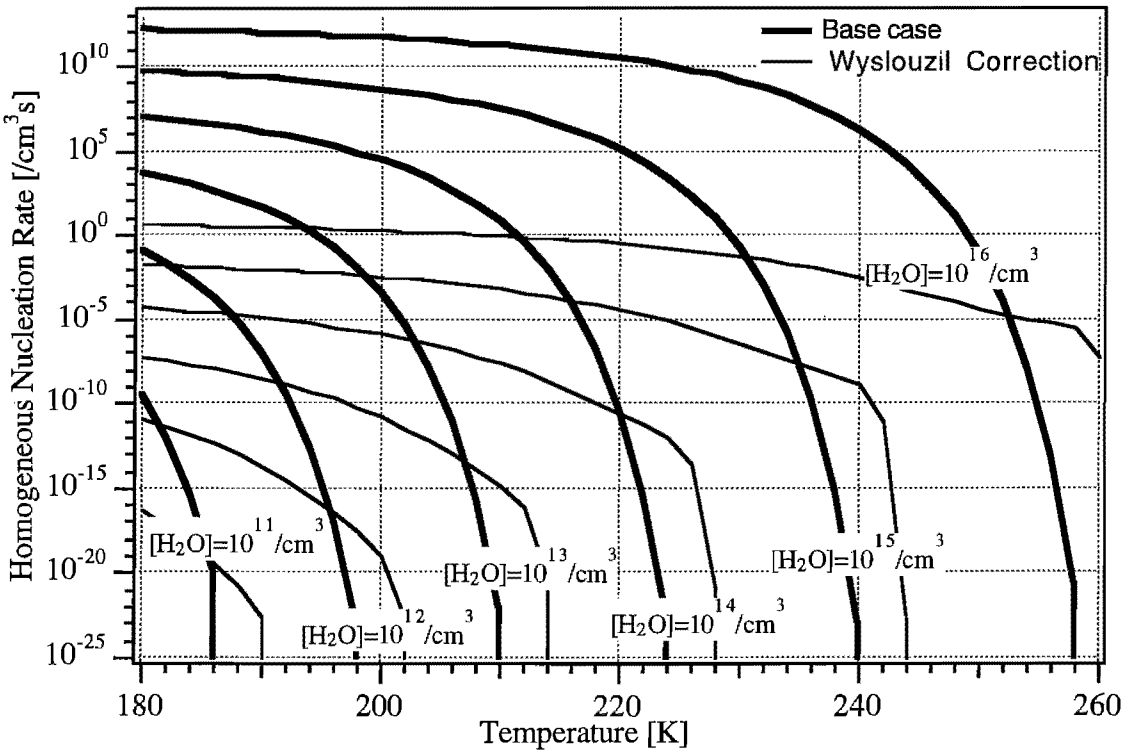

Figure 3-5 Effect of Wyslouzil's empirical correction factor on calculated nucleation rates.

formation rather dramatically in the lower stratosphere, where a large number of small particles form. These sensitivity studies are discussed further in Chapter 4.

3.2 Condensation and Evaporation

Condensation and evaporation are important processes in the evolution of aerosol particle size distributions in the atmosphere. The model calculates the effects on particle sizes of gas-liquid exchanges of water, sulfuric acid, sulfur trioxide, and nitric acid. These gases equilibrate on different timescales and are important at different conditions in the atmosphere, making their respective exchanges rather distinct microphysical processes. Water vapor exchange is very rapid, and is treated as an equilibrium process. Rates of sulfuric acid exchange and SO_3 uptake must be calculated explicitly from kinetic and diffusive considerations. Nitric acid condensation occurs only at the very low stratospheric temperatures that occur in polar winter. At

these low temperatures nitric acid composition is calculated as an equilibrium solution to the ternary system thermodynamics.

Water

Stratospheric concentrations of water vapor are large compared to those for sulfuric acid. Steele and Hamill (1981) calculate that water molecules impinge upon particles at a rate 10^8 times faster than sulfuric acid molecules, and that the characteristic timescale for water to equilibrate between vapor and aerosol phases is on the order of seconds. Model calculations therefore assume that over the microphysical time step (20 minutes) water will have established such an equilibrium, in which the number of water molecules condensing onto aerosol per unit time will be exactly equal to the number evaporating.

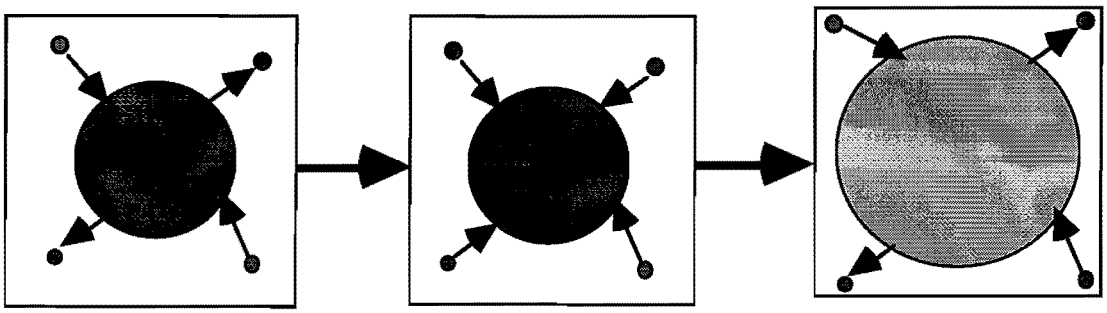

Figure 3-6 Water condensation, or "swelling", maintains gas-liquid water equilibrium through changes in temperature and ambient water vapor pressure.

Water vapor is in equilibrium between vapor and aerosol phases only when the ambient vapor pressure matches the equilibrium vapor pressure over a droplet. As discussed in section 3.1, the equilibrium vapor pressure is a function of a droplet's acidity (composition) and ambient temperature. With the exception of the very cold Antarctic stratosphere, where aerosol sedimentation is responsible for significant dehydration, the effect of condensation on the concentration of water in the vapor phase is negligible. Imposing the condition that ambient water vapor pressure and

temperature be unaffected by condensation permits a simple equilibrium solution for aerosol fractional composition (acidity). Aerosol composition is selected such that the equilibrium water vapor pressure matches the ambient water vapor pressure. Employing the thermodynamic calculations of Gmitro and Vermeulen (1964), Steele and Hamill (1981) have tabulated the equilibrium composition (weight percent sulfuric acid, W) as a function of temperature and water vapor pressure. The model makes use of the following parameterization to this data, presented in Hanson *et al.* (1993):

$$W = \frac{\left(0.6246 \cdot \log p_{H_2O} - 14.458\right) \cdot T + 3565.0}{1.3204 \cdot \log p_{H_2O} - 0.19988 \cdot T + 44.777} \qquad 3.9$$

The altitude profile of acid composition that the model calculate using this parameterization matches well that published by Turco *et al.* (1979a).

As a particle descends in altitude to colder temperatures in the stratosphere, the equilibrium vapor pressure of water it can sustain will decrease, and water will condense on the particle rapidly to reach a new equilibrium weight fraction (figure 3-6). This effect, called deliquescence or "swelling," can be very pronounced at temperatures below 200K. Stratospheric aerosol particles, which average 75% or more acid (by weight) can be diluted to 25% or less in supercooled liquids.

Sulfuric Acid and Sulfur Trioxide

In contrast to water, sulfuric acid is not in equilibrium between the drop and the vapor. The model therefore calculates the rate of acid condensation and evaporation and consequent droplet growth or decline as sulfuric acid approaches equilibrium. As the number of acid molecules in a droplet changes, the water vapor adjusts to maintain the appropriate fractional composition (figure 3-7). Sulfur trioxide (SO_3) impinging on aerosol particles is quickly oxidized to sulfate within the liquid droplet. The model assumes such oxidation occurs with a reaction probability of 1, treating SO_3 condensation in a manner analogous to sulfuric acid condensation. SO_3 condensation

is counted as a production term for total sulfuric acid (gas phase plus liquid sulfate) in equation 3.1, and evaporation of the resultant sulfate produces gas-phase sulfuric acid.

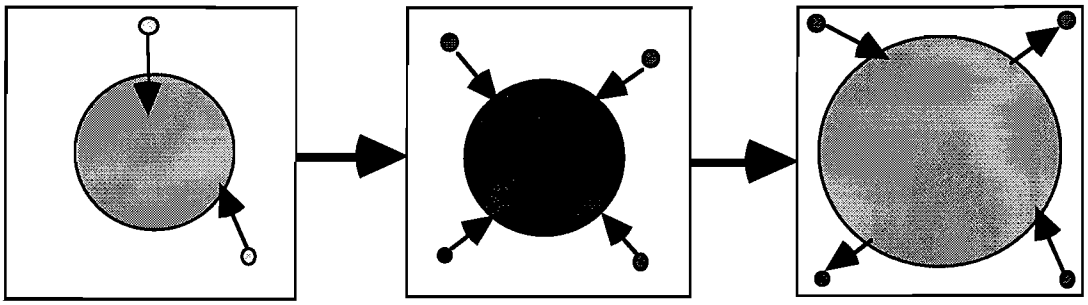

Ambient sulfuric acid exceeds equilibrium vapor pressure. Acid molecules condense slowly.

Droplet experiences increased acidity. Water condenses to maintain equilibrium.

Weight fraction acid remains constant.

Figure 3-7 Sulfuric acid condenses slowly on stratospheric particles, at rates calculated explicitly. Water vapor adjusts rapidly to maintain constant fractional composition.

The flux of molecules of species x (H_2SO_4 or SO_3), C_i^X, to a droplet with radius r_i varies greatly with Knudsen number, Kn, which is the ratio of the mean free path of the condensing molecules to droplet radius. Our model calculates the growth of particles from radii much less than 0.01 μm to several microns, corresponding to a wide range of Knudsen numbers. The "effective" mean free path of molecules in air is calculated using the equation of Hamill *et al.* (1977b):

$$l_{eff} = \frac{1}{\pi \cdot n_{air} \cdot d^2 \sqrt{\frac{M_{air}}{M_{air}+M_X}}} \qquad 3.10$$

where n_{air} is the number density of air molecules, $d=4.3\times10^{-8}$ cm is the mean collision diameter of an H_2SO_4 molecule with air, $M_{air}=28.96$ g/mol is the molecular weight of air, and M_X is the molecular weight of the condensing molecule (98.07 g/mol for H_2SO_4, 80.06 g/mol for SO_3).

Our model uses an approximate expression valid for all Knudsen numbers to calculate the flux of impinging sulfuric acid and SO_3 molecules (Hamill *et al.*, 1977b):

$$C_i^{H_2SO_4} = \frac{4\pi D r_i}{1+\lambda Kn}\left(\left[H_2SO_4{}^{(g)}\right]-\left[H_2SO_4{}^{(g)}\right]^o\right) \quad 3.11$$

$$C_i^{SO_3} = \frac{4\pi D r_i}{1+\lambda Kn}\left[SO_3{}^{(g)}\right] \quad 3.12$$

The rate of condensation or evaporation of sulfuric acid is dependent on the difference in acid concentration (/cm^3) between ambient air $\left[H_2SO_4{}^{(g)}\right]$ and equilibrium $\left[H_2SO_4{}^{(g)}\right]^o$. The model derive sulfuric acid equilibrium vapor pressure from the parameterization of Ayers *et al.* (1980), consistent with its nucleation calculation. The equilibrium vapor pressure term is ignored in equation 3.12, as SO_3 is not maintained as such in aerosol but converted to sulfate.

In equations 3.11 and 3.12, λ is a correction factor defined thus (Hamill *et al.*, 1977b):

$$\lambda = \frac{1.333+\frac{0.71}{Kn}}{1+\frac{1}{Kn}} + \frac{4(1-\alpha)}{3\alpha} \quad 3.13$$

where α is the reaction probability for H_2SO_4 or SO_3 condensation, which the model takes to be unity. The diffusion coefficient, D, is given as follows:

$$D = \frac{v_{thermal}\cdot l_{eff}}{3} = \frac{l_{eff}}{3}\sqrt{\frac{8RT}{\pi M_X}} \quad 3.14$$

where R=8.31441x10^7 erg/mol/K is the molar gas constant (Hamill *et al.*, 1977b).

The equilibrium vapor pressure of sulfuric acid over aerosol droplets will increase slightly with the curvature of the droplet surface. In taking into account this phenomenon, known as the Kelvin effect, the model assumes the droplets are spherical. The factor, K_f, by which vapor pressure increases as a function of droplet radius, r_i, is given by Pruppacher and Klett (1978):

$$K_f(r_i) = \exp\left(\frac{2M_{H_2SO_4}\sigma}{RT\rho r_i}\right) \quad 3.15$$

Aerosol surface tension, σ, and aerosol density, ρ, are extrapolated linearly from measurements (NRC, 1928; Sabinina and Turpugow, 1935) as described in section 3.1. The Kelvin factor reduces particle growth by condensation and favors evaporation. The effect is greater on smaller particles, which have greater curvature relative to larger ones. Thus in regions where the ambient sulfuric acid vapor pressure is close to the equilibrium vapor pressure, large particles may grow while small ones are evaporating.

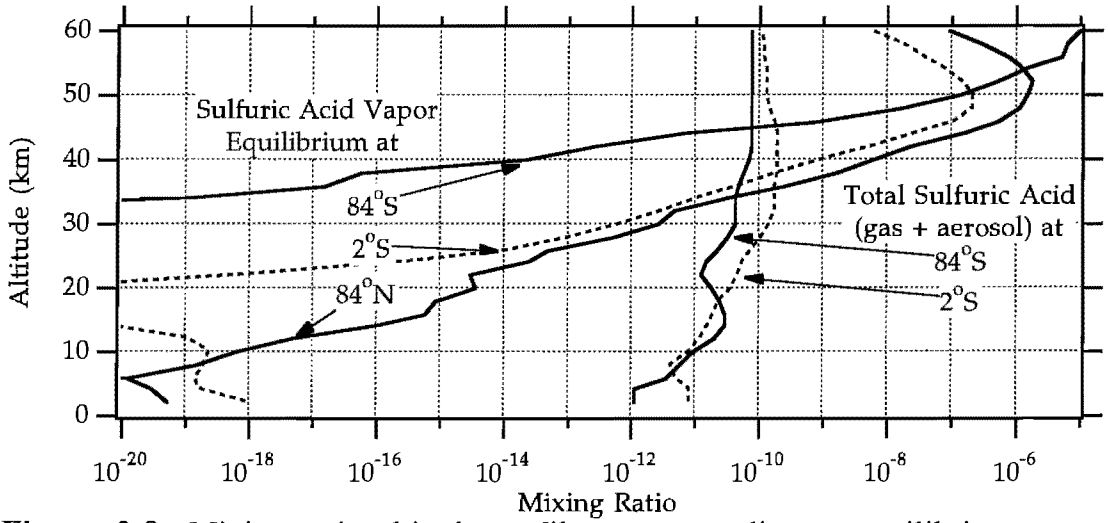

Figure 3-8 Mixing ratio altitude profiles corresponding to equilibrium vapor pressures for sulfuric acid and total sulfuric acid (gas + aerosol) at various latitudes on model day 240 (September 1). Gas-phase sulfuric acid mixing ratios tend toward equilibrium via nucleation, condensation, and evaporation. Thus where equilibrium is much greater than the total, all liquid tends to evaporate.

The model calculates sulfuric acid condensation rates similar to those previously published (Hamill *et al.*, 1977b; Turco *et al.*, 1979a). In the lower stratosphere, equilibrium vapor pressures are much less than total sulfuric acid pressures, and nucleation and condensation favor aerosol over the gas phase (see figure 3-8). As altitude increases, equilibrium vapor pressures increase with temperature, and ambient sulfuric acid vapor pressures decrease with atmospheric pressure. In the upper stratosphere, where equilibrium vapor pressures are greater than ambient sulfuric acid, aerosol evaporates. As shown in figure 3-9, the altitude at which equilibrium equals total sulfuric acid (representative of the top of the aerosol layer) varies with season.

The seasonal variation is greatest in the polar regions, where the aerosol layer extends as high as 43 km in winter, but to only 30 km in summer.

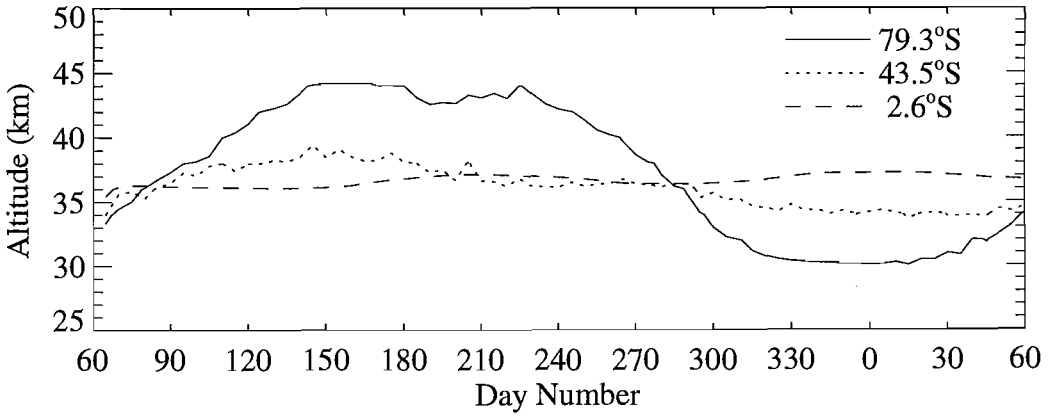

Figure 3-9 Latitudinal and seasonal variation of the 100 pptv contour in equilibrium mixing ratio of H_2SO_4, corresponding approximately to the top of the aerosol layer.

Our model uses the calculated sulfuric acid condensation and evaporation rates to determine the number of particles from each size bin, i, to be promoted or demoted to adjacent size bins, i±1. Size bins are defined by average number of acid molecules per drop, Na_i, and are geometrically spaced such that $Na_{i+1}=2Na_i$. Given the current population of particles in any given size bin, n_i, and the rate of change of sulfate molecules, $C_i = C_i^{H_2SO_4} + C_i^{SO_3}$, the model calculates the rate of change of the population due to condensation or evaporation thus:

$$\left.\frac{\partial n_i}{\partial t}\right|_{cond} = P_i^{cond} - L_i^{cond} \cdot n_i \qquad 3.16$$

$$= \left\{ \begin{array}{l} \dfrac{C_{i-1} n_{i-1}}{Na_i - Na_{i-1}},\ C_{i-1} > 0 \\ \qquad\qquad condensation \\ \dfrac{|C_{i+1}| n_{i+1}}{Na_{i+1} - Na_i},\ C_{i+1} < 0 \\ \qquad\qquad evaporation \end{array} \right\} - \left\{ \begin{array}{l} \dfrac{C_i}{Na_{i+1} - Na_i},\ C_i > 0 \\ \qquad\qquad condensation \\ \dfrac{|C_i|}{Na_i - Na_{i-1}},\ C_i < 0 \\ \qquad\qquad evaporation \end{array} \right\} \bullet n_i$$

Production of particles in each size bin occurs by growth or evaporation from adjacent bins. Loss of particles in each bin results from growth into the next larger bin or evaporation into the next smaller bin. Particles are lost completely when they evaporate from the smallest bin (Na=2 molecules). Condensational growth out of the largest size

bin is not allowed. Growth in the larger bins is very slow due to the geometric spacing, and these bin populations are affected more by transport and sedimentation, as will be discussed later in this chapter.

Nitric Acid

Throughout most of the stratosphere, aerosol particles are composed almost entirely of sulfuric acid and water. At the very cold temperatures experienced in the polar lower stratosphere in winter, however, uptake of nitric acid can become significant. At temperatures below 215K and water vapor pressures between $2x10^{-5}$ and $2x10^{-3}$ mbar, the model employs the code of Carslaw *et al.* (1995), which calculates the composition of $HNO_3/H_2O/H_2SO_4$ aerosol under such conditions. This code makes use of analytic parameterizations for the ternary system that agrees well with thermodynamic models and measurements, and considers the loss of ambient HNO_3 vapor pressure due to aerosol uptake. In polar winter, aerosol takes up significant amounts of nitric acid and water, possibly removing both from the stratosphere permanently via sedimentation. Our model partitions concentrations of both species between gas and aerosol phases, accounting for removal by particle sedimentation and transport.

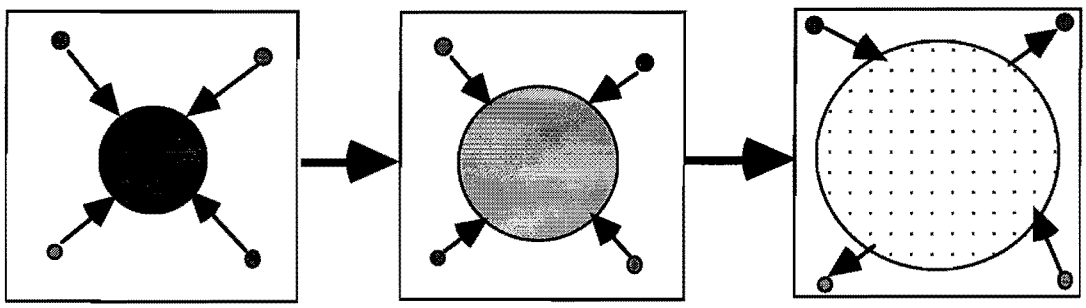

At very cold temperatures HNO_3 begins to condense.

$H_2O/HNO_3/H_2SO_4$ ternary solution. Nitric acid & water continue to condense.

H_2SO_4 becomes insignificant. H_2O & HNO_3 predominate.

Figure 3-10 Nitric acid condensation

3.3 Coagulation

Coagulation occurs when two aerosol particles merge to form one larger particle (figure 3-11). The model accounts for spontaneous coagulation, due to thermal motions of the particles. The model does not include enhanced coagulation that may occur due to other motions, such as gravitational sedimentation, shear, turbulence, or Van der Waals attractions.

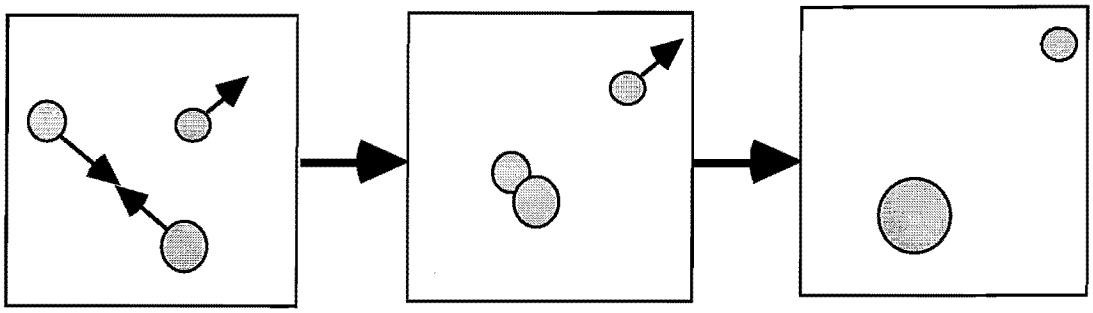

Figure 3-11 Coagulation

Coagulation can be a computationally intensive process to simulate. Because particles from each of the model's forty-five size bins can merge with particles from any size bin, the number of calculations required is proportional to the square of the number of size bins. For this reason many models include only "self-coagulation," occurring between particles that are the same size. Cross-coagulation, neglected by such a scheme, is, however, an important sink for small particles. Our model accounts for coagulation between all bins.

Table 3-1 Geometric spacing of size bins

Bin #	i-3	i-2	i-1	i	i+1	i+2	i+3
n=ave # of molecules	$\frac{A}{8}$	$\frac{A}{4}$	$\frac{A}{2}$	A	2A	4A	8A

Because the aerosol size bins are geometrically spaced (see table 3-1), it is not possible to accurately account for what happens when a small drop coagulates with a large drop. The resulting drop will not be twice the size of the original large drop, and will hence remain in the same size bin. To conserve mass and volume, therefore, the model counts such a coagulation as a fractional increase in the number of particles in the larger bin. For example, the coagulation of a particle from bin i-3 with a particle from bin i is counted as an increase in the population of bin i of one-eighth of a particle. In reality, such a coagulation would not increase the bin population; it would increase the volume of one particle by one-eighth. Such a volume increase in a single particle can not be resolved with the model's geometric bin spacing.

The following differential equation describes the rate of change of the population of bin i due to coagulation with all other bins:

$$\left.\frac{\partial n_i}{\partial t}\right|_{coag} = \ldots + k_{i-3,i} n_{i-3} n_i \cdot \frac{1}{8} + k_{i-2,i} n_{i-2} n_i \cdot \frac{1}{4} + k_{i-1,i} n_{i-1} n_i \cdot \frac{1}{2} \quad \text{smaller bins} \qquad 3.17$$

$$+ \frac{1}{2}\left(k_{i-1,i-1} n_{i-1} n_{i-1} - 2k_{i,i} n_i n_i\right) + \frac{1}{2}\left(k_{i,i} n_i n_i - 2k_{i,i} n_i n_i\right) \quad \text{self-coagulation}$$

half promoted half remain

$$- k_{i,i+1} n_i n_{i+1} - k_{i,i+2} n_i n_{i+2} - \ldots \quad \text{larger bins}$$

where n_i (/cm^3) is the density of particles in bin i, and $k_{i,j}$ (cm^3/s) is the coagulation constant for collisions between particles in bins i and j, as will be described shortly. The factor of one-half on the self-coagulation terms reflects my convention that half of all coagulations between two particles in bin i will result in particles large enough to move to bin i+1. The other half will not be large enough, and will produce one new particle in bin i at the expense of two. In summation form, equation 3.17 is:

$$\left.\frac{\partial n_i}{\partial t}\right|_{coag} = P_i^{coag} - L_i^{coag} \cdot n_i \qquad 3.18$$

$$= \left\{ n_i \sum_{j=1}^{i-1} k_{j,i} n_j \cdot \left(\frac{1}{2}\right)^{i-j} + \frac{1}{2} k_{i-1,i-1} n_{i-1}^2 \right\} - \left\{ \frac{3}{2} k_{i,i} n_i + \sum_{j=i+1}^{n} k_{i,j} n_j \right\} \bullet n_i$$

The rates of production and loss due to coagulation, shown in equation 3.18, are incorporated into the differential equations for particle bin populations as will be discussed in the section 3.5.

The model's coagulation scheme conserves total aerosol volume, but cannot give a proper treatment to particle number and surface area. Geometrically spaced discrete size bins allow the model to account for large populations of particles in the atmosphere, but limit its accuracy in accounting for aerosol interactions. However, the volume-doubling scenario provides sufficiently high resolution and minimizes numerical errors.

Coagulation coefficients in the model are taken from Fuchs (1964, p. 294):

$$k_{i,j} = \frac{8\pi \bar{D}\bar{r}}{\frac{4\bar{D}}{\bar{v}\bar{r}} + \frac{\bar{r}}{\bar{r}+\Delta'}} \qquad 3.19$$

where $\bar{r} = \left(r_i + r_j\right)/2$ is the average radius of the coagulating particles. $\bar{D} = \left(D_i + D_j\right)/2$ is the average particle diffusion constant, $\bar{v} = \sqrt{v_i^2 + v_j^2}$ is the average thermal speed of the particles, and $\bar{\delta} = \sqrt{\delta_i^2 + \delta_j^2}$ is an average mean free path correction factor, given by Fuchs (1964, p. 291). The individual particle diffusion constants, D_i and D_j, are calculated from the experimentally determined Cunningham slip-flow form (Pruppacher and Klett, 1978, p. 361):

$$D_i = \frac{kT(1+\alpha_i Kn_i)}{6\pi\eta_a r_i} \qquad 3.20$$

The term $1+\alpha Kn$ is the Cunningham slip-flow correction, where Kn is the particle Knudsen number and $\alpha = 1.257 + 0.400\exp(-1.10/Kn)$. η_a (g/cm/s) is the coefficient of viscosity of air, given by Sutherland's equation (ESSA *et al.*, 1966, p. 7):

$$\eta_a = \frac{\beta \cdot T^{1.5}}{T+S} \qquad 3.21$$

where $\beta = 1.458\text{x}10^{-5}$ g s^{-1} cm^{-1} K$^{-1/2}$ and S=110.4 K.

The coagulation kernels calculated by this method are presented in figure 3-12. The coagulation kernels for identical conditions calculated by Turco *et al.* (1979) are shown for comparison. The previous calculations are uniformly greater than mine by a factor of 2. The specific cause of this discrepancy in calculations remains unclear at this time. However, this factor is relatively minor compared to the multiple-order-of-magnitude variation in coagulation rates with altitude and particle size.

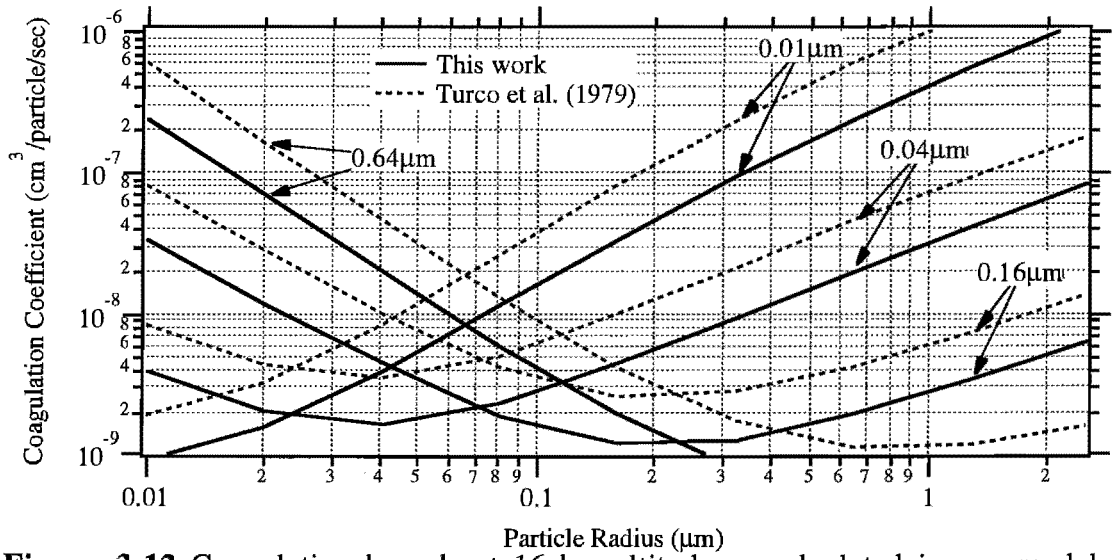

Figure 3-12 Coagulation kernels at 16 km altitude as calculated in our model, compared to calculations presented in Turco *et al.* (1979). For both calculations ambient temperature is 216K and air density is 3.5×10^{18} molecules/cm^3.

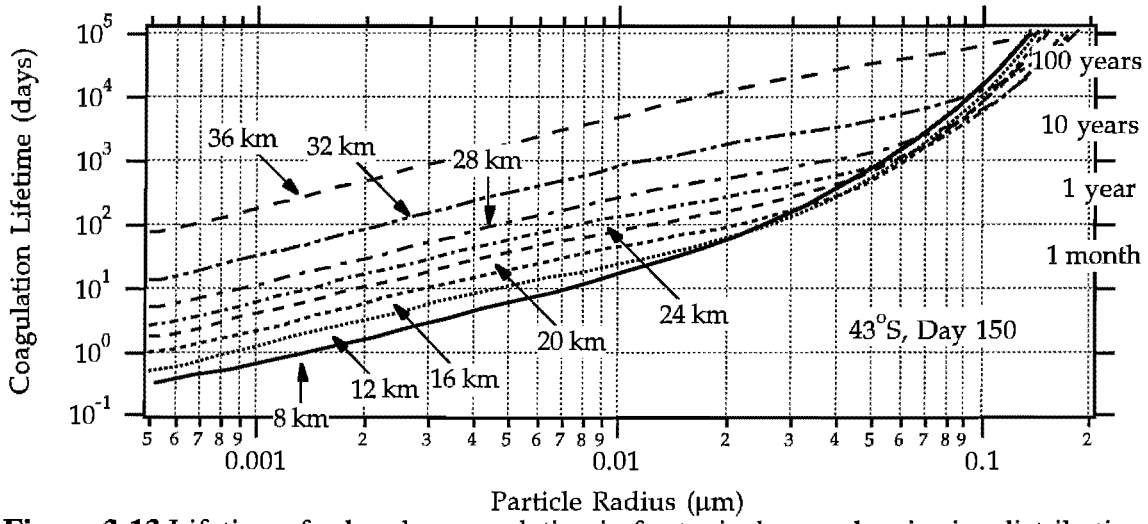

Figure 3-13 Lifetimes for loss by coagulation in for typical nonvolcanic size distributions.

Coagulation is a slow process, reducing populations of small particles on timescales of weeks to years, and increasing populations of large particles by negligible amounts. Figure 3-13 shows the lifetime for loss of particles of different sizes and altitudes for a typical nonvolcanic scenario at mid-latitudes. These calculations agree generally with those of Hamill *et al.* (1977), which reports that roughly half of all particles in the 0.01 to 0.1 μm range are lost to coagulation within a year, and that losses of larger particles are negligible. Very small particles ($r<10^{-3}$ μm) can be lost to coagulation within a day in the lower stratosphere, although such lifetimes increase to a month or more near the top of the aerosol layer. The rate of coagulation is, of course, highly dependent on the size distribution of ambient particles, and these lifetimes are decreased when greater numbers of large particles are present, such as in volcanic scenarios.

3.4 Transport

Atmospheric dynamics

Particles which are suspended in the atmosphere without significant fall velocities behave dynamically in the same manner as the air parcels that suspend them. Hence particle mixing ratio (particles/mg air) is conserved in dynamical processes. Eddy diffusion and the meridional circulation transport the population of each particle size bin in the same way as individual chemical species (see Chapter 2). At any given gridpoint, particles of all sizes are advected at the same velocity, determined by the meridional circulation. Sub-grid scale mixing (or eddy diffusion), on the other hand, may affect particles of different sizes in different ways. Eddy diffusion has the effect of smoothing out latitudinal and vertical gradients in individual particle sizes.

Computation would be greatly reduced by calculating a transport term only for the total number of particles of all sizes, and distributing the total proportionately among the size bins. Such a scheme would rely on an assumption of rapid

repartitioning of aerosol size populations by coagulation, condensation, and evaporation. Aerosol redistribution can often be slow compared to the model timestep, however, making it more realistic to calculate separate transport terms for individual size bins. As I show in the next section, the model's sedimentation calculation requires this anyway. For each size bin, the model calculate the rate of change of particle mixing ratio due to diffusion and advection in the same manner as for chemical species. A separate transport term is then calculated to account for particle sedimentation.

Sedimentation

Gravitational settling, or sedimentation, of particles occurs when particles are too heavy to be supported by the thermal energy of atmospheric gases (figure 3-14). When this occurs particles no longer behave in the same manner as air parcels. Sedimenting particles of any given size fall at a given terminal velocity through air parcels rather than with them. Thus during sedimentation the particle concentration (particles/cm^3) of each size bin is conserved, rather than mixing ratio (particles/mg air). The model treats falling particles and the transport of condensed material within them (sulfate, water, and nitric acid) accordingly.

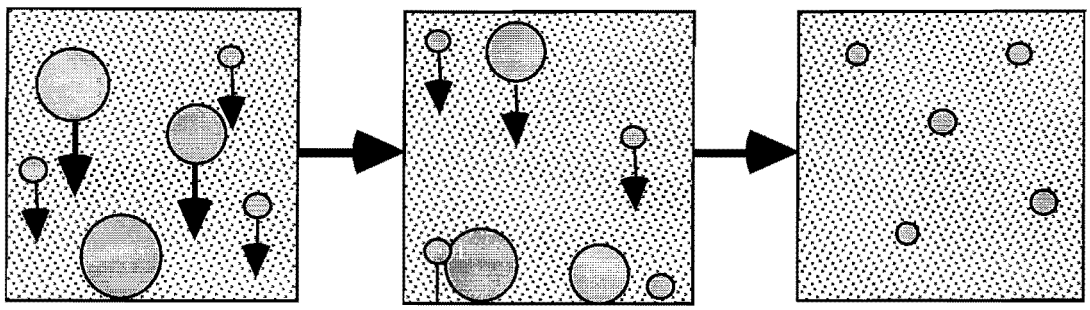

Figure 3-14 Sedimentation

The speed at which small particles gravitationally settle is given by the terminal velocity in slip-corrected Stokes flow (Pruppacher and Klett, 1978, p. 362):

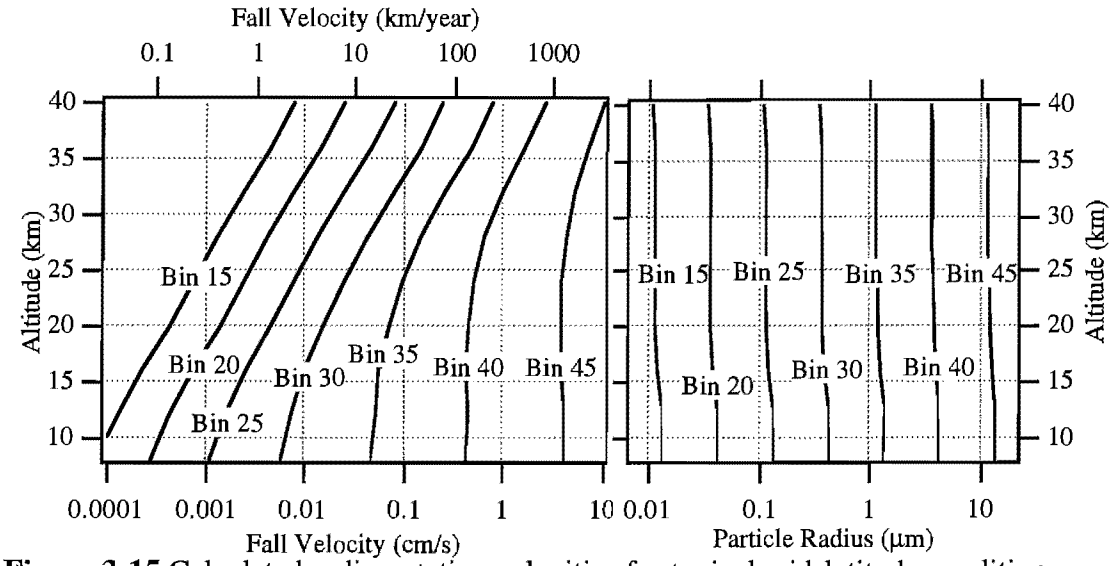

Figure 3-15 Calculated sedimentation velocities for typical mid-latitude conditions.

$$V_s = \frac{2(1+\alpha Kn)r^2 g(\rho_p - \rho_a)}{9\eta_a} \qquad 3.22$$

where r (cm) is particle radius, g (cm/s^2) is gravitational acceleration, ρ_p (g/cm^3) is particle density, ρ_a (g/cm^3) is air density, η_a (g/cm/s) is the coefficient of viscosity of air, and $1+\alpha Kn$ is the Cunningham slip-flow correction. The particle fall velocities are then used in a semi-Lagrangian aerosol transport scheme, similar to that used for advection of gaseous constituents (see Chapter 2). The difference in the sedimentation scheme is that particle concentration is transported, rather than mixing ratio.

Figure 3-15 shows sedimentation velocities calculated for various particle size bins at stratospheric altitudes. Because size bins are defined by the number of sulfuric acid molecules per drop, the average particle radius for each bin varies somewhat with water content, as shown on the right. For this typical mid-latitude case, particle composition is relatively uniform with altitude, and the bins shown correspond roughly to particles of 0.01, 0.03, 0.1, 0.3, 1, 3, and 10 micron radii. Comparison is very good to a similar plot of calculated fall velocities for particles of such radii, shown in Pruppacher and Klett (1978, p. 362).

Figure 3-16 shows the variation of sedimentation velocity with radius for the same calculations. Figures 3-15 and 3-16 both show that particles of radius 1μm or greater will fall out of the stratosphere within a few months at most. Particles of such size can be maintained only when they are generated on a similar timescale. Particles larger than 1μm are seen in the model only in the winter polar lower stratosphere, when rapid cooling leads to rapid condensation and swelling. Throughout the rest of the stratosphere, rates of particle growth are slow enough that particles fall out before they reach 1μm in radius.

The semi-Lagrangian code produces additional transport terms representing the effects of sedimentation on the populations of each size of particle. Similar terms are calculated to express the rate of change in the mixing ratio of total sulfuric acid/sulfate, nitric acid, and water due to sedimentation. These terms are added to other transport terms (for diffusion and advection, as discussed above), and incorporated into constituent finite difference equations. Sedimentation of aerosol is believed to be responsible for the ultimate removal of significant proportions of nitric acid and water from the polar lower stratosphere. Wilson *et al.* (1992) report measurements in which denitrification in the polar stratosphere is correlated to a reduction in number of the very

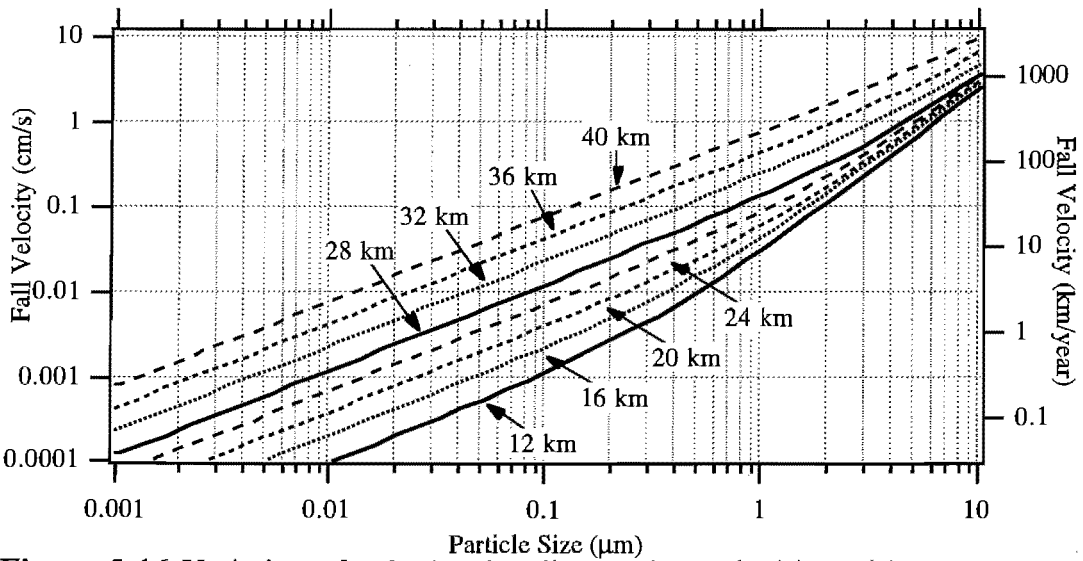

Figure 3-16 Variation of calculated sedimentation velocities with particle size for various altitudes for typical mid-latitude conditions.

largest particles, with smaller particles (which comprise the vast majority in number) remaining.

Tropospheric deposition

Wet and dry precipitation in the troposphere is an important sink for sulfate aerosol. Warneck (1988, p. 364-366) presents considerable evidence that scavenging of aerosol by precipitation is an efficient process, with a residence time between 5 and 7 days. Since this residence time is much shorter than the timescale for vertical transport through the troposphere (absent deep convection), virtually all of the aerosol in the rainout region will be removed. However, this residence time is likely to be longer in the upper troposphere, where particle nucleation is thought to represent a significant source of stratospheric aerosol (Brock *et al.*, 1995). The model employs a 4-day residence time for aerosol at 2 km, decreasing the removal rate linearly to zero at 2 km below the tropopause.

3.5 Particle Populations

The population of particles in each of the 45 size bins is calculated by solving the following finite difference equation:

$$\frac{n_i(t+\Delta t)-n_i(t)}{\Delta t} = \delta_{i,i_{crit}} \cdot J_{nuc} + P_i^{cond} + P_i^{coag} + T_i^{dyn} + T_i^{sed} - \left(L_i^{cond} + L_i^{coag} + \lambda_{aer}\right) \cdot n_i(t) \qquad 3.23$$

where J_{nuc} is the particle nucleation rate, i_{crit} is the bin of the critical nucleus for nucleation, P_i^{cond} and L_i^{cond} are defined in equation 3.16, P_i^{coag} and L_i^{coag} are defined in equation 3.18, T_i^{dyn} and T_i^{sed} are transport terms due to atmospheric dynamics and particle sedimentation, and λ_{aer} is the rainout rate for particles at the given altitude and latitude. The model tests the loss timescale for each size bin and

integrate accordingly by either explicit forward Euler or photochemical equilibrium methods, as discussed in chapter 2.

The model calculates the total sulfuric acid in aerosol by subtracting gas-phase sulfuric acid (calculated from equation 3.2) from total sulfuric acid (calculated from equation 3.1), checking to ensure that total sulfuric acid is conserved. This quantity is then partitioned amongst the particle bins proportionally to the size distribution resultant from equation 3.23. In the next chapter I present the resultant size distributions and corresponding parameters such as surface area, mass mixing ratio, and total particle number concentrations. I compare these calculations to observations and discuss sensitivities to various uncertainties.

Chapter 4

The Nonvolcanic Aerosol

The observational history of stratospheric aerosol demonstrates the influence of large perturbations corresponding to major volcanic eruptions. Measurements of stratospheric aerosol are obtained from *in situ* instruments as well as remote sensors. Several decades of *in situ* measurements from particle counters aboard balloons and aircraft provide records over many volcanically active and quiescent periods. Such instruments report total concentrations of particles, imposing various lower size limits, and offering the best-resolved measurements of aerosol size distributions. From these attributes such as total surface area concentration are calculated. Additional *in situ* instruments measure the total mass of liquid sulfate.

Following the dramatic increases caused by the eruptions of Fuego in 1974 and El Chichón in 1982, stratospheric aerosol levels decreased steadily for about four and six years, respectively, followed by a leveling off. Determination of whether decreases actually halted is somewhat difficult due to the relatively short intervals before subsequent eruptions (St. Helens in 1980 and Pinatubo in 1991, respectively). Hofmann (1990) argues that a steady nonvolcanic "background" layer is indicated in Northern Hemisphere mid-latitude measurements for the periods 1978-79 and late 1988-90. Hofmann further notes that the ratio of large to small particles is seen to

increase between these "background" periods, and concludes that nonvolcanic sources of stratospheric sulfate must therefore be increasing. In this chapter I calculate aerosol resulting from various nonvolcanic sources, comparing with observations to determine the role of each source.

Near-global coverage of aerosol extinction has been provided by a series of long-term limb occultation experiments aboard satellites. The Stratospheric Aerosol Measurement (SAM) II measured extinction at 1μm wavelength between 64° and 80° in both hemispheres from October 1978 until January 1994. The Stratospheric Aerosol and Gas Experiment (SAGE) I measured 0.45 and 1μm extinction between 79°S and 79°N from February 1979 until November 1981. SAGE II has operated from October 1984 until the present time, measuring extinction at 0.385, 0.453, 0.525, and 1.02 μm between 80°S and 80°N. Thomason and Poole (1993) describe a parameterization for calculating surface area concentrations from single-wavelength extinction measurements based on a multi-spectral principal components method. Surface areas thus derived are found to match multi-wavelength estimates to within 20-30%. Using the 1 μm channel from these observations, Thomason *et al.* (1995) derive a near-global seasonal climatology of surface area concentration, which is used here for comparison to model calculations.

4.1 Contribution of Carbonyl Sulfide

Chin and Davis (1995) have examined the budget of carbonyl sulfide, comparing its contribution of active sulfur to the stratosphere with estimates of the flux required to maintain the aerosol observed in volcanically quiescent periods. From source strength estimates and mixing ratio observations, they calculate the global atmospheric lifetime to be 4.3 years, less than half the stratospheric lifetime for OCS derived using a 1-dimensional photochemical model. Chin and Davis conclude therefore, that most of the OCS that enters the stratosphere returns intact to the troposphere and is ultimately lost by surface uptake by vegetation. The flux of active

sulfur they calculate as resulting from dissociation of OCS in the stratosphere is 2 to 5 times less than recent estimates of the flux required to maintain the background aerosol, derived from observations of mass and estimates of lifetime.

Golombek and Prinn (1993) have examined the contributions of OCS and SO_2 from the troposphere with three-dimensional modeling studies. They calculate that advection of SO_2 from the troposphere is the dominant source of SO_2 between the tropopause and 20 km. In this region, convergence due to advection contributes 2 to 3 times more SO_2 than oxidation of OCS, according to their model. This calculation is based on a 3-D representation of dynamics not possible in our 2-D model. However, the complexity of the three-dimensional problem mandated a number of simplifications in terms of microphysics. Sulfuric acid is partitioned between gas and liquid assuming vapor is equal to its equilibrium concentration for a 75% sulfuric acid solution. Liquid particle sizes are assumed to be distributed according to a uniform exponential about a parameterized mean radius. One sedimentation velocity is calculated for particles of all sizes at each gridpoint, based on the mean radius of the size distribution. Golombek and Prinn's tabulated sedimentation velocities are much smaller than those calculated in our model, never exceeding 1 mm/sec. The effects and feedbacks of microphysical processes on size distributions are not explicitly calculated. Relation of Golombek and Prinn's SO_2 source calculation to production of liquid sulfate is not straightforward, and requires a more complete treatment of the microphysical problem.

Chin and Davis (1995) employ a one-dimensional model to calculate that 1.8×10^{25} molecules/s of OCS are oxidized in the stratosphere. Previous work had consistently determined this flux to be much greater, by factors of 3 to 5 (Crutzen, 1976; Sze and Ko, 1979; Sze and Ko, 1980; Turco *et al.*, 1980; Servant, 1986). Chin and Davis (1995) explain this discrepancy as due to their improved understanding of OCS vertical distribution and of reaction rates for loss of OCS. Our two-dimensional model calculates an annual average of 2.7×10^{25} molecules/s of OCS lost in the

stratosphere, 50% higher than the calculation of Chin and Davis, but still several times lower than the previous estimates.

Several estimates of the flux of sulfur to the stratosphere required to maintain the observed background aerosol layer are listed in table 4-1. These calculations are based on estimates of the total mass of sulfate in the stratosphere (deduced from observations) and assumed lifetimes, also listed. This method of calculating the flux fails, however, to account for the concomitant mass of gas-phase sulfuric acid and sulfur dioxide in the stratosphere. The source of sulfur to the liquid aerosol must also sustain these sulfur-bearing gases. Counting all non-OCS sulfur-bearing molecules, rather than just sulfate, increases the stratospheric burden by 60 to 250% in our model, depending on the source scenario. In addition, the estimated lifetimes shown in table 4-1 are likely to be too long. Servant (1986) assumed sedimentation to be negligible, and chose a residence time (14 months) representative of that for air in the stratosphere. My calculations predict that sedimentation significantly reduces stratospheric residence times for sulfur.

Table 4-1 Previous estimates of sulfur flux required to maintain background aerosol compared to flux and mass resulting from OCS, calculated in this work.

Source	Total stratospheric sulfate (molecules)	Lifetime	Flux (molecules/s)
Crutzen (1976)	1.6×10^{33}	2 years	2.6×10^{25}
Servant (1986)	2.4×10^{33}	14 months	6.6×10^{25}
Hofmann (1991)	1.2×10^{33}	1 year	3.8×10^{25}
This work (OCS only)	4.4×10^{32}	9 months	3.0×10^{25}

Assuming OCS is the only source of sulfur, our model calculates only 4.4×10^{32} molecules of sulfate above the tropopause. To this I add a calculated 1.1×10^{32} molecules of gas-phase H_2SO_4 and 1.5×10^{32} molecules of SO_2, giving a total of 7.0×10^{32} oxidized sulfur-bearing molecules above the tropopause. Together with OCS, these three oxidized species comprise over 99% of non-OCS stratospheric sulfur

in our model. As stated previously, the model calculates that $2.7x10^{25}$ molecules/s of OCS are oxidized in the stratosphere. Assuming that this oxidation of OCS in the stratosphere is the sole source of the oxidized sulfur-bearing compounds in the stratosphere, I divide the total by this flux to calculate a residence time for reduced sulfur of 10 months.

This analysis, however, does not account for transport of SO_2 from the troposphere, which must also be considered. Even with OCS as our only source, a small but significant mixing ratio of this SO_2 is produced in the troposphere by the slow oxidation of OCS there. Although OCS is long-lived in the troposphere, more than a third of the total number of OCS oxidation reactions in the model occur in the troposphere, which contains the bulk of the atmosphere's mass. In our OCS-only calculation, 0.2-0.8 pptv of SO_2 reaches the tropopause, contributing to the stratospheric sulfur budget. The total rate of SO_2 oxidation in the stratosphere is $3.0x10^{25}$ molecules/s, roughly 10% greater than the stratospheric rate of SO_x production by OCS. The remaining SO_2 molecules are produced by OCS oxidation in the troposphere, and is transported to the stratosphere. Consideration of this additional source reduces the calculated average stratospheric residence time for non-OCS sulfur proportionately, to 9 months.

My microphysical calculations confirm that carbonyl sulfide does not dissociate sufficiently in the lower stratosphere to be the dominant source of background aerosol. The total burden of stratospheric sulfate the model calculates as resulting from OCS is 3 to 6 times less than the estimates of total background stratospheric sulfate listed in table 4-1. The deficit between observed sulfate and that calculated from OCS is more pronounced, however, in the lower stratosphere, where the maxima in aerosol mass, surface area, and particle concentration are observed. Numerous observations of background sulfate mass, aerosol surface area, and particle concentration are compared to model calculations in figure 4-1. Observations of mass mixing ratio from 1979 and

1989 were obtained by balloon launches from Laramie, Wyoming (Hofmann, 1990a), as well as the original measurements of Junge *et al.* (1961). An ER-2 aircraft flight from December 28, 1988 also provides profiles of liquid sulfate mass mixing ratio, aerosol surface area, and particle concentration (Hofmann, 1995). Additional surface area profiles are inferred from satellite extinction measurements retrieved over 3-month periods beginning in December of 1979, 1988, and 1989 (Thomason and Poole, 1993; Thomason *et al.*, 1995).

At altitudes below its peak at 20 km, observed liquid sulfate mass mixing ratios are consistently 10 to 30 times greater than those calculated as resulting from carbonyl sulfide. Clearly OCS dissociation cannot provide sufficient sulfur to the mid-latitude lower stratosphere to account for the bulk of the sulfate mass observed there. The

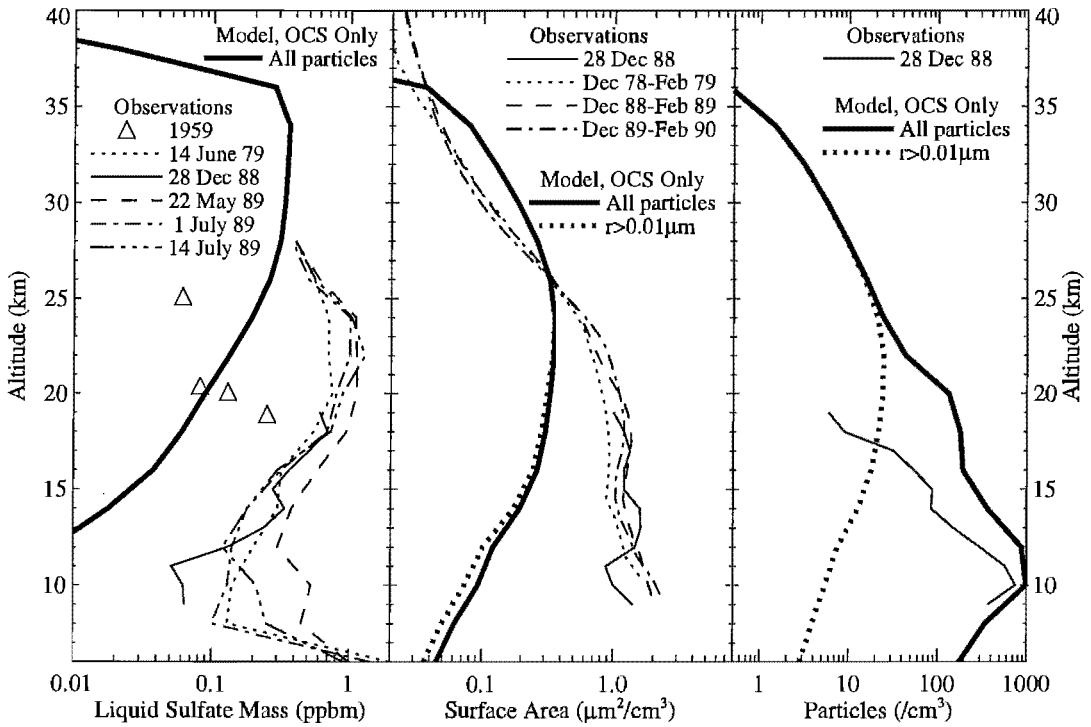

Figure 4-1 Calculated and measured aerosol properties at mid-latitudes. Measurements are retrieved from satellites, aircraft, and balloon flights (see text). Calculations are shown for the model latitude centered at 38°N, averaged for the months of December-February, and assume OCS is the sole source of sulfur to the stratosphere. A lower boundary condition of 510 pptv is assumed for OCS. Calculations of surface area and number are separated to show the contribution by particles of measurable size (radius larger than 0.01 μm).

measurements of Junge *et al.*, from 1959, indicate much lower mass mixing ratios of sulfate than that measured in later years. However, these measurements cover a very limited size range of aerosol, and thus are not readily comparable to our model results.

Surface area measurements below 20 km are consistently 3 to 10 times greater than those calculated from OCS alone. Particle counters used in aircraft and balloon flights are capable of measuring particles only as small as 0.01 μm. I therefore separate the contribution of particles of measurable size in calculated surface area and particle number profiles. The vast majority of particles the model calculates below 20 km are too small to be observed. At its peak near 10 km, observed particle concentration exceeds my calculated measurable number by 2 orders of magnitude when only OCS is considered. The calculated profile for concentration of particles greater than 0.01 μm peaks much higher, at 22 km, where more OCS-derived sulfur is available to create larger particles. In contrast, the rapid decrease in observed particle number (even as sulfate mass increases) from 10 to 19 km indicates fast coagulation combined with little nucleation of new particles in this region.

Figure 4-2 compares the OCS-only calculation to surface areas derived from near-global satellite extinction measurements. The lowest extinctions of the entire satellite record are observed in the period 1978-1979. In-situ measurements also suggest this period to be less perturbed by volcanic influences than any period since. Satellite-derived surface areas from this background period, shown for the December-February season, exceed my calculations at all latitudes in the lowest 10 km of stratosphere. Comparisons to satellite observations in other seasons within this background period show similar deficits for the OCS-only calculation.

The reason for this sulfur deficit becomes apparent when by comparing calculated SO_2, as shown in figure 4-3, to observations. Georgii and Meixner (1980) measured SO_2 in April and December 1978, as well as in 1977, at altitudes up to 5 km

above the tropopause. They report a mean of 500 pptv SO_2 in the free troposphere, 30

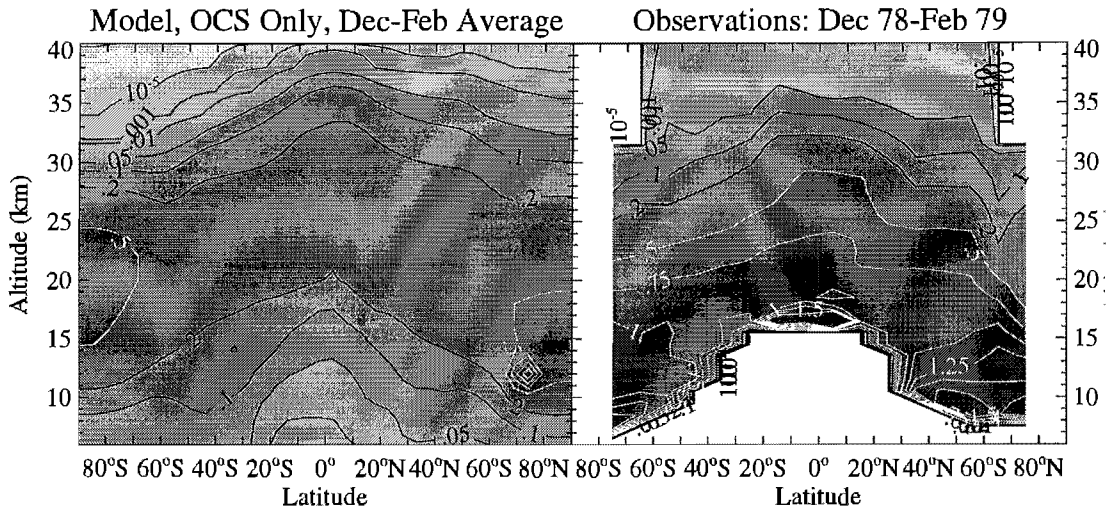

Figure 4-2 Comparison of calculated and observed global surface area distributions. The model calculation assumes OCS is the only source of sulfur to the stratosphere. Surface area units are $\mu m^2/cm^3$.

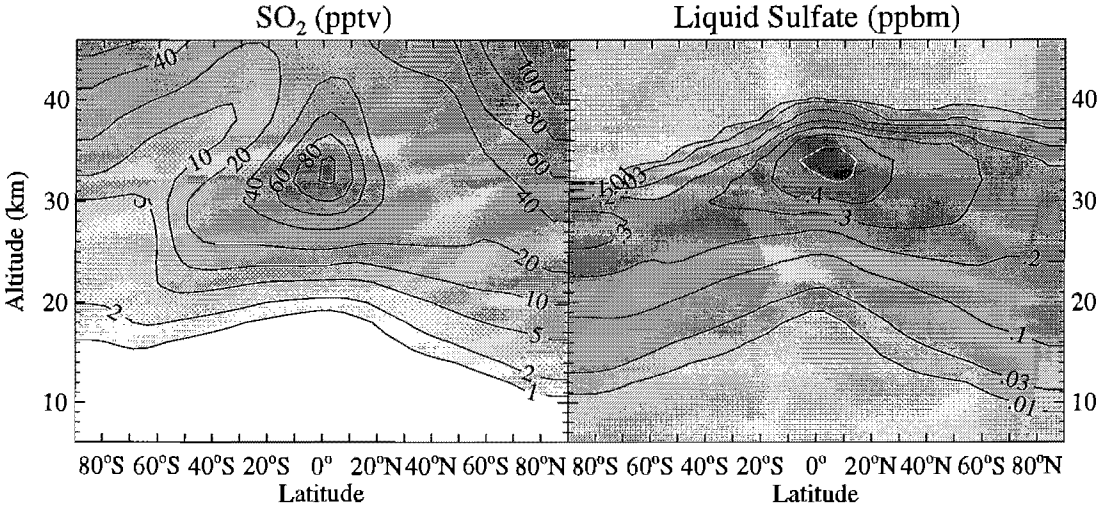

Figure 4-3 Calculated mixing ratios of SO_2 (parts per trillion by volume) and dissolved H_2SO_4 in aerosol (parts per billion by mass) resulting from observed tropospheric OCS mixing ratios (510 pptv). Model calculations are time-averaged over the December-February season.

to 170 pptv at the tropopause, with similar values in the lower stratosphere. Other measurements in the lower stratosphere report little variation with altitude, with mixing ratios between 30 and 70 pptv (Jaeschke *et al.*, 1976; Inn *et al.*, 1981). Möhler and Arnold (1992) report little vertical dependence in the troposphere, with mixing ratios varying between 50 and 400 pptv; and sharp decreases above the tropopause, with only

10 pptv just 2.5 km above the tropopause. These measurements indicate that two orders of magnitude more SO_2 is present at the tropopause than our model calculates as resulting from OCS-oxidation in the lower stratosphere. SO_2 of tropospheric origin is therefore likely to provide a major source of sulfate to the lower stratosphere.

4.2 Contribution of Tropospheric SO_2

Tropospheric SO_2, derived from a variety of sources discussed in Chapter 2, clearly does enter the stratosphere, thereby contributing to sulfate aerosol mass. I have run various cases, varying tropospheric conditions for SO_2 within observed parameters. In this section I discuss calculations that include a fixed, uniform mixing ratio for SO_2 throughout the troposphere. I do not attempt to deal with tropospheric sources and sinks for SO_2. Cases A and B maintain 200 and 400 pptv, respectively, of SO_2 in the troposphere.

Figure 4-4 shows the steady state average over one season for SO_2 in the case A and case B calculations. SO_2 mixing ratios in the troposphere and lower stratosphere match observations well, in contrast to the OCS-only case. Much as observed, SO_2 is

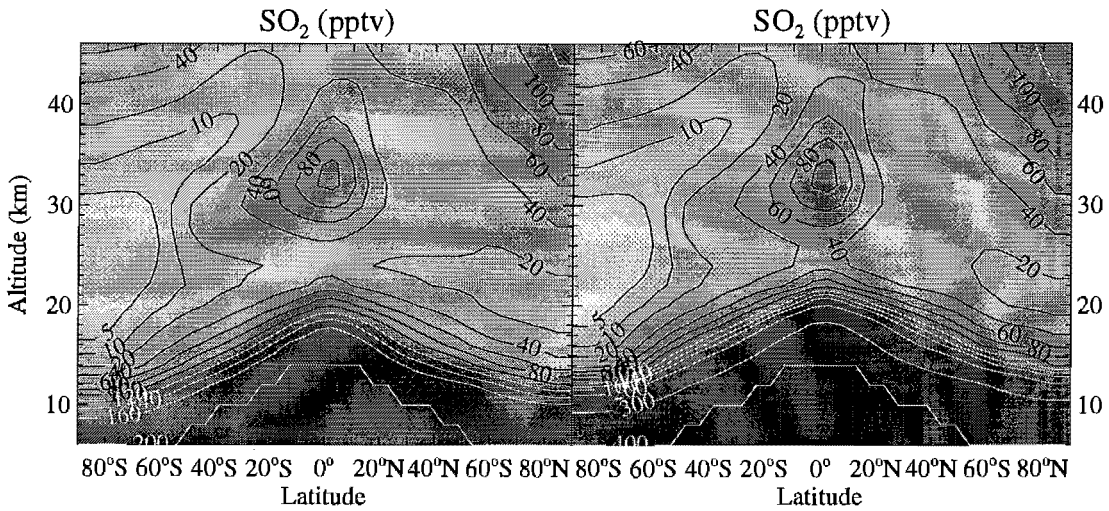

Figure 4-4 Calculated volume mixing ratios of SO_2 for case A (left) and case B (right), varying tropospheric conditions for SO_2 (see text). Calculations are averaged over the December-February season, after a run of sufficient length to reach a steady state.

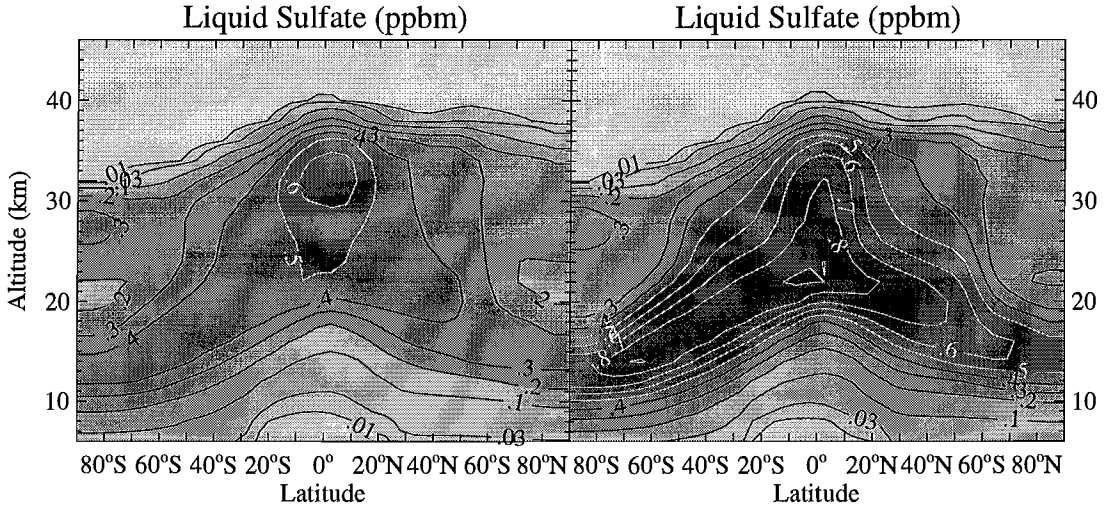

Figure 4-5 Calculated mass mixing ratios of dissolved H_2SO_4 for case A (left) and case B (right).

calculated to decrease rapidly in the first few kilometers above the tropopause. Decreasing SO_2 in the lower stratosphere corresponds to increasing liquid sulfate, shown in figure 4-5.

Above 25 km, SO_2 mixing ratios vary little in magnitude from the OCS-only calculation. SO_2 is produced at such altitudes by photolysis of gas-phase sulfuric acid.

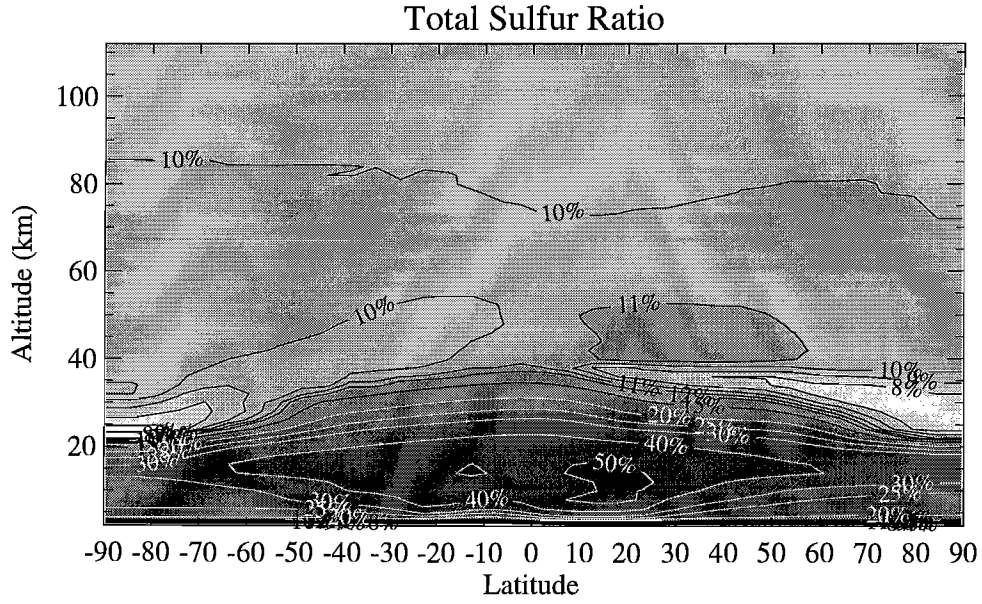

Figure 4-6 Percent increase in total sulfur from OCS-only case to case B (400 pptv SO_2 in the troposphere). Calculations are averaged over the December-February season.

The insensitivity of SO_2 in the upper stratosphere to mixing ratios in the lower stratosphere indicates that active sulfur cannot easily penetrate the sulfate layer. This conclusion is borne out in figure 4-6, which shows the percent increase in total calculated sulfur due to the addition of tropospheric SO_2. The calculated influence of tropospheric SO_2 is greatest in the lower part of the stratosphere, where it is responsible for increasing total sulfur by 30 to 50% in case B relative to the OCS-only case. At the top of the sulfate layer, however, sulfur has increased by only 10%, indicating that little of the additional sulfur provided by tropospheric SO_2 has survived. Sulfur is not conserved in the atmosphere due to sedimentation, which is the dominant loss for sulfate aerosol. Because tropospheric SO_2 is converted to sulfate aerosol rapidly upon entering the stratosphere, sulfur from this source is likely to be lost to sedimentation before it can reach the upper stratosphere.

Calculated and Observed Sulfate Mass

In examining the possible importance of SO_2 of tropospheric origin as a source of stratospheric aerosol, I begin by comparing observed and calculated sulfate mass. As figure 4-5 has illustrated, calculated sulfate mass is proportional to the chosen tropospheric mixing ratio. While, as I will show in the next section, particle size distributions and aerosol surface areas are sensitive to variations in nucleation and coagulation rates, I find that total sulfate mass is not. This finding eliminates uncertainties in my representation of these microphysical processes as a cause for discrepancies between calculated and observed mass. Calculated sulfate mass, therefore, is a good indicator of the role of tropospheric SO_2, as well as of the adequacy of my representation of other microphysical processes, notably sedimentation. I compare first the total global burden of stratospheric sulfate as calculated and as deduced from observations. I then examine my results further by comparing observed and calculated vertical distributions.

Stratospheric burdens

Table 4-2 presents the annually averaged stratospheric burdens of the major sulfur-bearing compounds for cases A and B, as well as the OCS-only case. Including 200 pptv of SO_2 in the troposphere increases the calculated sulfate burden by a factor of 5 relative to the OCS-only case, bringing it within the range of estimates derived from calculations (table 4-1). Further addition of tropospheric SO_2 generates a non-linear response in stratospheric sulfate. In case B I increase tropospheric SO_2 by an additional 200 pptv over case A. The increase in stratospheric sulfate from case A to case B is 90% of that from the OCS-only case to case A. Stratospheric sulfur other than OCS is partitioned 62% as aerosol, 16% as gas-phase sulfuric acid, and 22% as SO_2 in the OCS-only case. In case A, the partitioning is 42% aerosol, 2.2% gas-phase sulfuric acid, and 55% SO_2. In case B, the model calculates only 39% in aerosol, 1.2% as gas-phase sulfuric acid, and 59% as SO_2. The causes of these responses and repartitionings are clarified by examination of the rates of the relevant chemistry, transport, and microphysics.

The residence time of each species in the stratosphere is determined by the rate of loss due to both chemistry and transport. Above the tropopause, oxidation by OH is the only chemical loss for SO_2. I present the annually averaged rate of this reaction above the tropopause in table 4-2. Dividing the stratospheric burden of SO_2 in each case by this rate yields the lifetime for chemical loss of SO_2, shown in table 4-3. The OCS-only calculation shows that on average SO_2 oxidizes within 2 months of its production in the stratosphere. SO_2 oxidation is much slower in the lower stratosphere relative to higher altitudes due to lower concentrations of OH. Therefore SO_2 entering from the troposphere is longer-lived than that produced in the upper stratosphere by OCS oxidation. When the dominant source of stratospheric SO_2 is tropospheric SO_2, as in cases A and B, the lifetime for chemical loss increases to 4 months. For all cases,

Table 4-2 Annually averaged calculated stratospheric burdens of sulfur-bearing compounds

Tropospheric SO_2 mixing ratio		**OCS Only --**	**Case A 200 pptv**	**Case B 400 pptv**
Stratospheric burden (molecules)				
Sulfate	$[H_2SO_4(l)]$	4.38x10^{32}	2.21x10^{33}	3.80x10^{33}
Gas-phase H_2SO_4	$[H_2SO_4(g)]$	1.12x10^{32}	1.18x10^{32}	1.22x10^{32}
SO_2	$[SO_2]$	1.54x10^{32}	2.90x10^{33}	5.69x10^{33}
OCS	$[OCS]$	1.11x10^{34}	1.11x10^{34}	1.11x10^{34}
Total sulfur	$[SO_y]$	1.18x10^{34}	1.63x10^{34}	2.07x10^{34}
Non-OCS sulfur	$[SO_y]-[OCS]$	7.15x10^{32}	5.26x10^{33}	9.67x10^{33}
Stratospheric rate (molecules/s)				
OCS $\rightarrow$ SO_x	$(R_{OCS\rightarrow SO_x})$	2.69x10^{25}	2.69x10^{25}	2.69x10^{25}
SO_2+OH$\rightarrow$$HSO_3$	(R_{SO_2+OH})	2.97x10^{25}	2.92x10^{26}	5.24x10^{26}
SO_3+$H_2$0(g)$\rightarrow$$H_2SO_4$(g)	$(R_{SO_3+H_2O})$	3.09x10^{25}	3.04x10^{26}	5.44x10^{26}
SO_3 condensation	(C_{SO_3})	3.29x10^{22}	5.16x10^{23}	1.52x10^{24}
H_2SO_4 condensation	$(C_{H_2SO_4})$	2.85x10^{25}	2.74x10^{26}	4.98x10^{26}
H_2SO_4 nucleation	(R_{nuc})	4.36x10^{22}	3.26x10^{25}	5.76x10^{25}
H_2SO_4(g)+hv$\rightarrow$$SO_2$	$(J_{H_2SO_4})$	3.28x10^{24}	3.43x10^{24}	3.57x10^{24}
H_2SO_4 sedimentation	$(-T_{sed})$	2.37x10^{25}	4.95x10^{25}	7.87x10^{25}
Net H_2SO_4 (g) transport out	$\left(-T_{H_2SO_4^g}\right)$	-1.03x10^{24}	2.65x10^{23}	4.34x10^{23}
Net H_2SO_4 transport out	$(-T_{H_2SO_4})$	4.05x10^{24}	2.51x10^{26}	4.63x10^{26}
Net SO_2 transport in	(T_{SO_2})	5.35x10^{22}	2.74x10^{26}	5.16x10^{26}

however, the average oxidation time is much shorter than the average stratospheric residence time for air, suggesting that transport of SO_2 back to the troposphere represents a negligible loss for the total stratospheric burden. The SO_2 chemical loss lifetimes shown in table 4-3 are therefore good estimates for the total stratospheric lifetimes.

Table 4-3 Stratospheric lifetimes of sulfur-bearing compounds in units of days.

		OCS Only	Case A	Case B
SO_2 chemical loss	$\left(\frac{[SO_2]}{R_{SO_2+OH}}\right)$	60	115	126
SO_2 transport production	$\left(\frac{[SO_2]}{T_{SO_2}}\right)$	34000	115	128
SO_2 chemical production	$\left(\frac{[SO_2]}{R_{OCS\rightarrow SO_x}}\right)$	66	1250	2500
H_2SO_4 loss	$\left(\frac{[H_2SO_4(g)+(l)]}{-T_{sed}-T_{H_2SO_4}+J_{H_2SO_4}}\right)$	207	89	83
H_2SO_4 production	$\left(\frac{[H_2SO_4(g)+(l)]}{R_{SO_3+H_2O}+C_{SO_3}}\right)$	207	89	83
Sulfate production	$\left(\frac{[H_2SO_4(l)]}{C_{SO_3}+C_{H_2SO_4}+R_{nuc}}\right)$	178	83	79
H_2SO_4 (g) production	$\left(\frac{[H_2SO_4(g)]}{R_{SO_3+H_2O}}\right)$	42	4.5	2.6
Non-OCS sulfur oxidation	$\left(\frac{[SO_y]-[OCS]}{R_{SO_2+OH}}\right)$	277	208	214
Non-OCS sulfur loss	$\left(\frac{[SO_y]-[OCS]}{-T_{sed}-T_{H_2SO_4}}\right)$	299	203	206

I now examine the relative timescales for production of stratospheric SO_2 by transport and chemistry in each of these cases. I define the SO_2 transport lifetime as the ratio of the total SO_2 stratospheric burden to the net flux of SO_2 from the troposphere to the stratosphere. Because very little SO_2 escapes back to the troposphere unoxidized, this net flux is essentially the flux of all SO_2 molecules entering the stratosphere from the troposphere. The chemical production lifetime is the ratio of the same burden to the total rate of OCS oxidation by OH, O, and photolysis. In the OCS-only case transport of SO_2 from the troposphere is minimal, and would require an unphysical accumulation over 90 years to produce the calculated stratospheric burden. Stratospheric SO_2 production is therefore dominated by OCS oxidation in this case, as confirmed by the proximity of the chemical production lifetime to the loss lifetime. By contrast, OCS oxidation would require 3.5 to 7 years to produce the stratospheric SO_2 burdens in cases A and B. In these cases it is the transport lifetimes which are comparable to the

chemical loss lifetimes. The stratospheric SO_2 burden is clearly driven by transport from the troposphere in cases A and B.

Production of sulfuric acid (gas-phase plus sulfate aerosol) is dominated by chemistry, while loss is largely dynamical, with some loss to photolysis in the upper stratosphere and mesosphere. In table 4-3 I present the lifetimes for loss and production of sulfuric acid. The latter is defined solely by chemistry, as the ratio of the total stratospheric burden to the rate of SO_3 oxidation by either gas- or aerosol-phase water. Chemical production is dominated by the gas-phase reaction of SO_3 and water to produce gas-phase sulfuric acid. This reaction occurs much faster in my calculation than uptake and oxidation of SO_3 in aerosol, which produces sulfate (see table 4-2). In each case, the chemical production lifetime matches the lifetime for loss defined by atmospheric transport, particle sedimentation, and photolysis.

Particle sedimentation dominates loss of stratospheric sulfuric acid in the OCS-only case, removing sulfuric acid about six times faster than either atmospheric transport or photolysis. When I include tropospheric SO_2 in cases A and B, atmospheric transport overtakes sedimentation as the predominant removal mechanism. Tropospheric SO_2 produces aerosol predominantly in the lower stratosphere, where it is susceptible to the exchange of air parcels with the troposphere. OCS produces aerosol at higher altitudes, where it is more likely to grow large enough to fall out of the stratosphere before atmospheric transport removes it. Sedimentation removes sulfate on a timescale of 7 months in the OCS-only case, leaving little to be removed by the circulation. In contrast, sulfate is removed by atmospheric transport in case A on a timescale of only 3.4 months, leaving relatively few particles time to grow large enough to fall out.

In all of the model cases sedimentation plays a very important role in limiting mixing ratios of active sulfur in the mid- and upper-stratosphere. In case B, for example, 15% of sulfate particles are removed by sedimentation and 85% by

atmospheric transport. When sedimentation is not included, the steady-state stratospheric burden of sulfate increases by 70%, while the total removal rate decreases by 7.5%. The dynamical lifetime of sulfate therefore increases by 80%, to 150 days. The vertical distribution of sulfate also changes significantly, peaking at higher altitudes. The burden of stratospheric aerosol in background periods is limited by both sedimentation and exchange of air with the troposphere.

The stratospheric sulfur contributed by tropospheric SO_2 remains largely below altitudes at which sulfuric acid photolysis is likely to occur. Hence loss of sulfuric acid to photolysis increases little from the OCS-only case to cases A and B. The sharp decrease in the average stratospheric lifetime of sulfuric acid (gas plus liquid), from near 7 months in the OCS-only case to near 3 months in cases A and B, is entirely due to increased removal by atmospheric transport. Sulfate that reaches the mid- and upper-stratosphere is effectively removed by sedimentation. The remainder, in the lower stratosphere, is exchanged on a short timescale with tropospheric air.

The average lifetime of sulfuric acid can be further divided into the lifetimes of the gas and liquid phases, as is done in table 4-3. With the addition of tropospheric SO_2 in cases A and B, the average gas-phase H_2SO_4 lifetime decreases by a much greater factor than does the sulfate lifetime. In all cases loss of gas-phase sulfuric acid is dominated by condensation onto existing aerosol. The much larger concentrations of aerosol in the lower stratosphere in cases A and B increase condensation rates by an order of magnitude, reducing the lifetime proportionately. Loss of gas-phase H_2SO_4 to homogeneous nucleation also increases by two orders of magnitude. Nucleation is greatly favored in the lower stratosphere relative to higher altitudes. Despite the enormous relative increase, rates of loss of gas-phase H_2SO_4 to nucleation are still only one-tenth of those to condensation in cases A and B.

In the steady state generated in my calculations, total sulfur transported into the stratosphere equals total sulfur transported out. Sulfur is transported from the

troposphere to the stratosphere predominantly as OCS and SO_2. It is returned to the troposphere predominantly as OCS and sulfate. The reaction rate for SO_2 + OH is a good measure of the rate of the sulfur oxidative process in the stratosphere. By dividing the stratospheric burden of non-OCS sulfur by this rate, I derive an estimate of how long sulfur is present from its arrival as SO_2 (from either OCS oxidation or transport from the troposphere) to its exit as sulfuric acid (by sedimentation or the mean circulation). A similar estimate may be obtained by dividing the non-OCS sulfur burden by the rate of removal of sulfuric acid from the stratosphere.

Table 4-3 shows estimates of this stratospheric lifetime by both methods. For the OCS-only case I find that oxidized sulfur remains in the stratosphere for an average of 9 to 10 months. The residence time decreases in case A to 7 months, as the bulk of the oxidized sulfur moves to the lower in the stratosphere, where it is removed more rapidly. This residence time does not decrease further with the further addition of tropospheric SO_2 in case B, as the vertical profile of oxidized sulfur does not change dramatically.

Altitude profiles

Figure 4-7a compares the observed mid-latitude profiles of sulfate mass mixing ratio (see figure 4-1) to model calculations including tropospheric SO_2. Looking first at case A, with 200 pptv of SO_2 in the troposphere, I note a significant deficit in calculated sulfate mass between 16 and 26 km, where observations indicate the peak of the aerosol layer to be. As case B demonstrates, further increases in tropospheric SO_2 preferentially impact sulfate mass below 20 km, with lesser effect at higher altitudes. With these elevated SO_2 levels, calculated sulfate mass reaches a maximum in the lower stratosphere at mixing ratios similar to the observed background peak. However, while observed mass mixing ratio peaks between 22 and 24 km, my calculations peak between 18 and 20 km. The additional sulfur from the tropospheric SO_2 is not

transmitted high enough to account for the observed mid-latitude mixing ratios between 20 and 25 km.

Particle sedimentation limits the penetration of sulfur from tropospheric SO_2 into the stratosphere. I test, therefore, whether reduced sedimentation could improve calculated mid-latitude sulfate profiles in comparison to observations. Cases C and D repeat the conditions of cases A and B, respectively, with sedimentation rates reduced by a factor of 2. As shown in figure 4-7b, this adjustment does increase sulfate mass above 20 km. However, these increases are not distributed properly to improve comparison to observations. In particular, calculated sulfate mass does not decrease rapidly above 25 km, as is observed. Above 25 km, cases A and B resemble the observations better than cases C and D. Exaggerated sedimentation is therefore not likely to explain the discrepant mass profile.

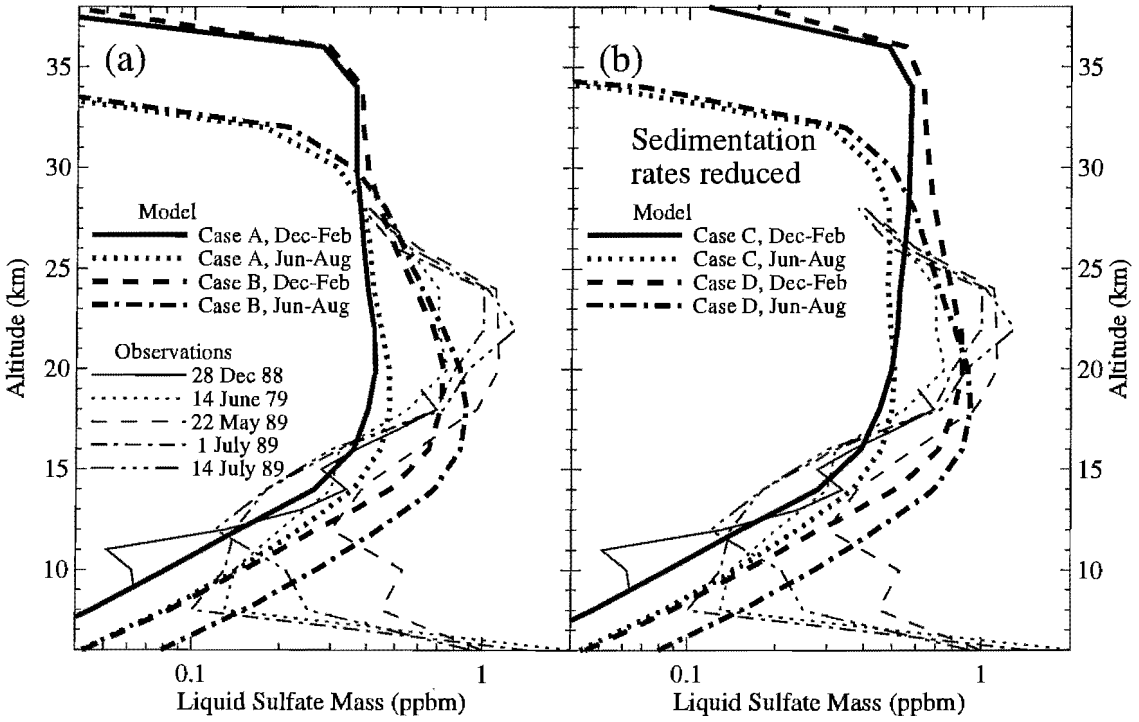

Figure 4-7 Observed and calculated mid-latitude profiles of sulfate mass mixing ratios. Calculations represent averages of steady-state results over the December-February and June-August seasons at 38°N. Cases A and C maintain 200 pptv of tropospheric SO_2, while cases B and D maintain 400 pptv. Cases C and D reduce calculated sedimentation rates by half. Observations are the same as those presented in figure 4-1 (see text).

Case B, with 400 pptv of SO_2 throughout the troposphere, represents the high end of observed tropospheric mixing ratios, especially near the tropopause. Case A is more representative of the average observed tropospheric SO_2. Figure 4-7a makes clear the significance of the mass deficit between 18 and 26 km for the case A calculation. I have shown that neither additional tropospheric sulfur nor decreased sedimentation improve comparison to observations in this region without degrading comparison at other altitudes. I have also found calculated sulfate mass to be insensitive to other microphysical parameters, such as nucleation and coagulation rates. It is likely therefore that the observations result from a source of sulfur not included in our model.

The source of the observed sulfate mass peak between 16 and 26 km remains unknown. This peak region shows the clearest distinction in observed mass mixing ratios between the 1979 and 1988-89 periods. The source of sulfur to this region is therefore likely to be time-varying. Hofmann (1990) notes this increase in mass and a corresponding increase in the number of large particles. Given the calculated residence times of less than one year for nonvolcanic sulfur, it is unlikely that stratospheric aerosol in the observed periods has retained significant sulfate mass from large recorded eruptions observed several years prior. Small unrecorded eruptions, which may have occurred more immediately before the observations, are a possible source. A significant reduced sulfur compound, one that is largely inert in the troposphere yet dissociates more rapidly than OCS in the stratosphere, remains another possibility. A definitive answer is not provided by this work.

Particle Number and Surface Area

While the discrepancies between calculated and observed sulfate mass suggest a missing source of sulfur, discrepancies in particle number and surface area reflect

uncertainties inherent in microphysical processes. Figure 4-8 compares observed aerosol surface area and particle number to various calculations. Both cases A and B overestimate aerosol surface area in the lower stratosphere and particle number throughout the stratosphere. Both also underestimate the number of large particles. There are large uncertainties inherent in the nucleation and coagulation rate calculations.

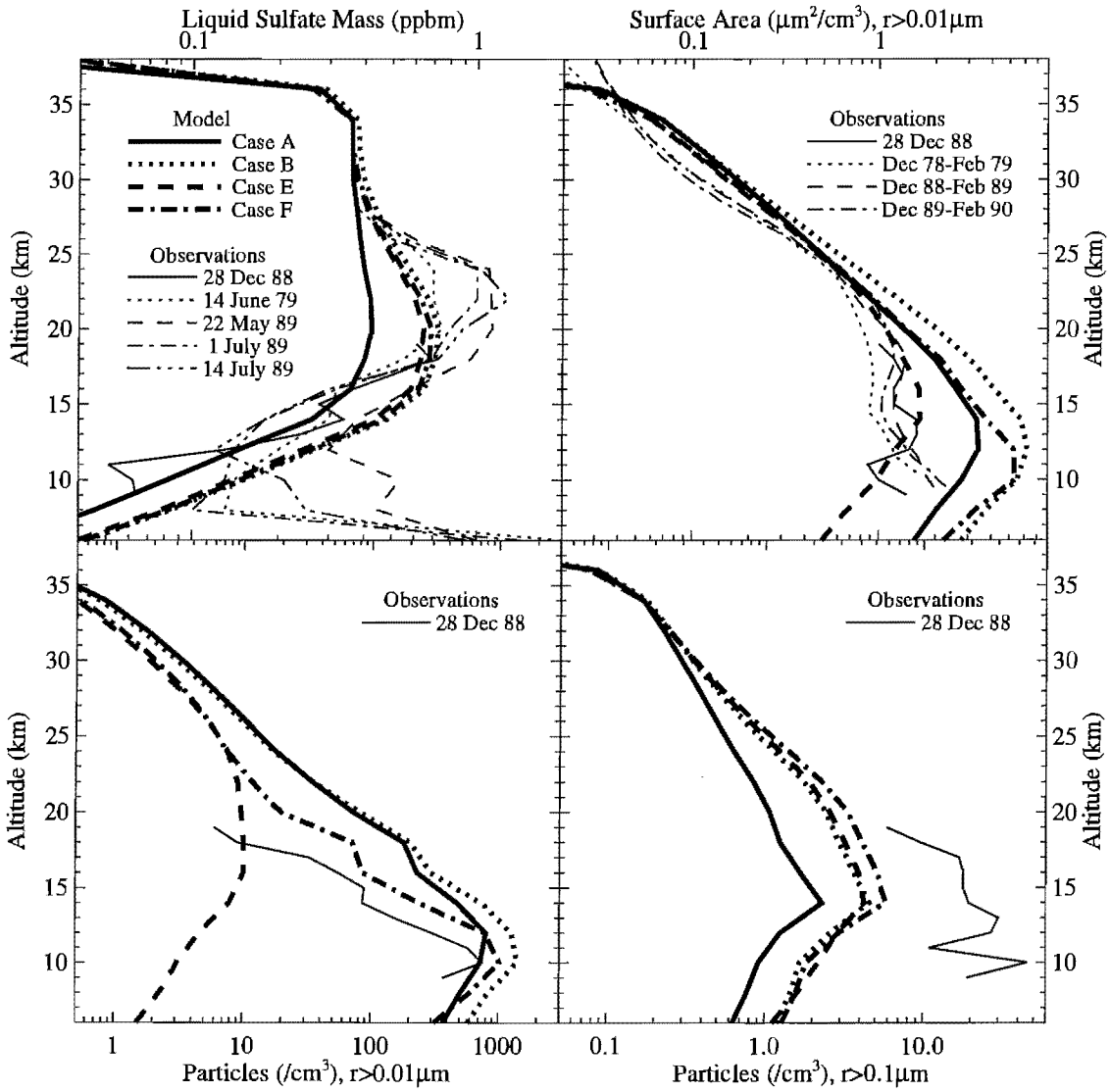

Figure 4-8 Comparison of measured aerosol mass, surface area, and number densities for particles greater than 0.01μm and 0.1μm to model cases. Calculations are shown at 38°N, averaged over the December-February season. Case A assumes 200 pptv SO_2 throughout the troposphere. Cases B, E, and F assume 400 pptv throughout the troposphere. Case E includes an empirical correction factor to nucleation rates. Case F decreases nucleation rates by a factor of 10, and increases coagulation rates by a factor of 4 (relative to case B).

By adjusting these rates within uncertainties, I can significantly change these calculated profiles, improving comparison to the observations.

I first examine the effect of the empirical correction for nucleation rates determined by Wyslouzil, and discussed in detail in Chapter 3. This correction factor dramatically reduces nucleation rates for critical nuclei containing less than 15 acid molecules, while enhancing nucleation rates for larger nuclei. The effect in my calculations is to greatly reduce nucleation rates in the lower stratosphere. Inclusion of this correction factor reduces aerosol surface area in the lower stratosphere, appearing to bring the calculations in line with observations (see case E in figure 4-8). The calculated particle density profile, on the other hand, has become dramatically worse in comparison to observations. Clearly the reduction in particle number due to this correction is far too large, and size distributions in the lower stratosphere are less accurate when it is included.

A better comparison to observations is obtained by less dramatic adjustment of microphysical parameters, as in case F. In this calculation I reduce particle number by decreasing nucleation rates uniformly by a factor of 10, and increasing coagulation rates by a factor of 4. As I have explained in Chapter 3, uncertainties in numerous physical parameters generate uncertainties of several orders of magnitude in the calculated nucleation rates. My coagulation calcuation may be in error; my calculated rates are lower by a factor of 2 than previous calculations. Van Dingenen and Raes (1990) show that Van der Waals forces, a factor not included in my model, enhance coagulation of sulfate aerosol particles less than 0.1 μm by up to a factor of 4.. Of the four cases shown case F compares best with the observed profiles of particles greater than 0.01 and 0.1 μm.

Figure 4-9 presents observed and calculated global distributions of aerosol surface area, an important parameter to heterogeneous chemistry. Surface area,

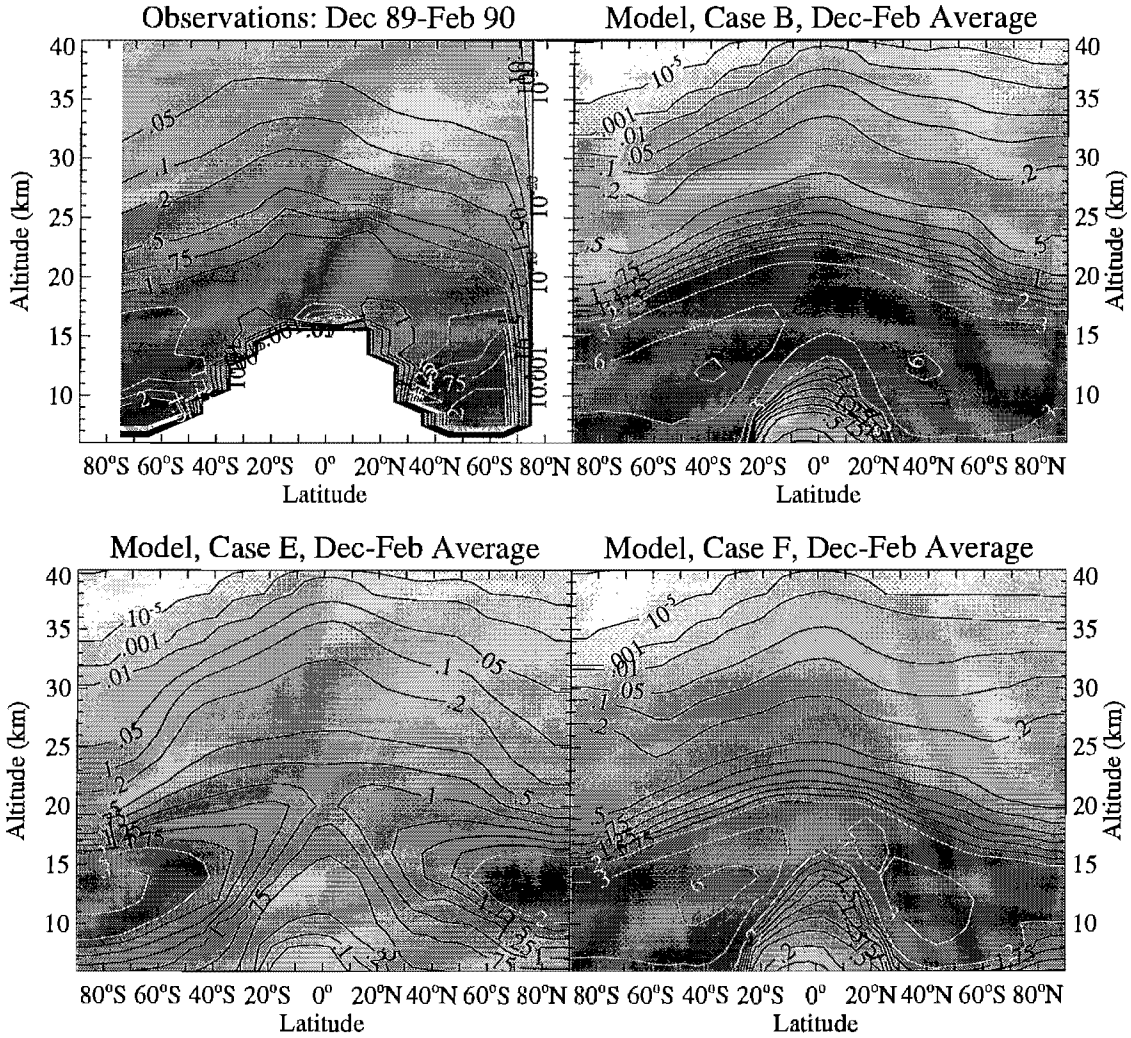

Figure 4-9 Observed and calculated global aerosol surface area ($\mu m^2/cm^3$) contribution from particles of radius greater than 0.01 μm. Observations are inferred from satellite measurements. Model cases B, E, and F assume 400 pptv of SO_2 throughout the troposphere, and results are averaged for the December-February season. Case E includes an empirical correction factor to nucleation rates. Case F reduces nucleation by a factor of 10, and increases coagulation rates by a factor of 4 relative to case B.

however, is not a good indicator of the accuracy of calculated size distributions. As I have already noted, case E appears to match observations well when we look only at surface area, but is actually incorrect by more than two orders of magnitude in particle number in the lower stratosphere. Likewise, case F significantly overestimates surface areas in the lower stratosphere, while proving the best match to particle concentration profiles. Profiles of particle number and sulfate mass are more unique constraints on

the calculations. Discrepancies between observed and calculated surface areas do, however, point to important uncertainties in the microphysics. The nature of these discrepancies is best revealed by comparison of observed and calculated particle size distributions.

Size Distributions

Finally, I compare calculated size distributions to those inferred from observations. Figure 4-10 shows size distributions inferred from various in-situ mid-latitude measurements presented in Turco *et al.* (1982). These observations were made at altitudes ranging from 0 to 12 km above the tropopause at mid-latitudes. Comparison to calculated size distributions reveals significant discrepancies. Model cases A and B predict much greater numbers of small particles ($r < 0.05$ μm) and lesser numbers of large particles ($r > 0.2$ μm) than are observed.

Calculated size distributions for model cases B, E and F are compared to the observations in Figure 4-10. These cases reveal the sensitivity of the calculations to adjustments in nucleation and coagulation rates. When the model includes Wyslouzil's empirical correction to calculated nucleation rates, calculated particles in the lower stratosphere conform to lognormal distributions, with relatively few particles smaller than 0.02 μm except within a few kilometers of the tropopause. Likewise, concentrations of particles larger than 0.2 μm increase relative case B, conforming better to observations. However, this dramatic reduction in nucleation reduces total particle concentrations near the tropopause well below those observed. The peak concentration of the size distributions increases with altitude in case E, whereas the observations show uniform decreases. Observations support the idea that nucleation is greatest near the tropopause. Our model predicts such behavior, except when the empirical correction is included, as in case E.

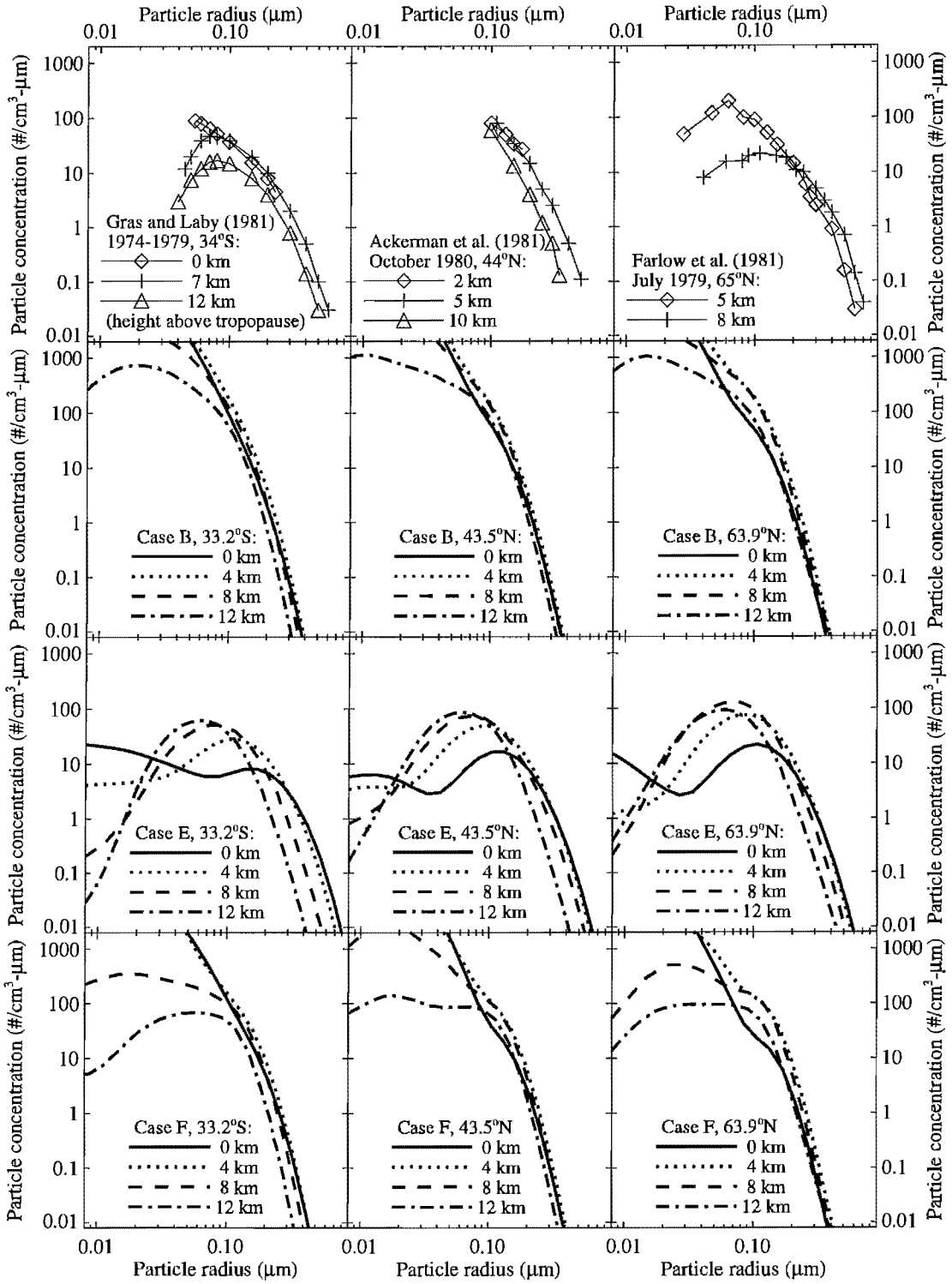

Figure 4-10 Particle size distributions derived from observations (top row) and calculated for model cases B, E and F, with height above the tropopause listed. Cases B, E, and F assume 400 pptv throughout the troposphere. Case E includes an empirical correction factor for calculated nucleation rates. Case F reduces calculated nucleation by a factor of 10 and increases coagulation by a factor of 4.

Case F demonstrates the sensitivity of calculated size distributions to much more moderate microphysical adjustments. By decreasing nucleation uniformly by a factor of 10 and increasing coagulation by a factor of 4 over case B, the model significantly decreases concentrations of small particles several kilometers above the tropopause and increase concentrations of large particles, improving comparison to observations. These adjustments are within the range of uncertainty inherent in the microphysical calculations. Discrepancies between the calculations and observations are likely due to such moderate uncertainties, rather than to the extreme empirical modification in nucleation rates suggested by Wyslouzil's experiments.

Figure 4-11 compares calculated median particle radii to those inferred from observations. The observed median radii, presented in Hofmann (1990), are inferred from integral counts of particles of radius greater than 0.01, 0.15, and 0.25 μm, assuming a lognormal size distribution. The calculated median radii for cases A and B correspond to the low end of the range of observations below about 14 km, and fit very

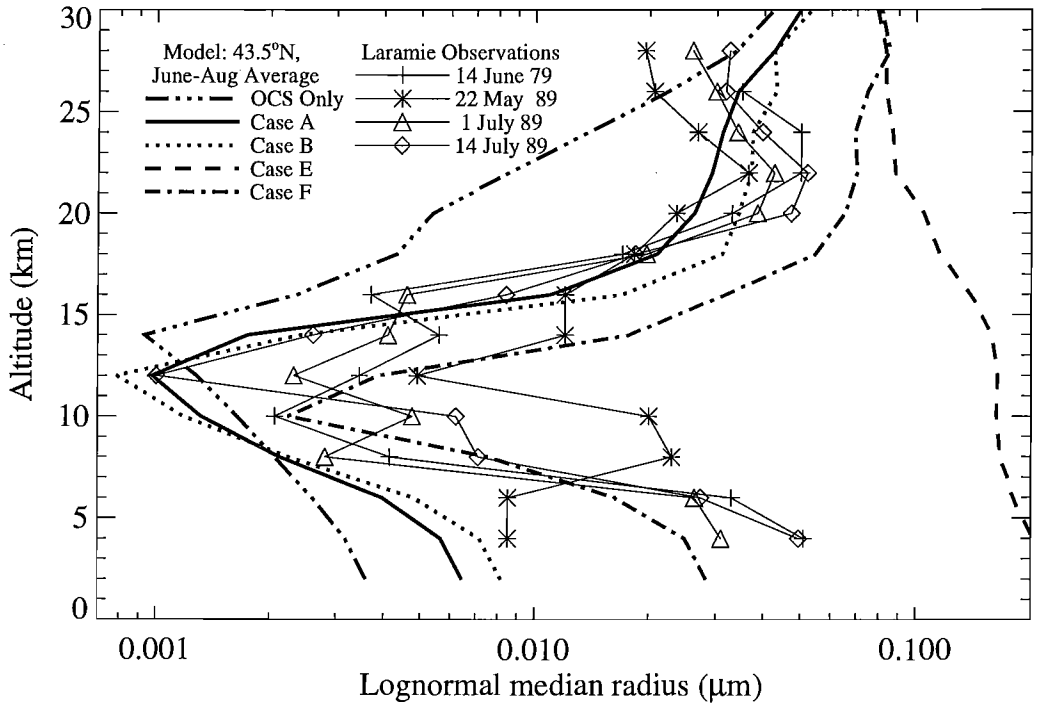

Figure 4-11 Calculated and observed median particle radius versus altitude.

well at higher altitudes. My model calculations indicate that Hofmann's assumption of a lognormal distribution appropriate to these higher altitudes than near the tropopause, where nucleation rates are high. The moderate decrease in nucleation and increase in coagulation in case F increase the median radius by a factor of about 4 at all altitudes, bringing calculations well within the observed range near the tropopause while appearing to worsen comparison at higher altitudes. Median radii in Case E are clearly well outside the range of observations at all altitudes, demonstrating again that the empirical nucleation correction does not improve comparison between the model and observations.

4.3 Conclusions

Model calculations indicate that carbonyl sulfide does not dissociate sufficiently in the lower stratosphere to provide the bulk of the sulfate observed in the stratospheric aerosol layer in volcanically quiescent periods. Within about 6 km of the tropopause, much of the deficit is likely made up by sulfur dioxide of tropospheric origin, observed at mixing ratios of up to 400 pptv throughout the troposphere. Between about 8 and 14 km above the tropopause, however, additional sources appear necessary to account for observed sulfate mixing ratios. Candidates include small volcanic eruptions and reduced sulfur compounds.

Calculated particle size distributions are quite sensitive to calculated nucleation rates, which are subject to large uncertainties. The base model scenario calculates too many small particles, and too few large particles compared to observations. Reduction of nucleation rates within current uncertainties can improve this comparison significantly. Observations are consistent with model calculations in which nucleation occurs predominantly within a few kilometers of the tropopause. The median radii of the calculated size distributions compare well to those observed.

Chapter 5

Polar Winter Nucleation and Nitric Acid

The behavior of aerosol in polar regions has been of particular interest to atmospheric chemists in recent years. Exceptionally low temperatures in winter and spring make the polar stratosphere particularly favorable for heterogeneous chemistry. Reactions on aerosol are, for example, key to the dramatic seasonal enhancement of halogen-catalyzed loss of ozone, known as the "ozone hole", in the vernal Antarctic lower stratosphere. Microphysical aerosol processes, such as uptake of nitric acid and sedimentation, play substantial roles in the establishment and maintenance of the ozone hole. In this chapter I investigate the effects of microphysical processes and heterogeneous chemistry in the lower and middle polar stratosphere. The calculations offer explanations of observed variations in aerosol and nitric acid in the region of the ozone hole and at higher altitudes.

5.1 The Anomalous "CN Layer"

Observations and Theories

Rosen and Hofmann (1983) noted an anomalous enhancement in particle concentration near 30 km at mid-latitudes in air of recent Arctic origin. Similar enhancements were later observed from September to November over Antarctica

(Hofmann *et al.*, 1985; Hofmann, 1988; Wilson *et al.*, 1989), and in January and February over the Arctic (Hofmann, 1990b; Wilson *et al.*, 1990). This high-altitude local maximum in particle number is not observed in summer, indicating that new particles form in the polar stratosphere between 20 and 30 km on a seasonal basis. The maximum is seen in the total particle measurement, which detects all particles larger than 0.01 μm radius. Experimentalists term this measurement the "condensation nuclei" (or "CN") count, indicating that the population count is dominated by the smallest particles. Thus the polar anomaly in total particles has become known as a "CN layer".

A series of Antarctic balloon measurements at McMurdo Station (78°S) show significant increases in particle number between 20 and 30 km coinciding with the arrival of sunlight in spring. Balloon-borne measurements from 1987 indicate a small layer of ~20 particles/cm^3 at 24-28 km developing by the time of the first measurement, on 31 August. Subsequent high-altitude observations inside the vortex in mid-October revealed a well-developed layer, with concentrations as high as 100 cm^{-3} between 20 and 24 km (Hofmann *et al.*, 1989). In 1988, measurements by the same method at the same site show the layer developing at 22-26 km from 20-30 cm^{-3} on 27 August, to over 100 cm^{-3} by 6 September (Hofmann, 1990b). Measurements in 1989 show the layer developing through September, with the peak increasing from ~60 cm^{-3} at 25 km in early September, to ~150 cm^{-3} at 23 km in late September (Hofmann and Deshler, 1991). A sequence of three balloon profiles from McMurdo in 1993 shows the layer already well-defined by 24 August, with a peak of ~50 cm^{-3} at 25 km; increasing to more than 200 cm^{-3} at 23.5 km on 9 September; and descending to 21 km on 23 September, with a slightly higher concentration (Deshler *et al.*, 1994). These isolated measurements indicate significant year-to-year variation in the timing and magnitude of the observed layer.

Rosen and Hofmann (1983) offer two hypotheses with their initial discovery. The first relates the seasonal variation in particle concentration to the variation of sunlight at high latitude. This photochemical theory conjectures that polar OCS might maximize in winter, due to lack of sunlight available to liberate the sulfur. With the return of sunlight in spring, OCS would dissociate, producing a burst of gas-phase sulfuric acid available to nucleate new particles. The lifetime of OCS against destruction by photolysis, OH, and O decreases rapidly with increasing altitude, and the available OCS might be thus oxidized on the order of weeks above 35 km.

Rosen and Hofmann's second hypothesis pertains to the rapid changes in temperature in polar winter. Sudden stratospheric warmings could evaporate existing sulfate aerosol. A subsequent drop in temperature associated with rapid transport to mid-latitudes would reduce the equilibrium concentration of sulfuric acid vapor over liquid, creating very large supersaturations. The excess of ambient vapor would then either condense on existing particles, or, in their absence, nucleate new ones. The region of new particle formation is confined in altitude by the presence of preexisting particles at lower altitudes, and by increasing equilibrium vapor pressures at higher altitudes. The upper limit, shown with seasonal and latitudinal variation in figure 3-9, is defined by the requirement that total ambient sulfuric acid must exceed equilibrium vapor pressure for liquid sulfate to exist. At higher altitudes, temperatures increase and sulfate boils away.

Rosen and Hofmann define the minimum altitude for nucleation by requiring that collisions between H_2SO_4 molecules occur more rapidly than condensation of these molecules onto existing particles. They calculate that the minimum gas-phase H_2SO_4 concentration required to satisfy this condition lies between 10^5 and 10^6 molecules/cm^3. Further, these new particles must grow to detectable size ($r > 0.01$ μm) in the time period available. Rosen and Hofmann calculate that such rapid condensation requires a minimum H_2SO_4 vapor concentration of 1.5×10^6

molecules/cm^3. Based on these upper- and lower-altitude constraints, Rosen and Hofmann predict that nucleation and growth to observable size is possible in polar regions between 30 and 35 km.

Hamill *et al.* (1990) take this explanation a step further, calculating nucleation rates from binary homogeneous nucleation theory. The conditions used in this calculation represent a single altitude profile of observed temperature and calculated sulfuric acid vapor, representative of the Antarctic before the onset of winter. Calculated nucleation rates were significant up to 27 km. Absent an interactive microphysical code accounting for condensation and coagulation of particles, the authors conclude that a translation of these nucleation rates to particle number is not straightforward. They expect coagulation and condensation on larger existing particles to quickly reduce concentrations of nucleated particles and sulfuric acid vapor, respectively, in the lower stratosphere. They also anticipate a source of sulfuric acid vapor at high altitudes, due to convergence of evaporated sulfate from lower latitudes and higher altitudes. According to Hamill *et al.*, these two effects explain increasing particle concentrations from 20 to 30 km in the polar stratosphere.

If new particle formation results simply from a sudden drop in temperature, we would expect to see the CN layer at the onset of winter. The observed dramatic increase in particle number over Antarctica, however, coincides with the return of sunlight in the spring. Rosen and Hofmann (1983) invoke sudden stratospheric warmings associated with the breakup of the polar vortex to explain the timing of this event. They reason that if such springtime warmings evaporate existing large ($r>0.1$ μm) particles, subsequent cooling could lead to production of many more small particles.

Zhao *et al.* (1995) question whether sufficient sulfuric acid is present in polar winter, absent photochemical production, to initiate the temperature-dependent mechanism of Rosen and Hofmann (1983). Using a 1-dimensional microphysical

model they calculate that OCS oxidation can not provide sufficient sulfuric acid vapor to allow new particles to grow to observable size. They postulate that "extra" sulfur required for the formation of the layer can be provided by SO_2 descending from the mesosphere. The source of this SO_2 is H_2SO_4 photolysis. By setting upper boundary conditions of 100 pptv for both SO_2 and H_2SO_4 at 60 km and allowing for vertical subsidence, Zhao *et al.* are able to calculate the formation of a layer of particles similar to that which is observed. The strength of the layer is found to be much more sensitive to the SO_2 concentration than the H_2SO_4 concentration. SO_2 accumulates in the polar night, serving as a sulfur reservoir until the return of sunlight in spring, while gas-phase sulfuric acid is lost on existing particles throughout the winter and does not accumulate to the required degree.

Model Calculations

The model produces a layer of particles in polar regions that conforms well to observations. Figure 5-1 shows calculated time and altitude variation for temperature, nucleation rates, and particle concentrations over one year at 79°S. The calculations shown are for the Case B scenario, which maintains 400 pptv SO_2 throughout the troposphere (see Chapter 4).

A small, but significant rate of nucleation initiates near 30 km as early as April (days 90-120), in the austral autumn. This slow nucleation phase continues throughout the winter, as cold temperatures (near 220 K) reach higher altitudes. At any given altitude nucleation returns to negligible rates within several weeks of its initiation, despite continued decreases in temperature. Nucleation terminates once ambient sulfuric acid vapor becomes depleted by both nucleation itself and subsequent condensation onto nucleated particles. The weak winter phase of nucleation produces small concentrations (10-50 /cm^3) of particles, of which fewer than 20 /cm^3 grow to observable size.

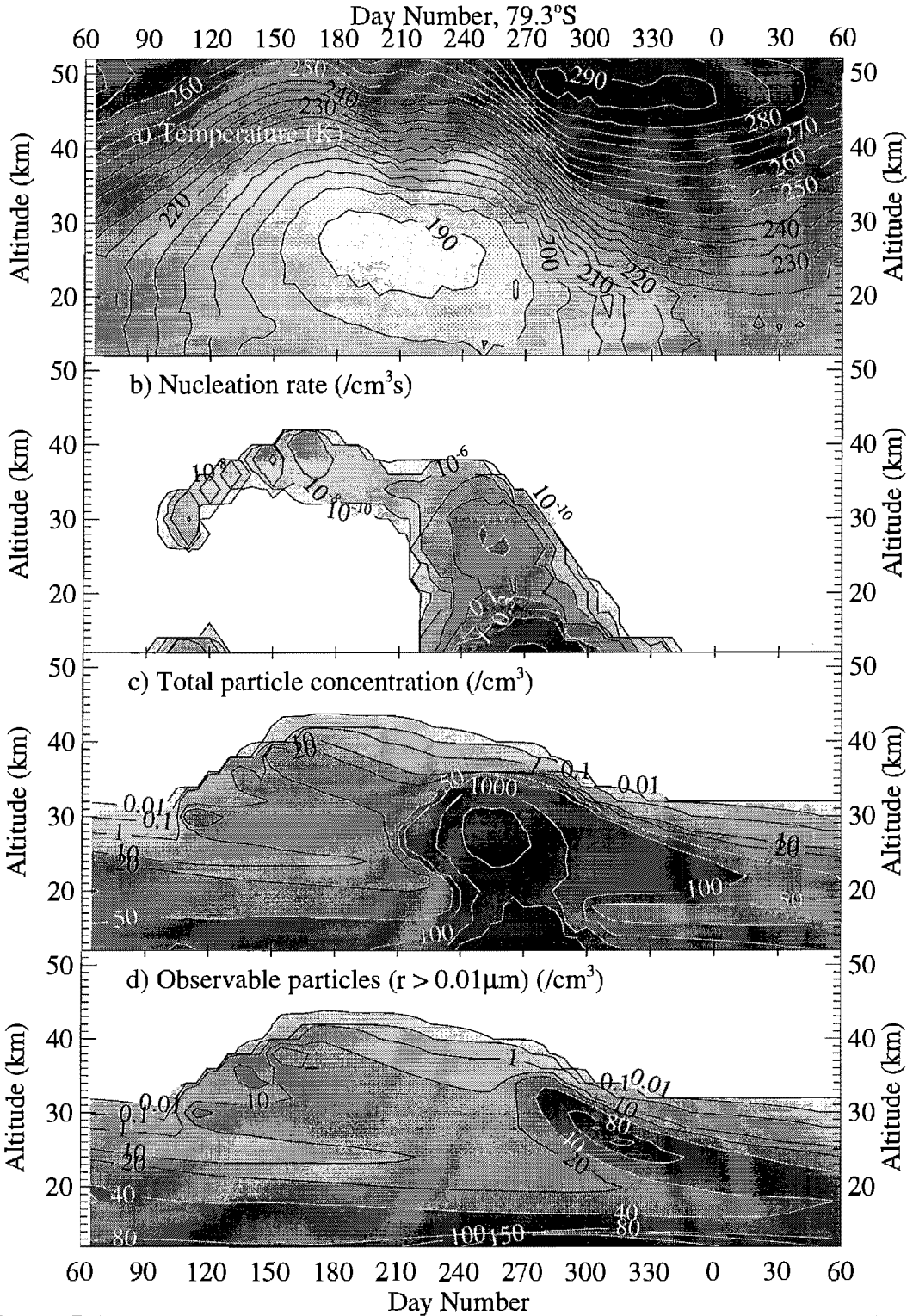

Figure 5-1 Model case B calculations of (a) temperatures, (b) homogeneous binary nucleation rates, (c) total particle concentrations, and (d) particles of radius greater than 0.01μm at 79°S. Calculations are presented for each altitude gridpoint (2 km resolution), averaged over 5-day periods. SO_2 mixing ratios are set to 400 pptv throughout the troposphere.

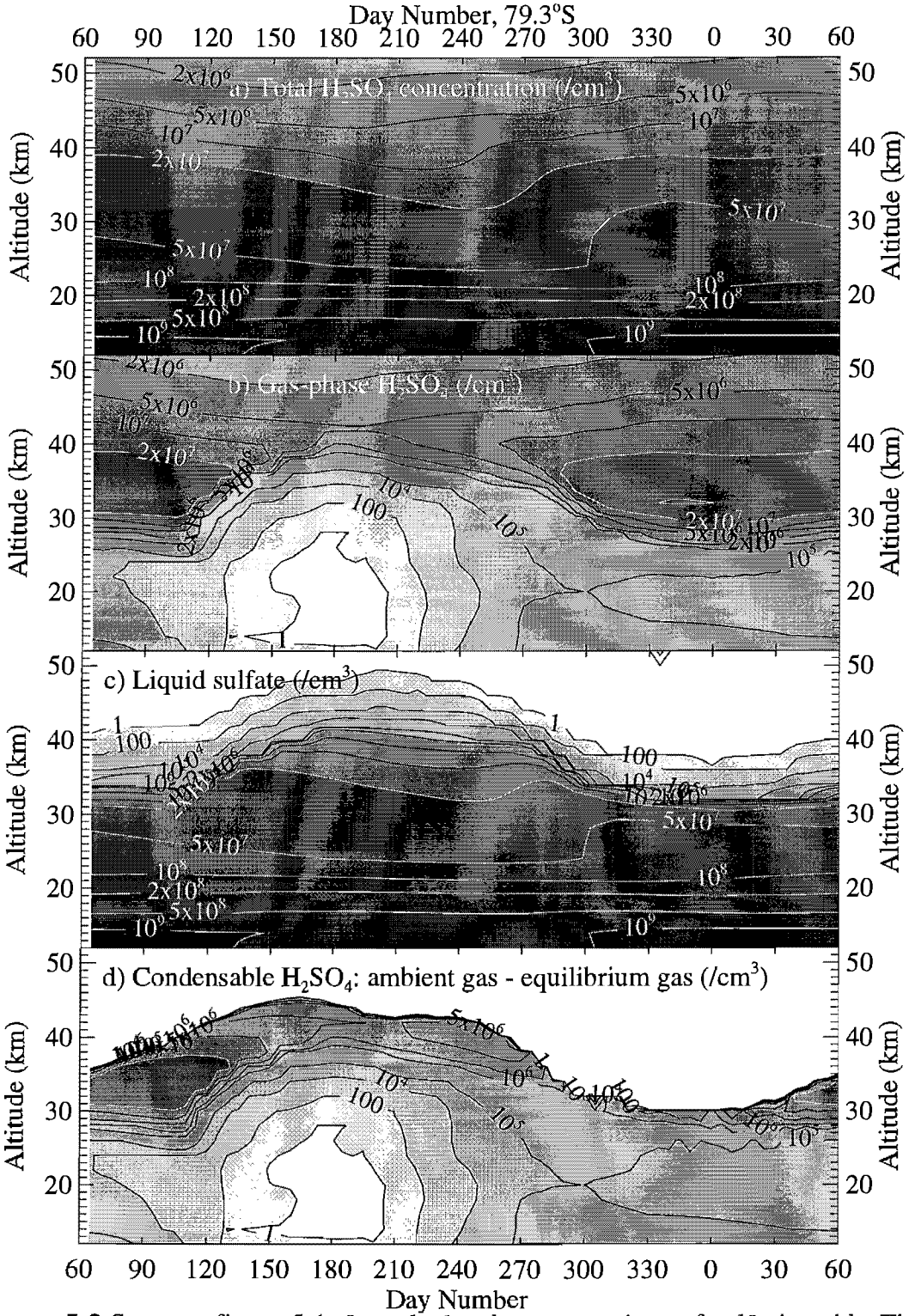

Figure 5-2 Same as figure 5-1, for calculated concentrations of sulfuric acid. The total concentration of ambient sulfuric acid (a) is partitioned between the gas (b) and liquid (c) phases. Condensable sulfuric acid (d) delineates the portion of gas-phase sulfuric acid in excess of the equilibrium concentration over the ambient aerosol.

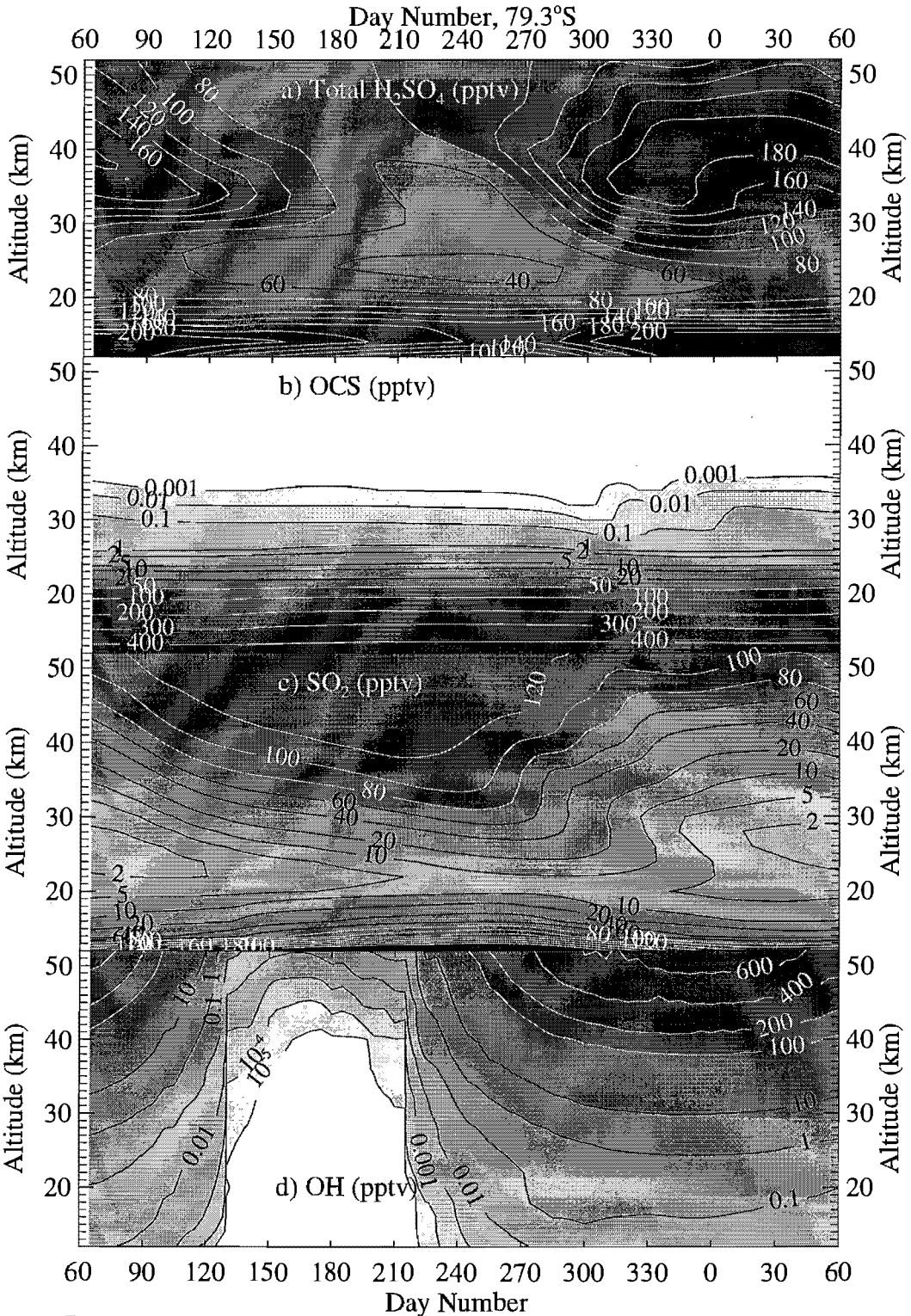

Figure 5-3 Same as figure 5-1, for mixing ratios of (a) H_2SO_4 (g + l), (b) OCS, (c) SO_2, and (d) OH.

Coincident with the return of sunlight at the end of August, nucleation increases dramatically at all altitudes below 36 km. Particle concentrations respond rapidly, peaking at over $10^4/cm^3$ between 22 and 30 km. Particles of observable size are seen a full month later, at the beginning of October. These larger particles form in a descending layer, correlating to observations described above.

The conditions responsible for the winter phase of nucleation are shown in figure 5-2. As temperatures decrease from February through April, the equilibrium concentration for gas-phase sulfuric acid drops well below the ambient concentration. The difference is shown as "condensable H_2SO_4" in figure 5-2d. In the absence of significant numbers of preexisting particles above 30 km, condensation is slow and large excesses of vapor accumulate over a period of several months. When temperatures fall below about 220 K, homogeneous nucleation begins, followed by rapid condensation of this excess onto the newly formed particles. This phase of nucleation results entirely from temperature decreases, despite decreasing concentrations of total sulfuric acid (figure 5-2a).

In contrast to the slow nucleation phase calculated through the winter, the rapid nucleation calculated in August is caused by abrupt increases in concentrations of total sulfuric acid, during a period of increasing temperature. Rapid increases are apparent first in August above 40 km, and propagate downward to 25 km by October. The rapid spring phase of nucleation initiates in August as a result of increasing sulfuric acid vapor pressures. As sulfuric acid vapor continues to increase in September, however, nucleation rates begin to decrease and halt entirely. After September, temperatures become too warm for significant nucleation to occur.

Clues to the sources of the additional sulfuric acid are provided by figure 5-3. The greatest seasonal variation in total sulfuric acid mixing ratio (shown in figure 5-3a) occurs above 30 km. At the onset of winter, mixing ratios near 50 km have already decreased to below 80 pptv from near 140 pptv in the summer. Depleted mixing ratios

persist and propagate downward through the winter. Springtime recovery of sulfuric acid also occurs first at the highest altitudes. By mid-spring, between 120 and 200 pptv of total sulfuric acid are calculated above 30 km. The pronounced seasonal variation is clearly unrelated to OCS, which never exceeds 1 pptv at altitudes above 30 km. OCS remains fairly invariant through the year (see figure 5-3b), and does not increase in polar night sufficiently to produce significant new sulfuric acid vapor in spring, as Rosen and Hofmann hypothesized it might.

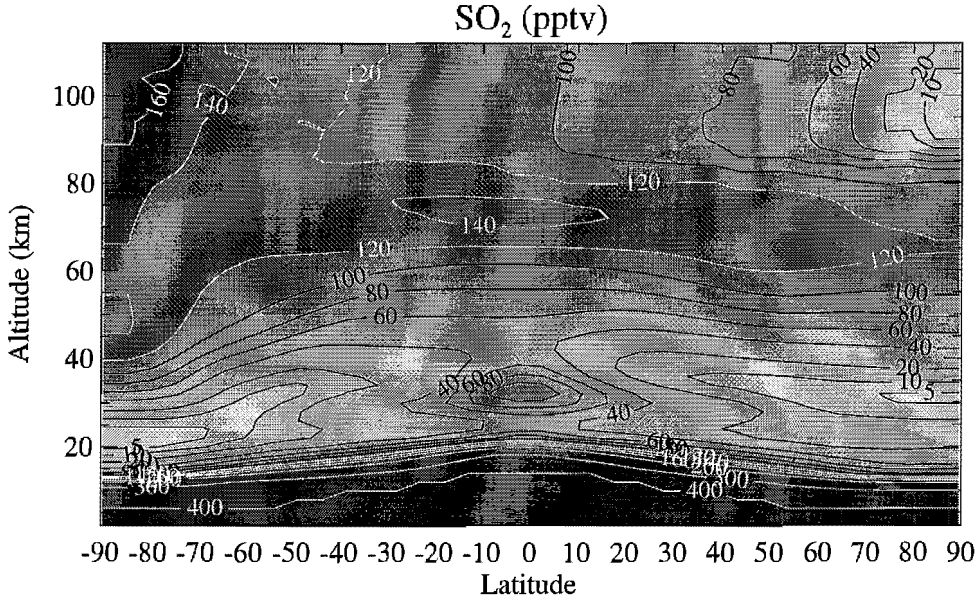

Figure 5-4 Calculated SO_2 vs. altitude and latitude, average for the period from model day 150 to 155 (June 1-5). SO_2 is produced above about 40 km by photolysis of H_2SO_4, and photolyzes above 70 km to form SO.

SO_2 mixing ratios, on the other hand, exhibit very large seasonal variations in the upper stratosphere, inverse to those of sulfuric acid. The dominant source of SO_2 to the upper stratosphere in this calculation is photolysis of sulfuric acid, which becomes significant at altitudes above about 40 km, with some latitudinal variation. Above about 70 km, SO_2 is itself photolyzed to SO, which becomes the dominant sulfur species in the upper mesosphere. During polar night, however, these processes cease, and SO converts rapidly back to SO_2 (see figure 5-4). The major influence of mesospheric SO_2 on the stratosphere results from a seasonal reversal of dynamics. In the summer mesosphere, the mean circulation is upward, while in the winter

mesosphere it is downward. Winter downwelling brings air partitioned with high SO_2 and low sulfuric acid from the mesosphere into the stratospheric polar vortex. With the return of sunlight and OH in the spring, this SO_2 oxidizes to produce sulfuric acid.

The importance of mesospheric SO_2 in the development of the observed particle layer is clearly demonstrated by a model calculation that does not include H_2SO_4 photolysis. The steady-state result for this case, which I designate NP (for "no photolysis"), is shown in figure 5-5. In contrast to case B, air descending from the mesosphere is, in case NP, partitioned in favor of sulfuric acid, with less than 5 pptv SO_2. This small amount of SO_2 is produced by photolysis of OCS in the tropical upper stratosphere (see figure 5-6). Sulfuric acid remains at significantly higher mixing ratios than in case B throughout the fall and winter. The weak winter phase of nucleation initiates with the similar vertical and temporal variations as case B, leading to approximately the same number (10-20/cm^3) of observable particles through the winter. In spring, however, the dramatic increase in nucleation rates between 20 and 35 km seen in figure 5-1 does not occur. The distinct springtime CN layer does not form absent H_2SO_4 photolysis.

What distinguishes these two cases such that they produce such different outcomes in polar spring? Figure 5-7 shows various case B calculations minus corresponding calculations for case NP. Springtime nucleation rates are higher by as much as five orders of magnitude in case B compared to case NP. The most active nucleation lies between 20 and 35 km from day 210 to 270. Figure 5-7a reveals that these higher nucleation rates occur despite lower mixing ratios of total sulfuric acid (gas plus liquid) in this region for case B. In case NP, however, a far greater proportion of this sulfuric acid is present in aerosol form . As figure 5-7b indicates, gas-phase mixing ratios are higher for case B in the region of highest nucleation . Although the difference is but a fraction of a part per trillion, this represents 10 to 20 times the vapor present in case NP.

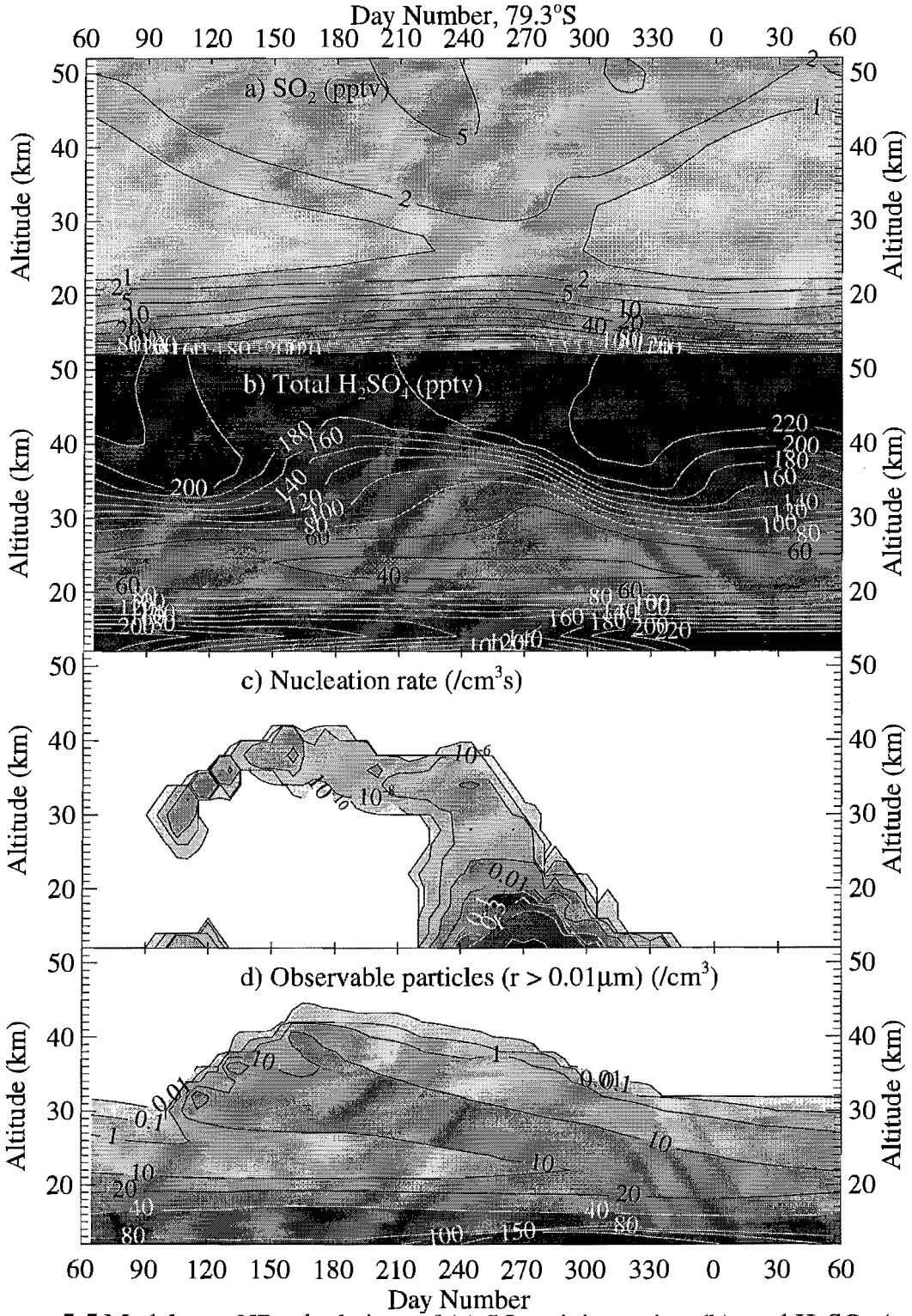

Figure 5-5 Model case NP calculations of (a) SO_2 mixing ratios, (b) total H_2SO_4 (g + l) mixing ratios, (c) nucleation rates, and (d) observable particles. Photolysis of H_2SO_4 vapor is turned off in case NP, and the same boundary conditions as case B are maintained for tropospheric SO_2.

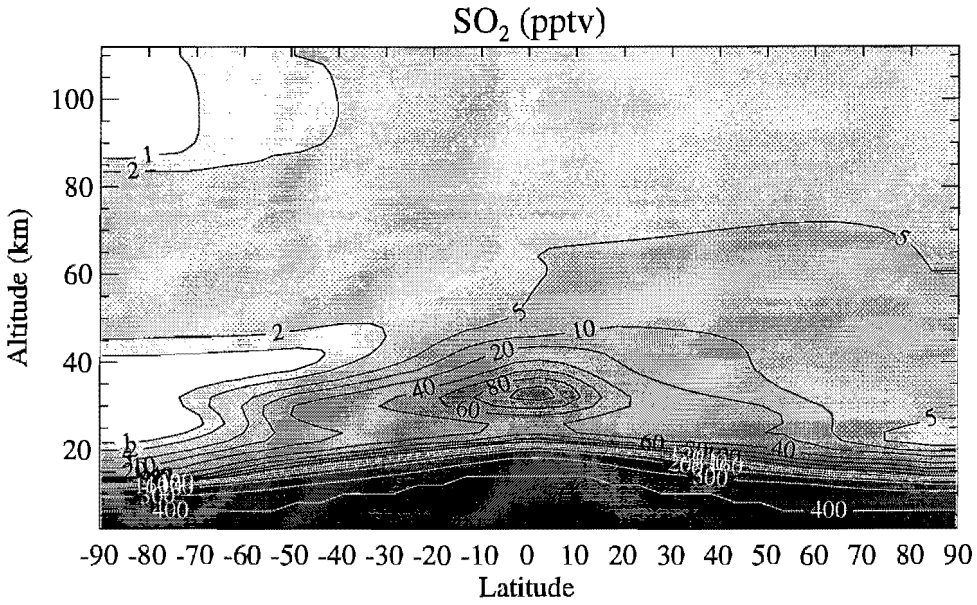

Figure 5-6 Global distribution of sulfur dioxide in the absence of sulfuric acid vapor photolysis (case NP). The source of SO_2 seen in the tropics near 30 km is OCS destruction.

Nucleation rates are a function only of temperature and gas-phase concentrations of sulfuric acid and water. Water and temperature do not vary significantly between cases B and case NP. The difference in nucleation rate (figure 5-7c) is clearly correlated to the difference in sulfuric acid vapor. As figure 3-3 illustrated, a difference of one order of magnitude in concentration can translate into many orders of magnitude in nucleation rate. In order to discern the cause of the springtime nucleation, we must understand why sulfuric acid vapor in the spring near 30 km is greater when photolysis is included.

Turning off photolysis eliminates a loss mechanism for sulfuric acid vapor. Yet, somewhat non-intuitively, this leads to smaller mixing ratios for sulfuric acid vapor. This odd behavior occurs because, absent photolytic loss to SO_2, more vapor is lost by condensation to liquid aerosol. With more liquid sulfate aerosol and higher surface areas, the lifetime for condensational loss of sulfuric acid vapor is greatly reduced. The result is that more vapor is lost without photolysis than with it, reducing gas-phase mixing ratios throughout the winter.

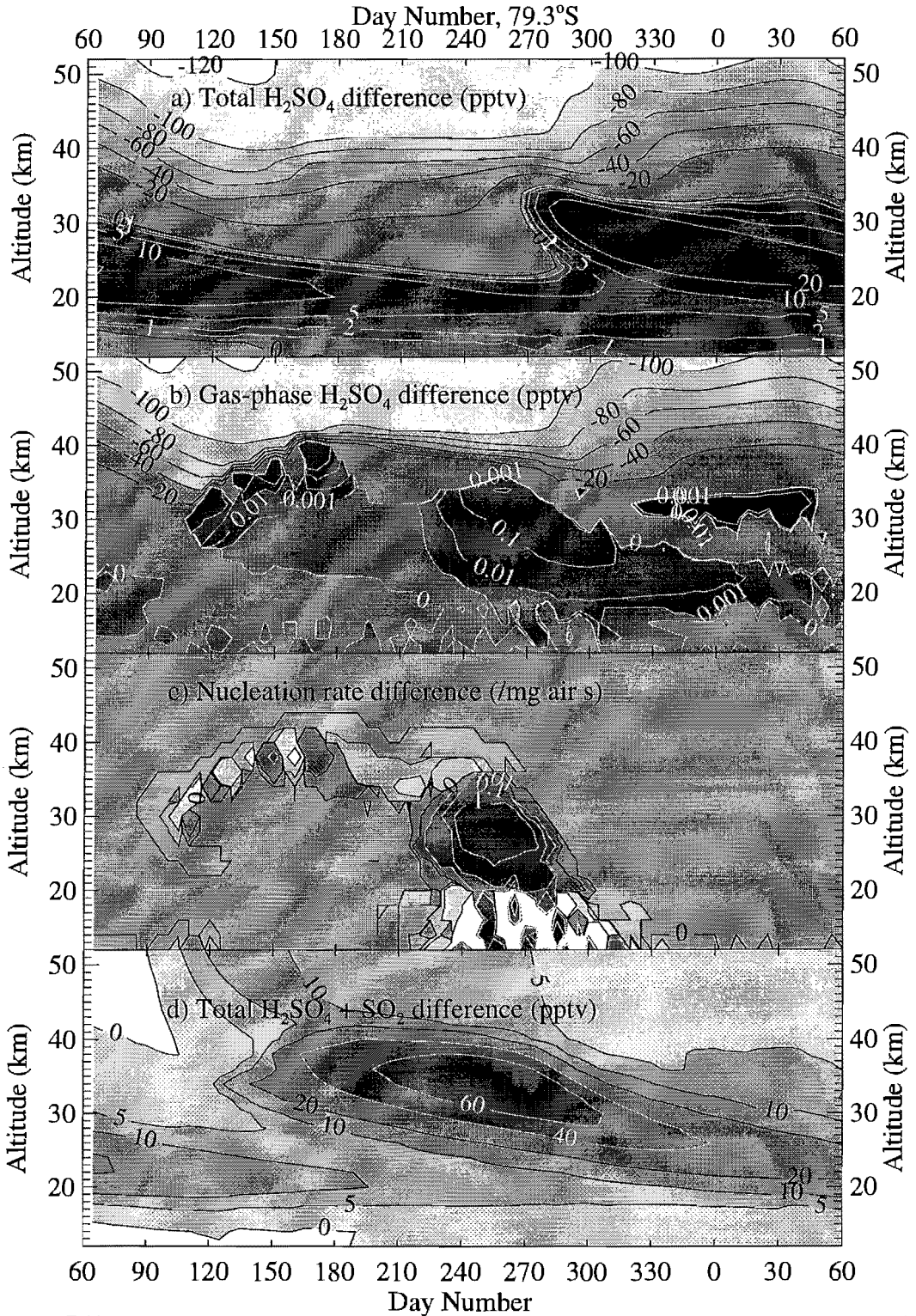

Figure 5-7 Difference due to sulfuric acid photolysis (case B minus case NP). Model calculated differences in a) total H_2SO_4 (g + l), b) gas-phase H_2SO_4, c) nucleation rate, and d) the sum of H_2SO_4 and SO_2 are presented.

With the return of sunlight and accompanying hydroxyl radicals in the spring, SO_2 may oxidize, providing the gas-phase source for sulfuric acid vapor. Because SO_2 of tropospheric origin oxidizes quickly upon entering the stratosphere in the tropics, the dominant source in case NP of accumulated SO_2 in polar winter is the slow local oxidation of OCS. This source provides but a few parts per trillion of SO_2, compared to more than 100 pptv that result from sulfuric acid photolysis in case B. Thus in the spring, sulfuric acid vapor is created much more rapidly in case B compared to case NP. The sudden springtime increase in vapor in case B, combined with lingering low temperatures, leads to the dramatic increase in binary homogeneous nucleation.

As temperatures fall in the winter, aerosol particles take up much more water and nitric acid, increasing their mass and sedimentation rates. In case NP, the seasonal variation in total sulfuric acid (see figure 5-5b) is due predominantly to this seasonal variation in sedimentation. In case B, on the other hand, additional variation is created by photolysis and accumulation of SO_2 (see figures 5-3a and c). In the case NP, more sulfate mass is present in aerosol; hence sedimentation rates are greater than in case B. The greater rate of loss is reflected in figure 5-7d, which shows the difference between these cases in the sum of SO_2 plus sulfuric acid. This sum accounts for very nearly all sulfur above 20 km in polar regions. The two cases maintain approximately the same amount of total sulfur in the upper stratosphere through summer and autumn. Faster winter sedimentation in case NP, however, depletes sulfur at 30 km to half that available in case B by spring.

By late September nearly all of the SO_2 descending below 40 km in case B has been oxidized back to sulfuric acid. At this time total sulfuric acid mixing ratios in case B exceed those in case NP by about 20 pptv (figure 5-7a), a discrepancy that is similar to that in total sulfur shown in figure 5-7d. The excess of total sulfuric acid in case B, which results from differing sedimentation rates, occurs exactly where the model calculates an enhanced layer of observable particles (see figure 5-1d). Absent the

reserve of sulfur immune from winter sedimentation provided by photolysis-generated SO_2, insufficient sulfuric acid is available in springtime to allow particles generated near 30 km to grow to observable size.

Timing of CN layer appearance

The calculated CN layer appears one month later in the season than that observed. New particles are nucleated in August, but do not grow to observable size until the beginning of October. The CN layer is generally first observed in early September, and grows throughout that month. The timing of both nucleation and growth correlates to the return of sunlight, which generates the OH required to oxidize SO_2. The pace at which the new particles can grow to observable size is limited by the concentrations of sulfuric acid vapor available for condensation.

As figure 5-8 shows, the model calculates the CN layer as forming in early September at 64°S, a full month earlier than at the pole. This latitudinal variation correlates with the return of sunlight in springtime, which occurs later at higher latitudes. The observed appearance of the layer at high latitudes in September may be due to recent excursions to lower latitudes of air observed in polar regions.

Air in the polar vortex rarely moves strictly along latitude circles. The center of the vortex wobbles off the geographic pole, and the shape of the vortex changes due to the influence of atmospheric waves. Hence air observed in regions of polar night is likely to have recently been exposed to sunlight at lower latitudes as it travels around the vortex. The Garcia-Solomon model accounts for such asymmetrical dynamics by first calculating the influence of planetary wave number 1 on the vortex. Air in the vortex is then exposed to photolysis rates calculated for the highest and lowest latitudes of its circuit for one day on each period of its circulation. Such a parameterization may not be sufficient to fully account for the influence of excursions to higher latitudes in the real atmosphere.

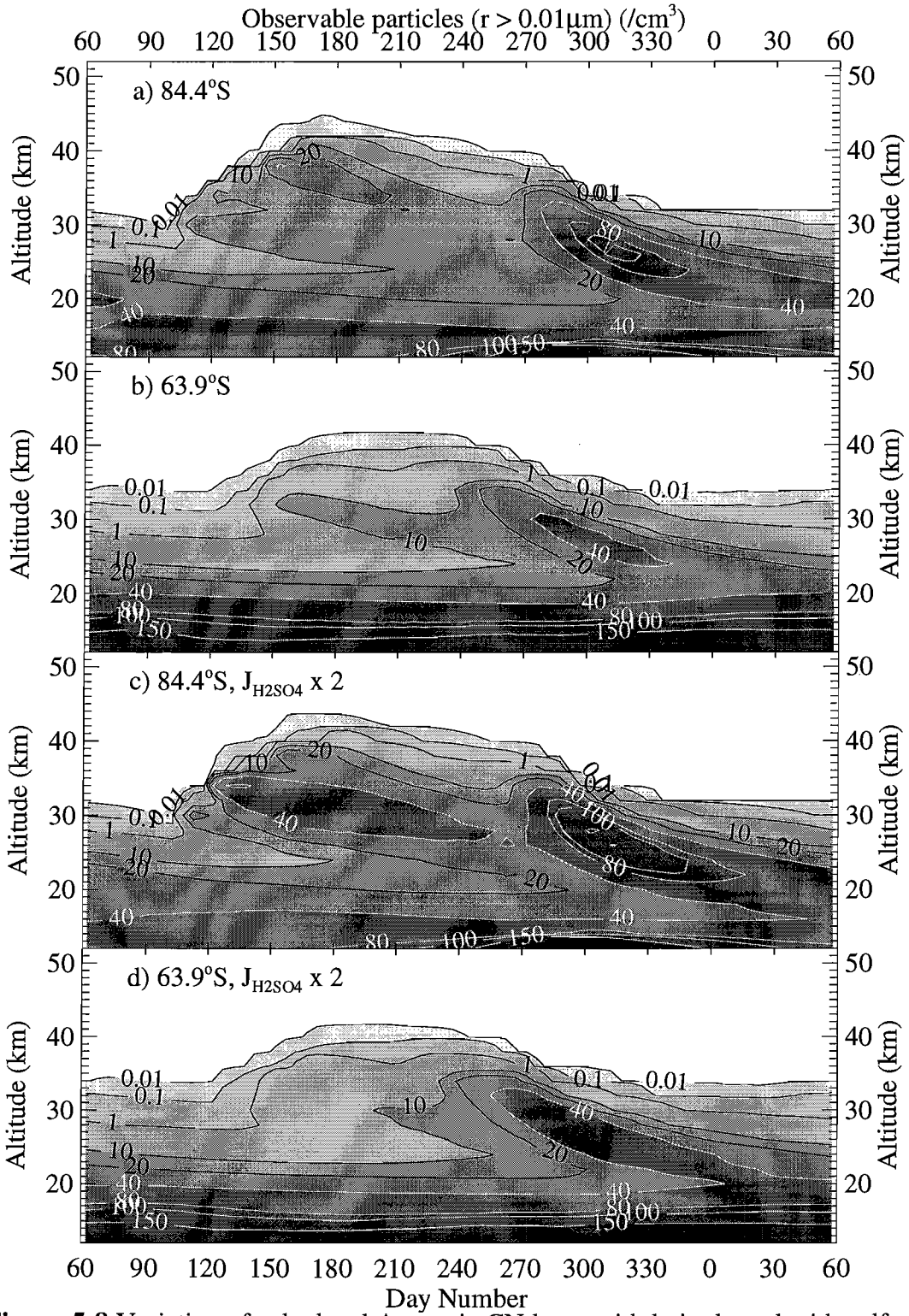

Figure 5-8 Variation of calculated Antarctic CN layer with latitude and with sulfuric acid photolysis rate. The layer is not calculated until October at 84°S, although it forms a month earlier at 64°S, albeit with half the peak particle concentrations. Doubling the photolysis rate for sulfuric acid increases the number of particles calculated.

While excursions across latitudes might explain the appearance of the polar CN layer in September, our model indicates that such excursions should also decrease the number concentrations of particles observed in the layer. I find, however, that this number concentration is sensitive to the photolysis rate of sulfuric acid, a rate that has not been measured. Figures 5-9 c and d show results from a case in which I have doubled this photolysis rate in the model. In this case, air descending from the mesosphere in winter is even more strongly partitioned towards SO_2, generating greater concentrations of sulfuric acid vapor with the return of OH in spring. The calculated concentrations of observable particles increase at all latitudes with increased sulfuric acid photolysis. Clearly measurements of sulfuric acid photolysis cross-sections would greatly benefit future modeling work.

5.2 Nitric Acid

Observations and Theories

Austin *et al.* (1986) present satellite observations revealing the presence of a double peak in nitric acid mixing ratio throughout the polar night, with the secondary maximum near 4 mbar (38 km). As that paper points out, the Garcia-Solomon model, absent heterogeneous chemistry, calculates a distribution of nitric acid quite similar to observations in the summer hemisphere, while profoundly different in the winter hemisphere. Calculated mixing ratios throughout the hemisphere were substantially less than those observed, and the secondary maximum in polar night was completely absent in the model.

Subsequently Garcia and Solomon (1994) improved their model by, among other things, adding heterogeneous chemistry on a parameterized distribution of stratospheric aerosol. Calculated nitric acid mixing ratios increase substantially throughout the winter hemisphere with this revision, comparing better to observations. However, relying on WMO/UNEP (1991) recommendations for aerosol surface areas,

the model did not calculate the formation of the secondary maximum in nitric acid at high altitudes. Because observations did not show particles at higher altitudes, these recommendations provided surface area estimates only up to 32 km. When, however, Garcia and Solomon included aerosol at higher altitudes (assuming an exponential decrease with a 7 km scale height), calculated nitric acid mixing ratios increase substantially at these altitudes in polar night.

The importance of descending mesospheric air in supplying odd nitrogen to the upper stratosphere in high-latitude winter has long been recognized (Frederick and Orsini, 1982; Solomon *et al.*, 1982; Russell *et al.*, 1984; Horvath and Frederick, 1985). Odd nitrogen passes below the stratopause as NO, NO_2, and N_2O_5. In Garcia and Solomon's (1994) modified model, N_2O_5 descending from the mesosphere reacts heterogeneously with water when in encounters the top of the stratospheric aerosol layer, producing nitric acid. Inclusion of the exponentially decreasing aerosol surface areas above 32 km extends nitric acid production to well above 40 km in polar night. This extension is not seen at other latitudes, and clearly results from the strong descent of odd nitrogen at the winter pole. The simple extrapolation of aerosol surface area in Garcia and Solomon (1994), however, does not appear to explain the secondary maximum in nitric acid near 38 km.

Kawa *et al.* (1995) compare satellite measurements of HNO_3 and N_2O_5 in the Northern Hemisphere to calculations of a 3-dimensional chemistry/transport model. Inside the polar vortex, elevated mixing ratios of nitric acid and reduced mixing ratios of N_2O_5 are observed, but not calculated, at the 1200 K potential temperature surface (35-40 km). This comparison strongly indicates that important chemistry is missing from the model. Referring to the calculations of Garcia and Solomon (1994), Kawa *et al.* conclude that heterogeneous reactions on sulfate aerosol are not likely to explain the double maximum in nitric acid. Instead they propose that hydrated ion clusters may be the site for heterogeneous conversion of N_2O_5 to nitric acid. However, in order to

produce the double peak with this mechanism in a model, Kawa *et al.* had to increase ion reactivity above 7 mbar by a factor of 10 over the background expected from galactic cosmic rays.

Additional observations of nitric acid have been provided by ground-based millimeter spectroscopy in Antarctica. De Zafra *et al.* (1996) present vertical profiles at the South Pole taken at 3- to 6-day intervals from April 1993 to January 1994 (see figure 5-9a). The measurements show the development of the secondary maximum, centered at 40-42 km, in late June. At the same time rapid loss of nitric acid is evident below about 20 km. Through July and August, removal of gas-phase nitric acid extends upward to about 25 km, while the secondary peak descends and grows, appearing to merge with the primary HNO_3 maximum. De Zafra *et al.* (1996) qualify the contours presented between days 200 and 225, saying that two layers of nitric acid are difficult to resolve by their technique when centered less than 10 km apart. Many of the convolutions of the contours above 30 km in this time period may be artifacts of the altitude retrieval method, which relies on pressure broadening. They propose that the two nitric acid layers descend with prevailing dynamics, the lower at appropriately slower speeds than the upper.

Model Calculations

The microphysical calculations show a secondary maximum in nitric acid near 40 km, resulting from heterogeneous chemistry on sulfate aerosol. As I have discussed in the first part of this chapter, sulfate particles nucleate at the top of the aerosol layer throughout polar winter. This new particle production results in enhanced aerosol surface areas, rather than the exponential decay with altitude above 32 km assumed by Garcia and Solomon (1994). As odd nitrogen descends, heterogeneous hydration of N_2O_5 maximizes near 40 km. Winter polar nucleation of sulfate aerosol

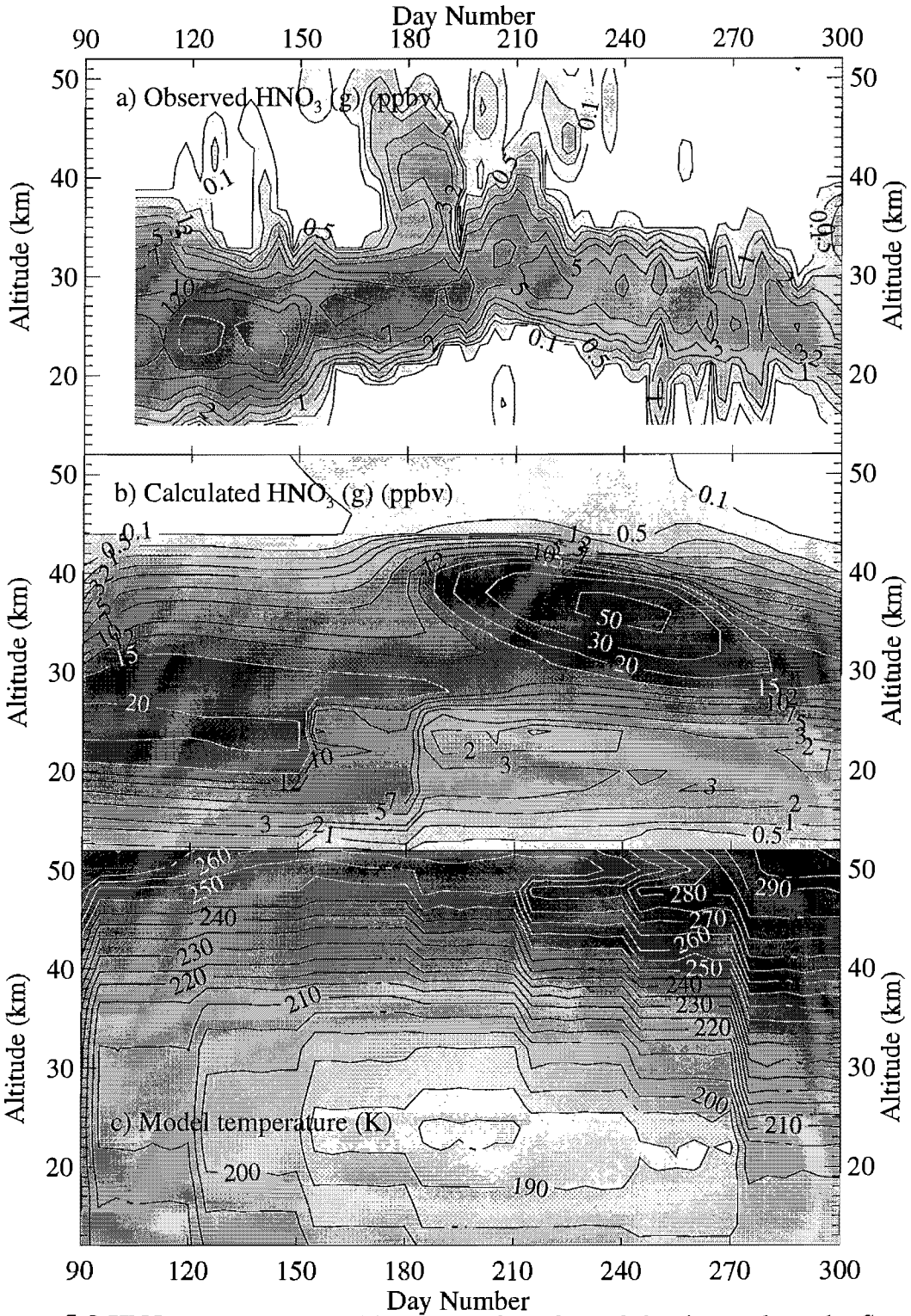

Figure 5-9 HNO_3 measurements (a) were made at 3- to 6-day intervals at the South Pole in 1993 by millimeter-wave spectroscopy (de Zafra *et al.*, 1996). Model calculations (b) are for a 20 x background sulfate layer, at 84°S, using 1993 monthly mean zonal-average temperatures (c) interpolated from those compiled by the National Meteorological Center (Randel, 1996).

therefore plays an important role in the formation of the secondary maximum in nitric acid.

I have made two adjustments to the model as presented thus far to aid comparison to the observations of de Zafra *et al.* (1996). While the scenarios I have presented up to this point have been for nonvolcanic sulfate, the observations were made in a period heavily influenced by the volcanic eruption of Mt. Pinatubo. I have therefore multiplied all sulfur-bearing compounds to 20 times those present in the background case B. While the model temperatures, derived from dynamics, generally compare well to a multi-year average of zonal mean observed temperatures, specific years may exhibit significant departures. I therefore drive model chemistry and microphysics in the comparison case with monthly averaged zonal-mean temperatures from the same year (1993) as de Zafra's observations. The data set of observed temperatures, compiled by the National Meteorological Center (Randel, 1996), covers 40 latitudes from 87°S to 87°N and 17 pressure levels from 1000 to 1 mbar (0.1 to 48 km). The model interpolates this grid in latitude and pressure, and sets zonal mean temperatures to their monthly mean values for the duration of each month. Temperature perturbations are added to provide variation about the observed mean. Above 48 km, temperatures derived from model dynamics are used, as before. I call this model scenario case G.

Figures 5-9b and c show calculated nitric acid mixing ratios and model-interpolated temperatures for case G. In the lower stratosphere, the model calculates removal of gas-phase nitric acid beginning in June, extending up to 25 km. This result parallels observations, although the observed removal is more extensive, indicating loss of all detectable nitric acid from the gas phase below 20 km. This is the region in which polar stratospheric clouds are observed, some composed of solid particles of nitric acid trihydrate (NAT) or water-ice. Because the model does not include details of PSC formation or any treatment of the growth of solid particles, it can not simulate

removal of gas-phase nitric acid fully. The model does show that much of the observed removal can be explained simply by uptake of nitric acid into supercooled ternary solutions (STS), in accordance with the parameterization of Carslaw *et al.* (1995).

The microphysical model shows that a secondary maximum in nitric acid at high altitudes in polar winter may result from heterogeneous chemistry on sulfate aerosol. As I will discuss, the calculated layer differs from that observed in several significant ways. However, the model specifically overcomes four problems with the aerosol theory outlined in de Zafra *et al.* (1996):

One problem mentioned is that observed nitric acid does not taper off smoothly at high altitudes, as one might expect from an exponentially decreasing aerosol layer, but forms in a clearly defined layer centered near 40 km. The model shows that such a layer results from heterogeneous hydration of N_2O_5 as it descends through the top of the aerosol layer. Figure 5-10 shows the factors that create the maximum in nitric acid at the top of the sulfate layer in July. As temperatures drop in winter, the volcanic aerosol layer extends to higher altitudes, providing significant surface area concentrations as high as 44 km. When descending mesospheric air, containing abundant odd nitrogen, meets the top of the aerosol layer, heterogeneous hydration of N_2O_5 occurs. The rate of this reaction is proportional both to N_2O_5 mixing ratio, which increases with increasing altitude, and to aerosol surface area, which increases with decreasing altitude. It happens that the reaction rate maximizes at 38-40 km. This is where I calculate and observe the peak of the high-altitude nitric acid layer.

A second problem mentioned is that the formation of the secondary maximum in late June is delayed several months from the onset of polar night. De Zafra *et al.* correctly point out that N_2O_5 forms at night with a lifetime of a few days, and they thus expect N_2O_5 hydrolysis to peak shortly after the onset of polar night. In this calculation, however, the important event in the timing of the formation of the

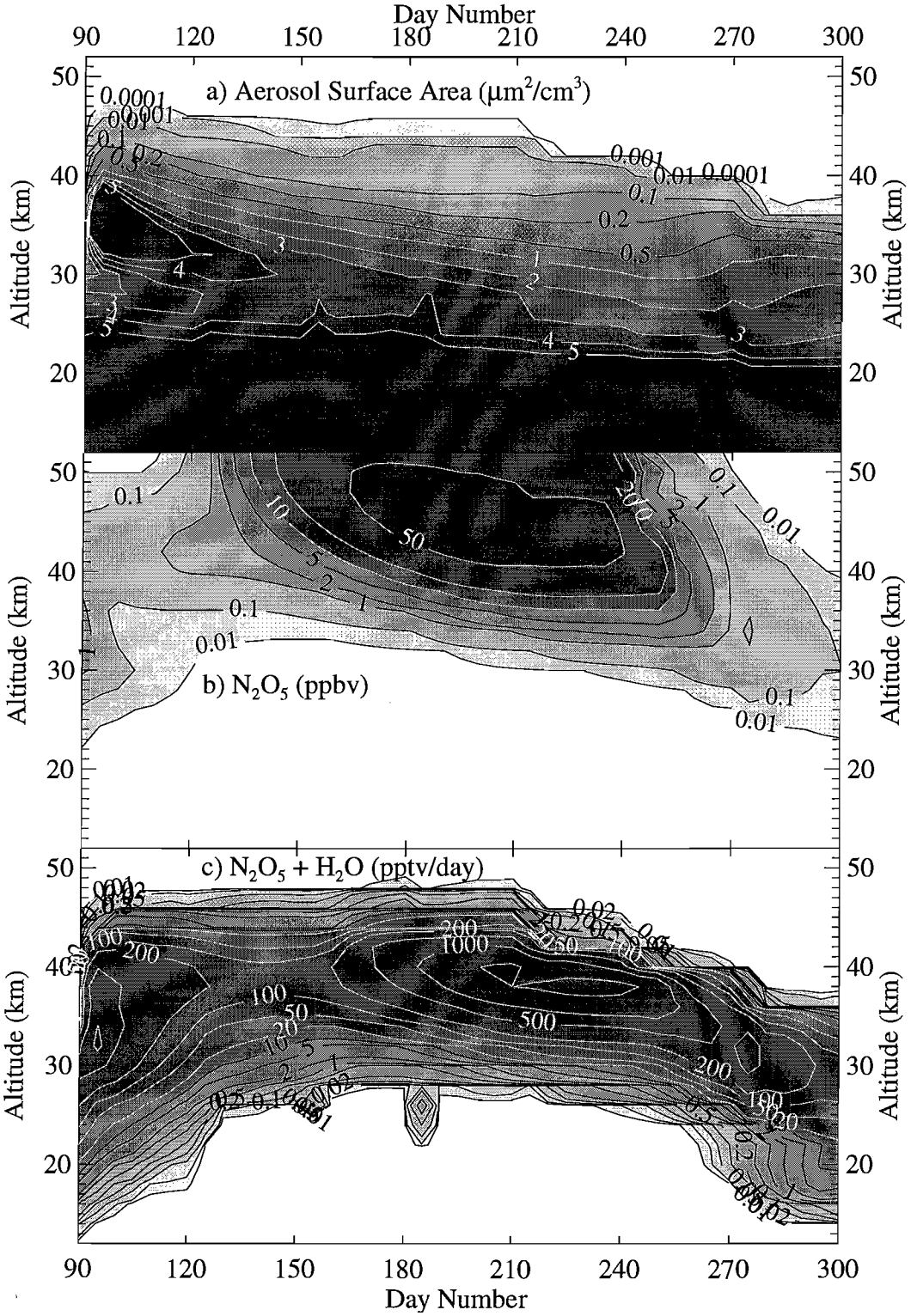

Figure 5-10 Calculated aerosol surface area, N_2O_5 mixing ratio, and heterogeneous hydration rate of N_2O_5 for case G at 84°S.

secondary maximum is not the onset of polar night, but the arrival of odd nitrogen from the mesosphere. While heterogeneous hydrolysis of ambient N_2O_5 occurs throughout the winter, it is this descending abundance that creates the secondary maximum. The model calculates that this odd nitrogen reaches 40 km in June, just in time to explain the observations.

A third problem mentioned is that the rapid downward transport that occurs at the poles throughout the winter ought to suppress the aerosol layer. The microphysical model shows this not to be the case. The altitude of the top of the aerosol layer is determined by temperature and available sulfur, not by dynamics. As temperatures drop, the equilibrium vapor pressure of sulfuric acid falls below ambient partial pressures of sulfuric acid vapor, and nucleation occurs. Thus in the winter the aerosol layer extends to higher altitudes, rather than being pushed to lower altitudes.

Finally, de Zafra *et al.* (1996) mention that, while the surface reaction probability (γ) for N_2O_5 hydrolysis had been thought to be 0.1 invariant with temperature, recent laboratory work by Zhang *et al.* (1995) suggests that it may be significantly reduced in the presence of nitric acid. Zhang *et al.* found reaction probability decreases linearly as temperature decreases, when $5x10^{-7}$ torr of HNO_3 is present. This partial pressure would correspond to mixing ratios of 200 ppbv at 40 km, or 830 ppbv at 50 km in the model. Observations indicate the presence of less than 4 ppbv in the high-altitude layer. Zhang's measurements do not indicate whether such small partial pressures might affect reaction probability. In addition, while Zhang's measurements indicate a reaction probability as low as 0.02 at 195K, the probability is 0.09 at 218K, the highest temperature at which measurements were made. NMC data shows temperatures to be even higher at the time of the secondary maximum, ranging from 225 K at 40 km to 250 K at 48 km. Thus the use of a reaction probability of 0.1 seems well justified.

The calculated mixing ratios of nitric acid are greater everywhere than those observed. Between 20 and 30 km calculated nitric acid is about 50% greater than that observed. For these higher pressures and lower temperatures, the reduction in reaction probability measured by Zhang *et al.* may have some effect. The discrepancy is much more severe, however, for the high-altitude layer.

Exaggeration of the calculated upper layer may result from unrealistic abundances of N_2O_5 in the model's polar night. N_2O_5 can only form at night by reaction of NO_2 and NO_3 on a third body. In the model N_2O_5 accumulates throughout the polar night, forming at rates proportional to the ambient air density. By July, more than 50 ppbv of N_2O_5 are calculated in the model between 40 and 50 km. It is unlikely that such large mixing ratios are present in this region in the real atmosphere. Excursions of polar air into sunlit regions are likely to reduce the abundance of both N_2O_5 and the NO_3 required to form it. Nighttime measurements of N_2O_5 from CLAES and ISAMS, presented in Kawa *et al.* (1995) indicate that mixing ratios remain well under 10 ppbv, and average 2 or 3 ppbv at 1200 K (~40 km) in polar regions. The model's overestimate of N_2O_5 mixing ratios likely contributes to the overestimate of nitric acid produced as the air descends through the aerosol layer in July and August.

The high altitudes to which significant mixing ratios of nitric acid extend in the observed secondary maximum in June and July present another problem for the model. However, other observations of the secondary maximum do not show the same vertical extent. CLAES data, presented in Kawa *et al.* (1995), show mixing ratios below 0.5 ppbv at altitudes above 2 mbar (~33 km in the model), while peak mixing ratios of 3 to 4 ppbv are seen at 4 mbar (~39 km). De Zafra *et al.* (1996) rely on pressure broadening of microwave emissions to determine their altitude of origin. The strength of the microwave signal retrieved is proportional to the concentration of nitric acid. De Zafra *et al.* claim that their retrieval method works well over the altitude range of 15 to 48 km. As air rarefies at the top of this range, however, small mixing ratios of nitric

acid may present signals close to the noise level, given the much stronger signals from lower altitudes. It seems likely that de Zafra's observations at the upper end of his altitude range will have greater uncertainties than his observations from lower altitudes.

5.3 Conclusions

The microphysical model of sulfate aerosol that I have developed helps explain two observed stratospheric phenomena in polar winter. The observed CN layer in polar winter is explained as a result of binary homogeneous nucleation following rapid production of sulfuric acid vapor from SO_2 in spring. The model also suggests that nucleation extends the aerosol layer to higher altitudes in polar winter despite the concurrent subsidence of polar air. When this subsiding air brings elevated mixing ratios of odd nitrogen down from the mesosphere, heterogeneous reactions at the top of this enhanced aerosol layer produce the observed secondary maximum in nitric acid.

The formation of the observed CN layer relies on the presence of sufficient sulfuric acid vapor in early and mid-spring. In early spring this vapor is required to nucleate new particles between 20 and 35 km. However, not all of these particles will grow to observable size. Rapid growth can only occur where sufficient sulfuric acid vapor concentrations are available in mid-spring. The presence of sufficient sulfuric acid vapor in both early and mid-spring relies on the photolysis of sulfuric acid. In the mesosphere, sulfuric acid vapor photolyzes extensively to SO_2, which descends to the stratosphere in polar winter. Sulfur is preserved as SO_2 through polar night rather than sulfuric acid, reducing sulfur loss to sedimentation and creating a burst of sulfuric acid vapor when sunlight returns. This springtime oxidation of SO_2 produces so much sulfuric acid vapor that nucleation rates increase dramatically. When temperatures increase in September, nucleation ceases, and the particles formed in early spring grow rapidly as the excess sulfuric acid vapor condenses. A resultant layer of particles of observable size is calculated to occur first above 30 km in early October, descending to near 25 km in November.

The microphysical model also explains the behavior of nitric acid in polar winter. Using observed monthly averaged zonal mean temperatures for 1993 and a 20 x background sulfate aerosol layer, the model reproduces a number of variations in nitric acid observed at the South Pole in 1993. The calculations indicate that much of the removal of gas-phase nitric acid observed in the lower stratosphere can be explained by uptake of nitric acid into supercooled ternary solutions, in accordance with the parameterizations of Carslaw *et al.* (1995). In the upper stratosphere, a distinct layer of nitric acid observed near 40 km in July is reproduced by the calculations. The layer results from heterogeneous hydration of N_2O_5 when descending air from the mesosphere, rich in odd nitrogen, intersects the top of the aerosol layer. The nitric acid produced descends with prevailing dynamics. The calculated layer greatly exceeds that observed, probably due to an excess of N_2O_5 in the model's polar night.

Chapter 6

Conclusions

6.1 Summary and Conclusions

I have developed and described here a numerical model for stratospheric sulfate aerosol microphysics, which I have incorporated in the Garcia-Solomon two-dimensional dynamical/chemical model. My calculations reveal much about the sources of ambient stratospheric aerosol, the causes of its observed seasonal behavior, and its effects on stratospheric chemistry. Carbonyl sulfide is shown to be a minor source of sulfate, important only at altitudes well above the bulk of the aerosol layer. At lower altitudes SO_2 of tropospheric origin is clearly important, although an additional source or sources is indicated. The anomalous CN layer observed in polar spring results directly from homogeneous nucleation, and indirectly from photolysis of sulfuric acid at higher altitudes. Homogeneous nucleation extends the aerosol layer to higher altitudes throughout polar winter. Heterogeneous reactions of descending odd nitrogen from the mesosphere on polar sulfate aerosol produce a secondary maximum of nitric acid in mid-winter near 40 km that qualitatively resembles observations.

A detailed description of sulfur chemistry affecting the stratosphere was added to the model's chemical scheme. Carbonyl sulfide and tropospheric SO_2 were the only sources of sulfur included in the model, although other sources were considered and discussed here. The transport and oxidation of these sources and intermediates were

calculated interactively with the chemistry and dynamics of the Garcia-Solomon model. The product of the chemical oxidation scheme is sulfuric acid vapor.

This sulfuric acid vapor is the source of sulfate aerosol in the stratosphere. New particles are generated by binary homogeneous nucleation of sulfuric acid and water vapors, when temperatures are sufficiently cold and ambient aerosol sufficiently scarce. In the presence of high surface areas of existing aerosol, gas-phase sulfuric acid in excess of its vapor pressure condenses onto these particles. When temperatures increase, sulfate evaporates to reform sulfuric acid vapor. Condensation and evaporation of water and nitric acid varies analogously. When particles collide, they coagulate, increasing particle size and reducing particle number. The prevailing dynamics of stratospheric air transports small particles, while larger particles can fall through the atmosphere. Each of these microphysical processes is modeled explicitly, and affects my calculated particle size distributions.

The importance of carbonyl sulfide as a source of stratospheric sulfur is relatively minor. Dissociation of OCS occurs predominantly at altitudes well above the bulk of the observed sulfate layer. Much of the mass of air in the stratosphere does not transit high enough for OCS dissociation to be important, and reenters the troposphere with OCS intact. A sulfate layer produced by OCS oxidation alone would contain only a sixth to a third of the total mass observed in volcanically quiescent periods. Deficits are more pronounced still in the lower stratosphere, where maxima in mass, surface area, and particle number are observed.

Sulfur dioxide of tropospheric origin reaches the stratosphere, providing the dominant source of sulfate aerosol. Mixing ratios of sulfur dioxide in the free troposphere appear to be strongly influenced by anthropogenic pollution, although natural sources, such as reduced sulfur compounds of oceanic origin and volcanic eruptions, may contribute as well. Human activities therefore have a great potential to increase stratospheric aerosol in volcanically quiescent periods. An increasing trend in

aerosol mass between three such periods in recent history, noted by Hofmann (1990a), may be due to increasing anthropogenic generation of SO_2.

Sedimentation of stratospheric aerosol limits the extent to which sulfate from tropospheric sulfur dioxide penetrates into the upper stratosphere. The predominant influence of tropospheric SO_2 on stratospheric aerosol is below 20 km. An additional source of sulfate is therefore indicated to account for the observed peak in sulfate mass between 20 and 25 km. Candidates include small volcanic eruptions and additional reduced sulfur compounds.

Model calculations compare well to observations of surface area, particle number, median particle radius, and particle size distributions in volcanically quiescent periods. These calculated parameters are sensitive to calculated nucleation rates, which have large uncertainties. Observations compare best with model calculations in which nucleation occurs predominantly within a few kilometers of the tropopause. Classical binary homogeneous nucleation theory produces results that match the observations much better than when the empirical correction factor of Wyslouzil *et al.* (1991) is incorporated.

My calculations explain the layer of new particles observed near 30 km in polar spring. As equilibrium vapor pressures fall with temperature throughout polar winter, binary homogenous nucleation extends the top of the aerosol layer to above 40 km. In spring, although temperatures begin to increase again, nucleation rates increase dramatically shortly after sunrise. SO_2, produced by photolysis of sulfuric acid in the mesosphere, has descended to the stratosphere in polar night. With the return of sunlight, OH oxidizes the SO_2, producing a burst of sulfuric acid vapor, which then boosts nucleation rates. Nucleated particles grow rapidly to observable size by condensation of the abundant sulfuric acid vapor.

If sulfuric acid were not photolyzed to SO_2 in the mesosphere, the descending mesospheric sulfur would arrive in the stratosphere as sulfuric acid vapor in winter.

This vapor would condense on existing aerosol throughout the winter, and increase loss due to sedimentation. The CN layer would not form in this case, absent a production mechanism for new sulfuric acid vapor in spring.

Subsiding mesospheric air in winter brings not only SO_2, but also odd nitrogen to the stratosphere. When this air descends to the top of the aerosol layer, its abundant N_2O_5 reacts heterogeneously with the water in the aerosol to produce nitric acid. Using monthly means of observed zonal average temperatures from 1993 as input, the model produces a secondary maximum in nitric acid near 40 km with timing similar to that observed in 1993 over the South Pole. The calculated upper layer of HNO_3 greatly exceeds observed mixing ratios, perhaps due to an excess of N_2O_5 in the model's polar night. The model also reproduces well the behavior of nitric acid the lower stratosphere in polar winter. The calculations indicate that much of the removal of gas-phase nitric acid observed in the lower stratosphere can be explained by uptake of nitric acid into supercooled ternary solutions, in accordance with the parameterizations of Carslaw *et al.* (1995).

6.2 Future Research

This study raises a number of questions that might be answered by future research. These involve improved microphysical calculations, as well as additional measurements.

Comparison of my calculations to observations indicates that a significant source of sulfate to the stratosphere in volcanically quiescent periods is needed. Additional modeling work could determine whether this additional sulfate originates as reduced sulfur compounds, such as CS_2 or DMS, or if it is a lingering effect of previous volcanic eruptions. Additional observational research might indicate if this extra sulfur comes from small, undetected volcanic eruptions.

Similarly, the sources of SO_2 to the free troposphere remain unclear. Because I have shown tropospheric SO_2 to be such a large source of the observed nonvolcanic

aerosol in the stratosphere, how SO_2 gets to the free troposphere is of keen interest. Important natural sources might be volcanic eruptions or reduced sulfur compounds emitted by the oceans. Determination of the extent to which man-made pollution contributes to observed mixing ratios of SO_2 in the free troposphere would indicate much about human impact on the stratosphere.

While the calculations presented here show for the first time that a layer of nitric acid near 40 km in polar winter could be produced heterogeneously on aerosol, clearly improvements should be made to obtain better correspondence with observations. The excessive production in the upper layer may be due to excessive mixing ratios of N_2O_5 in air descending from the mesosphere. Future modeling and observational work could determine whether this is the case.

This microphysical study leaves much to be discovered about stratospheric aerosol. Determination of the lifetime of volcanic perturbations and how removal rates vary over time remains of interest. I also would like to know the effects of increases in atmospheric CO_2 and consequent decreases in stratospheric temperature on the vertical extent of stratospheric aerosol and heterogeneous chemistry. These and many other questions await future microphysical modeling studies.

References

Andreae, M. O., H. Berresheim, T. W. Andreae, M. A. Kritz, T. S. Bates and J. T. Merrill, Vertical distribution of dimethylsulfide, sulfur dioxide, aerosol ions, and radon over the northeast Pacific Ocean, *J. Atmos. Chem.*, *6*, 149-173, 1988.

Andrews, D. G. and M. E. McIntyre, Planetary waves in horizontal and vertical shear: the generalized Eliassen-Palm relation and the zonal mean acceleration, *J. Atmos. Sci.*, *33*, 1976.

Andrews, D. G. and M. E. McIntyre, On wave-action and its relatives, *J. Fluid Mech.*, *89*, 1978.

Austin, J., R. R. Garcia, J. M. Russell, S. Solomon and A. F. Tuck, On the Atmospheric Photochemistry of Nitric Acid, *J. Geophys. Res.*, *91*, 5477-5485, 1986.

Ayers, G. P., R. W. Gillett and J. L. Gras, On the vapor pressure of sulfuric acid, *Geophys. Res. Lett.*, *7*, 433-436, 1980.

Bandy, A. R., D. L. Scott, B. W. Blomquist, S. M. Chen and D. C. Thornton, Low yields of SO_2 from dimethyl sulfide oxidation in the marine boundary layer, *Geophys. Res. Lett.*, *19*, 1125-1127, 1992a.

Bandy, A. R., D. C. Thornton, D. L. Scott, M. Lalevic, E. E. Lewin and A. R. D. III, A time series for carbonyl sulfide in the Northern Hemisphere, *J. Atmos. Chem.*, *14*, 527-534, 1992b.

Berresheim, H., M. O. Andreae, G. P. Ayers, R. W. Gillett, J. T. Merrill, V. J. Davis and W. L. Chameides, Airborne measurements of dimethylsulfide, sulfur dioxide, and aerosol ions over the Southern Ocean south of Australia, *J. Atmos. Chem.*, *10*, 341-370, 1990.

Beyer, K. D., A. R. Ravishankara and E. R. Lovejoy, personal communication, 1995

Boyd, J., The noninteraction of waves with the zonally averaged flow on a spherical earth and the interrelationship of eddy fluxes of energy, heat, and momentum, *J. Atmos. Sci.*, *33*, 2285-2291, 1976.

Brasseur, G. and C. Granier, Mount Pinatubo aerosols, chlorofluorocarbons, and ozone depletion, *Science*, *257*, 1239-1242, 1992.

Brasseur, G. and S. Solomon, *Aeronomy of the Middle Atmosphere*, 452 pages, D. Reidel Publishing Company, Boston, 1986.

Brock, C. A., P. Hamill, J. C. Wilson, H. H. Jonsson and K. R. Chan, Particle formation in the upper tropical troposphere: a source of nuclei for the stratospheric aerosol, *Science*, *270*, 1650-1653, 1995.

Carslaw, K. S., B. Luo and T. Peter, An analytic expression for the composition of aqueous HNO_3-H_2SO_4 stratospheric aerosols including gas phase removal of HNO_3, *Geophys. Res. Lett.*, *22*, 1877-1880, 1995.

Chatfield, R. B. and P. J. Crutzen, Sulfur Dioxide in Remote Oceanic Air: Cloud Transport of Reactive Precursors, *J. Geophys. Res.*, *89*, 7111-7132, 1984.

Chin, M. and D. D. Davis, A reanalysis of carbonyl sulfide as a source of stratospheric background sulfur aerosol, *J. Geophys. Res.*, *100*, 8993-9005, 1995.

Costen, R. C., G. M. Tennille and J. S. Levine, Cloud pumping in a one-dimensional photochemical model, *J. Geophys. Res.*, *93*, 15941-15954, 1988.

Crutzen, P. J., The possible importance of OCS for the sulfate layer of the stratosphere, *Geophys. Res. Lett.*, *20*, 1435-1438, 1976.

de Zafra, R. L., V. Chan, S. Crewell, C. Trimble and J. M. Reeves, Millimeter wave spectroscopic measurements over the South Pole, 3. The behavior of stratospheric nitric acid through polar fall, winter, and spring, *J. Geophys. Res.*, *101*, in press, 1996.

DeMore, W. B., S. P. Sander, D. M. Golden, R. F. Hampson, M. J. Kurylo, C. J. Howard, A. R. Ravishankara, C. E. Kolb and M. J. Molina, Chemical Kinetics and Photochemical Data for Use in Stratospheric Modeling, Jet Propulsion Laboratory Report JPL 92-90, August 15, 1992.

DeMore, W. B., S. P. Sander, D. M. Golden, R. F. Hampson, M. J. Kurylo, C. J. Howard, A. R. Ravishankara, C. E. Kolb and M. J. Molina, Chemical Kinetics and Photochemical Data for Use in Stratospheric Modeling, Jet Propulsion Laboratory Report JPL94-26, December 15, 1994.

Deshler, T., B. J. Johnson and W. R. Rozier, Changes in the character of polar stratospheric clouds over Antarctica in 1992 due to the Pinatubo volcanic aerosol, *Geophys. Res. Lett.*, *21*, 273-276, 1994.

Dunkerton, T., On the mean meridional mass motions of the stratosphere and mesosphere, *J. Atmos. Sci.*, *35*, 2325-2333, 1978.

ESSA, NASA and USAF, *US Standard Atmosphere Supplements*, US Government Printing Office, Washington, D.C., 1966.

Fahey, D. W., S. R. Kawa, E. L. Woodbridge, P. Tin, J. C. Wilson, H. H. Jonsson, J. E. Dye, D. Baumgardner, S. Borrmann, D. W. Toohey, L. M. Avallone, M. H. Proffitt, J. Margitan, M. Loewenstein, J. R. Podolske, R. J. Salawitch, S. C. Wofsy, M. K. W. Ko, D. E. Anderson, M. R. Schoeberl and K. R. Chan, *In situ* measurements constraining the role of sulphate aerosols in mid-latitude ozone depletion, *Nature*, *363*, 509-514, 1993.

Farman, J. C., B. G. Gardiner and J. D. Shanklin, Large losses of total ozone in Antarctica reveal seasonal ClO_X/NO_X interaction, *Nature*, *315*, 207-210, 1985.

Fiocco, G., A. Mugnai and W. Forlizzi, Effects of radiation scattered by aerosols on the photodissociation of ozone, *J. Atmos. Terr. Phys.*, *40*, 949-961, 1978.

Fishman, J. and P. J. Crutzen, The origin of ozone in the troposphere, *Nature, 274*, 855, 1978.

Frederick, J. E. and N. Orsini, The distribution and variability of mesospheric odd nitrogen: A theoretical investigation, *J. Atmos. Terr. Phys., 44*, 479, 1982.

Fuchs, N. A., *The Mechanics of Aerosols*, Permagon, New York, 1964.

Garcia, R. R., Parameterization of planetary wave breaking in the middle atmosphere, *J. Atmos. Sci., 48*, 1405-1419, 1991.

Garcia, R. R. and S. Solomon, The effect of breaking gravity waves on the dynamics and chemical composition of the mesosphere and lower thermosphere, *J. Geophys. Res., 90*, 3850-3868, 1985.

Garcia, R. R. and S. Solomon, A new numerical model of the middle atmosphere 2. Ozone and related species, *J. Geophys. Res., 99*, 12,937-12,951, 1994.

Garcia, R. R., F. Stordal, S. Solomon and J. T. Kiehl, A new numerical model of the middle atmosphere 1. Dynamics and transport of tropospheric gases, *J. Geophys. Res., 97*, 12,967-12,991, 1992.

Georgii, H.-W. and F. X. Meixner, Measurement of the tropospheric and stratospheric SO_2 distribution, *J. Geophys. Res., 85*, 7433-7438, 1980.

Giauque, W. F., E. W. Hornung, J. E. Kunzler and T. R. Rubin, The thermodynamic properties of aqueous sulfuric acid solutions and hydrates from 15 to 300°K, *J. Am. Chem. Soc., 82*, 62-70, 1960.

Gmitro, J. I. and T. Vermeulen, Vapor-liquid equilibria for aqueous sulfuric acid, *AIChE J., 10*, 740-746, 1964.

Golombek, A. and R. G. Prinn, A global three-dimensional model of the stratospheric sulfuric acid layer, *J. Atmos. Chem., 16*, 179-199, 1993.

Hamill, P., C. S. Kiang and R. D. Cadle, The Nucleation of H_2SO_4-H_2O Solution Aerosol Particles in the Stratosphere, *J. Atmos. Sci., 34*, 150-162, 1977a.

Hamill, P., O. B. Toon and C. S. Kiang, Microphysical Processes Affecting Stratospheric Aerosol Particles, *J. Atmos. Sci., 34*, 1104-1119, 1977b.

Hamill, P., O. B. Toon and R. P. Turco, Aerosol nucleation in the winter Arctic and Antarctic stratosphere, *Geophys. Res. Lett., 17*, 417-420, 1990.

Hamill, P., R. P. Turco, C. S. Kiang, O. B. Toon and R. C. Whitten, An analysis of various nucleation mechanisms for sulfate particles in the stratosphere, *J. Aerosol Sci., 13*, 561-585, 1982.

Heist, R. H. and H. Reiss, Hydrates in supersaturated binary sulfuric acid-water vapor, *J. Chem. Phys., 61*, 573-581, 1974.

Hofmann, D. J., Balloon-borne measurements of middle atmosphere aerosol and trace gases in Antarctica, *Rev. Geophys., 26*, 113-130, 1988.

Hofmann, D. J., Increase in the Stratospheric Background Sulfuric Acid Aerosol Mass in the Past 10 Years, *Science*, *248*, 996-1000, 1990a.

Hofmann, D. J., Measurement of the condensation nuclei profile to 31 km in the Arctic in January 1989 and comparisons with Antarctic measurements, *Geophys. Res. Lett.*, *17*, 357-360, 1990b.

Hofmann, D. J., Aircraft sulphur emissions, *Nature*, *349*, 659, 1991.

Hofmann, D. J., Stratospheric aerosols: morphology, chemistry and optics, draft chapter, AEAP Report, unpublished manuscript, 1995.

Hofmann, D. J. and T. Deshler, Stratospheric cloud observations during formation of the Antarctic ozone hole in 1989, *J. Geophys. Res.*, *96*, 2897-2912, 1991.

Hofmann, D. J., J. M. Rosen and W. Gringel, Delayed production of sulfuric acid condensation nuclei in the polar stratosphere from El Chichon volcanic aerosols, *J. Geophys. Res.*, *90*, 2341-2354, 1985.

Hofmann, D. J., J. M. Rosen, J. W. Harder and J. V. Hereford, Balloon-borne measurements of aerosol, condensation nuclei, and cloud particles in the stratosphere at McMurdo Station, Antarctica, during the spring of 1987, *J. Geophys. Res.*, *D94*, 11,253-11,269, 1989.

Hofmann, D. J. and S. Solomon, Ozone destruction through heterogeneous chemistry following the eruption of El Chichon, *J. Geophys. Res.*, *D94*, 5029-5041, 1989.

Horvath, J. J. and J. E. Frederick, *In situ* measurements of nitric oxide in the high-latitude upper stratosphere, *Geophys. Res. Lett.*, *12*, 496, 1985.

Hynes, A. J., P. H. Wine and J. M. Nicovich, *J. Phys. Chem.*, *92*, 3846-3852, 1988.

Inn, E. C. Y., J. F. Vedder and D. O'Hara, Measurements of stratospheric sulfur constituents, *Geophys. Res. Lett.*, *8*, 5-8, 1981.

Inn, E. C. Y., J. F. Vedder and B. J. Tyson, COS in the stratosphere, *Geophys. Res. Lett.*, *6*, 191-193, 1979.

Jaecker-Voirol, A. and P. Mirabel, Nucleation rate in a binary mixture of sulfuric acid and water vapor, *J. Phys. Chem.*, *92*, 3518-3521, 1988.

Jaeschke, W., R. Schmitt and H. W. Georgii, Preliminary results of stratospheric SO_2 measurements, *Geophys. Res. Lett.*, *3*, 517-519, 1976.

Junge, C. E., C. W. Chagnon and J. E. Manson, Stratospheric aerosols, *J. Meteorol.*, *18*, 81-108, 1961.

Kawa, S. R., J. B. Kumer, A. R. Douglass, A. E. Roche, S. E. Smith, F. W. Taylor and D. J. Allen, Missing chemistry of reactive nitrogen in the upper stratospheric polar winter, *Geophys. Res. Lett.*, *22*, 2629-2632, 1995.

Kinne, S., O. B. Toon and M. Prather, Buffering of stratospheric circulation by changing amounts of tropical ozone: A Pinatubo case study, *Geophys. Res. Lett.*, *19*, 1927-1930, 1992.

Kolb, C. E., J. T. Jayne, D. R. Worsnop, M. J. Molina, R. F. Meads and A. A. Viggiano, Gas phase reaction of sulfur trioxide with water, *J. Am. Chem. Soc.*, *116*, 10314-10315, 1994.

Lindzen, R. S., Turbulence and stress owing to gravity wave and tidal breakdown, *J. Geophys. Res.*, *86*, 9707-9714, 1981.

Louisnard, N., G. Fergand, A. Girard and L. Gramont, Infrared absorption spectroscopy applied to stratospheric profiles of minor constituents, *J. Geophys. Res.*, *88*, 5365-5376, 1983.

Maroulis, P. J., A. L. Torres and A. R. Bandy, Atmospheric concentrations of carbonyl sulphide in the southwestern and eastern United States, *Geophys. Res. Lett.*, *4*, 510-512, 1978.

Maroulis, P. J., A. L. Torres, A. B. Goldberg and A. R. Bandy, Atmospheric SO_2 Measurements on Project Gametag, *J. Geophys. Res.*, *85*, 7345-7349, 1980.

Michelangeli, D. V., M. Allen and Y. L. Yung, El Chichon volcanic aerosols: impact of radiative, thermal, and chemical perturbations, *J. Geophys. Res.*, *D94*, 18429-18443, 1989.

Mills, M. J., A. O. Langford, T. J. O'Leary, K. Arpag, H. L. Miller, M. H. Proffitt, R. W. Sanders and S. Solomon, On the relationship between stratospheric aerosols and nitrogen dioxide, *Geophys. Res. Lett.*, *20*, 1187-1190, 1993.

Möhler, O. and F. Arnold, Gaseous sulfuric acid and sulfur dioxide measurements in the Arctic troposphere and lower stratosphere: implications for hydroxyl radical abundances, *J. Geophys. Res.*, *19*, 1763-1766, 1992.

Molina, L. T., J. J. Lamb and M. J. Molina, Temperature Dependent UV Absorption Cross Sections for Carbonyl Sulfide, *Geophys. Res. Lett.*, *8*, 1008-1011, 1981.

NRC, *International Critical Tables of Numerical Data, Physics, Chemistry, and Technology*, III, ed., Density -- Aqueous Inorganic Solutions (11-2), pp. 56-57, McGraw-Hill, New York, 1928.

Okabe, H., *Photochemistry of Small Molecules*, Wiley, New York, 1978.

Pham, M., J.-F. Müller, G. P. Brasseur, C. Granier and G. Mégie, A three-dimensional study of the tropospheric sulfur cycle, *J. Geophys. Res.*, *100*, 26,061-26,092, 1995.

Pitari, G. and V. Rizi, An estimate of the chemical and radiative perturbation of stratospheric ozone following the eruption of Mt. Pinatubo, *J. Atmos. Sci.*, *50*, 3260-3276, 1993.

Pruppacher, H. R. and J. D. Klett, *Microphysics of Clouds and Precipitation*, D. Reidel, Boston, 1978.

Randel, W. J., personal communication, 1996

Rinsland, C. P., M. R. Gunson, M. K. W. Ko, D. W. Weisensten, R. Zander, M. C. Abrams, A. Goldman, N. D. Sze and G. K. Yue, H_2SO_4 photolysis: A source of sulfur dioxide in the upper stratosphere, *Geophys. Res. Lett.*, *22*, 1109-1112, 1995.

Rodhe, H. and I. Isaksen, Global distribution of sulfur compounds in the troposphere estimated in a height/latitude transport model, *J. Geophys. Res.*, *85*, 7401-7409, 1980.

Roedel, W., Measurement of sulfuric acid saturation vapor pressure: implications for aerosol formation by heteromolecular nucleation, *J. Aerosol Sci.*, *10*, 375-386, 1979.

Rosen, J. M., The boiling point of stratospheric aerosols, *Journal of Applied Meteorology*, *10*, 1044-1046, 1971.

Rosen, J. M. and D. J. Hofmann, Unusual behavior in the condensation nuclei concentration at 30 km, *J. Geophys. Res.*, *88*, 3725-3731, 1983.

Russell, J. M., S. Solomon, L. L. Gordley, E. E. Remsberg and L. B. Callis, The variability of stratospheric and mesospheric NO_2 in the polar winter night observed by LIMS, *J. Geophys. Res.*, *89*, 7267, 1984.

Sabinina, L. and L. Turpugow, The surface tension of the system sulfuric acid-water, *Z. Phys. Chem.*, *A173*, 237-241, 1935.

Sandalls, F. J. and S. A. Penkett, Measurements of carbonyl sulphide and carbon disulphide in the atmosphere., *Atmos. Env.*, *11*, 197-199, 1977.

Schoeberl, M. R., P. K. Bhartia, E. Hilsenrath and O. Torres, Tropical ozone loss following the eruption of Mt. Pinatubo, *Geophys. Res. Lett.*, *20*, 29-32, 1993.

Seinfeld, J. H., *Atmospheric Chemistry and Physics of Air Pollution*, 738 pages, John Wiley & Son, New York, 1986.

Servant, J., The burden of the sulphate layer of the stratosphere during volcanic "quiescent" periods, *Tellus*, *38(B)*, 74-79, 1986.

Solomon, S., The mystery of the Antarctic ozone hole, *Rev. Geophys.*, *26*, 131-148, 1988.

Solomon, S., P. J. Crutzen and R. G. Roble, Photochemical coupling between the thermosphere and the lower atmosphere, 1, Odd nitrogen from 50 to 120 km, *J. Geophys. Res.*, *97*, 7206, 1982.

Solomon, S., R. R. Garcia, F. S. Rowland and D. J. Wuebbles, On the depletion of Antarctic ozone, *Nature*, *321*, 755-758, 1986.

Solomon, S., R. W. Portmann, R. R. Garcia, L. W. Thomason, L. R. Poole and M. P. McCormick, The role of aerosol trends and variability in anthropogenic ozone depletion at northern mid-latitudes, *J. Geophys. Res.*, *101*, 6713-6727, 1996.

Steele, H. M. and P. Hamill, Effects of temperature and humidity of the growth and optical properties of sulphuric acid-water droplets in the stratosphere, *J. Aerosol Sci.*, *12*, 517-528, 1981.

Sze, N. D. and M. K. W. Ko, CS2 and OCS in the stratospheric sulfur budget, *Nature*, *280*, 308-310, 1979.

Sze, N. D. and M. K. W. Ko, Photochemistry of OCS, CS_2, CH_3SCH_3 and H_2S: Implications for the atmospheric sulfur cycle, *Atmos. Env.*, *14*, 1223-1239, 1980.

Thomason, L. W., G. S. Kent, C. R. Trepte and L. R. Poole, A comparison of the stratospheric aerosol background periods of 1979 and 1989-1991, *submitted to Science*, 1995.

Thomason, L. W. and L. R. Poole, Use of stratospheric aerosol properties as diagnostics of Antarctic vortex processes, *J. Geophys. Res.*, *98*, 23,003-23,012, 1993.

Thornton, D. C., A. R. Bandy, B. W. Blomquist, D. D. Davis and R. W. Talbot, Sulfur dioxide as a source of condensation nuclei in the upper troposphere of the Pacific Ocean, *J. Geophys. Res.*, *101*, 1883-1890, 1996.

Tie, X., G. Brasseur, B. Briegleb and C. Granier, Two-dimensional simulation of Pinatubo aerosol and its effect on stratospheric ozone, *J. Geophys. Res.*, *99*, 20,545-20,562, 1994.

Timmermans, J., *The physico-chemical constants of binary systems in concentrated solutions*, 2, Interscience Publishers, New York, 1960.

Toon, O. B., R. P. Turco, P. Hamill, C. S. Kiang and R. C. Whitten, A one dimensional model describing aerosol formation and evolution in the stratosphere, II. Sensitivity studies and comparison with observations, *J. Atmos. Sci.*, *36*, 718-736, 1979.

Torres, A. L., P. J. Maroulis, A. B. Goldberg and A. R. Bandy, Atmospheric OCS measurements on Project Gametag, *J. Geophys. Res.*, *85*, 7357-7360, 1980.

Tucker, B. J., P. J. Maroulis and A. R. Bandy, Free tropospheric measurements of CS2 over a 45°N to 45°S latitude range, *Geophys. Res. Lett.*, *12*, 9-11, 1985.

Turco, R. P., P. Hamill, O. B. Toon, R. C. Whitten and C. S. Kiang, The NASA-Ames Research Center stratospheric aerosol model, I, Physical processes and mathematical analogs, NASA Report 1362, April, 1979a.

Turco, R. P., P. Hamill, O. B. Toon, R. C. Whitten and C. S. Kiang, A one-dimensional model describing aerosol formation and evolution in the stratosphere, I, Physical processes and mathematical analogs, *J. Atmos. Sci.*, *36*, 699-717, 1979b.

Turco, R. P. and R. C. Whitten, A comparison of several computational techniques for solving some common aeronomic problems, *J. Geophys. Res.*, *79*, 3179-3185, 1974.

Turco, R. P., R. C. Whitten and O. B. Toon, Stratospheric aerosols: observations and theory, *Rev. Geophys. Space Phys.*, *20*, 233-279, 1982.

Turco, R. P., R. C. Whitten, O. B. Toon, J. B. Pollack and P. Hamill, OCS, stratospheric aerosols and climate, *Nature*, *20*, 233-279, 1980.

Van Dingenen, R. and F. Raes, Coagulation enhancement of H_2O-H_2SO_4 aerosols: experiments and model calculations in the transition regime, *J. Aerosol Sci.*, *21*, S237-S240, 1990.

Warneck, P., *Chemistry of the Natural Atmosphere*, 753 pages, Academic Press, San Diego, 1988.

Wilson, J. C., M. Loewenstein, D. W. Fahey, B. Gary, S. D. Smith, K. K. Kelly, G. V. Ferry and K. R. Chan, Observations of condensation nuclei in the Airborne Antarctic Ozone Experiment: Implications for new particle formation and polar stratospheric cloud formation, *J. Geophys. Res.*, *94*, 16,437-16,448, 1989.

Wilson, J. C., M. R. Stolzenburg, W. E. Clark, M. Loewenstein, G. V. Ferry and K. R. Chan, Measurements of condensation nuclei in the airborne Arctic stratospheric expedition: Observations of particle production in the polar vortex, *Geophys. Res. Lett.*, *17*, 361-364, 1990.

Wilson, J. C., M. R. Stolzenburg, W. E. Clark, M. Loewenstein, G. V. Ferry, K. R. Chan and K. K. Kelly, Stratospheric sulfate aerosols in and near the northern hemisphere polar vortex: The morphology of the sulfate layer, multimodal size distributions, and the effect of denitrification, *J. Geophys. Res.*, *D97*, 7997-8013, 1992.

Wine, P. H., W. L. Chameides and A. R. Ravishankara, Potential Role of CS_2 Photooxidation in Tropospheric Sulfur Chemistry, *Geophys. Res. Lett.*, *8*, 543-546, 1981.

WMO/UNEP, Scientific assessment of ozone depletion: 1991, World Meteorological Organization (WMO)/United Nations Environment Programme (UNEP) Report 25, Geneva, 1991.

Wyslouzil, B. E., J. H. Seinfeld, R. C. Flagan and K. Okuyama, Binary nucleation in acid-water systems. II. Sulfuric acid-water and a comparison with methanesulfonic acid-water, *J. Chem. Phys.*, *94*, 6842-6850, 1991.

Yung, Y. L. and W. B. DeMore, Photochemistry of the stratosphere of Venus: implication for atmospheric evolution, *Icarus*, *51*, 199-247, 1982.

Zander, R., C. P. Rinsland, C. B. Farmer, J. Namkung, R. H. Norton and J. M. R. III, Concentrations of carbonyl sulfide and hydrogen cyanide in the free upper troposphere and lower stratosphere deduced from ATMOS/ Spacelab 3 Infrared Solar Occultation Spectra, *J. Geophys. Res.*, *93*, 1669-1678, 1988.

Zhang, R., M. Leu and L. F. Keyser, Hydrolysis of N_2O_5 and $ClONO_2$ on $H_2SO_4/HNO_3/H_2O$ ternary solutions under stratospheric conditions, *Geophys. Res. Lett.*, *100*, 1493-1496, 1995.

Zhang, R., P. J. Wooldridge, J. P. D. Abbatt and M. J. Molina, Physical chemistry of the H_2SO_4/H_2O binary System at low yemperatures: Stratospheric implications, *J. Phys. Chem.*, *97*, 7351-7358, 1993.

Zhao, J.-X., Numerical studies of the stratospheric aerosol layer under background and perturbation conditions, Ph.D. dissertation, Univ. of Calif., Los Angeles, 1993.

Zhao, J. X., O. B. Toon and R. P. Turco, Origin of condensation nuclei in the springtime polar stratosphere, *J. Geophys. Res.*, *100*, 5215-5227, 1995.

Zhao, J. X. and R. P. Turco, Nucleation simulations in the wake of a jet aircraft in stratospheric flight, *J. Aerosol Sci.*, *26*, 779-795, 1995.